

REVIEW ARTICLE | JUNE 25 2025

From electron cyclotron emission and reflectometry to microwave imaging diagnostics in fusion plasmas: Progress and perspectives ^{EP}

Alf Köhn-Seemann   ; Rennan B. Morales 



Phys. Plasmas 32, 060502 (2025)

<https://doi.org/10.1063/5.0259713>



Articles You May Be Interested In

A new method of out-of-focus millimeter wave imaging in fusion plasma diagnostics using Bessel beams

Rev. Sci. Instrum. (September 2018)

Comparative study between the reflective optics and lens based system for microwave imaging system on KSTAR

Rev. Sci. Instrum. (October 2010)

Low-noise heterodyne receiver for electron cyclotron emission imaging and microwave imaging reflectometry

Rev. Sci. Instrum. (July 2016)

26 March 2026 11:39:46



AIP Advances

Why Publish With Us?

-  **21DAYS**
average time to 1st decision
-  **OVER 4 MILLION**
views in the last year
-  **INCLUSIVE**
scope

[Learn More](#)



From electron cyclotron emission and reflectometry to microwave imaging diagnostics in fusion plasmas: Progress and perspectives

Cite as: Phys. Plasmas **32**, 060502 (2025); doi: [10.1063/5.0259713](https://doi.org/10.1063/5.0259713)

Submitted: 20 January 2025 · Accepted: 28 May 2025 ·

Published Online: 25 June 2025



View Online



Export Citation



CrossMark

Alf Köhn-Seemann^{1,a)}  and Rennan B. Morales² 

AFFILIATIONS

¹Institute of Interfacial Process Engineering and Plasma Technology, University of Stuttgart, Stuttgart, Germany

²United Kingdom Atomic Energy Authority, CCFE, Culham Campus, Abingdon, United Kingdom

^{a)} Author to whom correspondence should be addressed: koehn@igvp.uni-stuttgart.de

ABSTRACT

Microwave diagnostics will be one of the few diagnostic techniques that can be operated in future fusion devices. In the past, they have contributed significantly to the understanding of the plasma dynamics, in particular electron cyclotron emission (ECE) and reflectometry. While these provide 1D measurements of plasma electron temperature and density along a line of sight, the advancement of electron cyclotron emission imaging (ECEI) and microwave imaging reflectometry (MIR) allows to obtain 2D images with high temporal and spatial resolution. Recent technological improvements will not only reduce the overall dimensions of these systems, thereby fulfilling requirements of future fusion devices, but also increase their sensitivity, reduce their costs, and ease maintenance, which increases operational time of the devices they are installed on. This paper aims to present an overview of ECE diagnostics and reflectometry. It first discusses their 1D implementations, followed by a more detailed examination of ECEI and MIR, including recent developments, and a perspective on future directions.

© 2025 Author(s). All article content, except where otherwise noted, is licensed under a Creative Commons Attribution (CC BY) license (<https://creativecommons.org/licenses/by/4.0/>). <https://doi.org/10.1063/5.0259713>

NOMENCLATURE

AM	Amplitude modulation	ECEI	Electron cyclotron emission imaging
ATF	Advanced Toroidal Facility	ECRH	Electron cyclotron resonance heating
AUG	ASDEX Upgrade, Axially Symmetric Divertor Experiment	EHO	Edge harmonic oscillation
CECE	Correlation electron cyclotron emission	ELM	Edge-localized mode
CER	Charge-exchange recombination	FADIS	Fast directional switch
CFETR	Chinese Fusion Engineering Testing Reactor	FDTD	Finite-difference time-domain
DBS	Doppler backscattering	FM	Frequency modulation
DIII-D	Divertor III D	FMCW	Frequency-modulated continuous-wave
DR	Doppler reflectometry	GAM	Geodesic acoustic mode
DTT	Divertor Tokamak Test facility	HDPE	High-density polyethylene
EAST	Experimental Advanced Superconducting Tokamak	HL-2A	Huan-Liuqi-2A
EBE	Electron Bernstein wave emission	HL-3	Huan-Liuqi-3
EBW	Electron Bernstein wave	IF	Intermediate frequency
ECCD	Electron cyclotron current drive	IFMIF-DONES	International Fusion Materials Irradiation Facility-DEMO Oriented Neutron Source
ECE	Electron cyclotron emission	IMAS	Integrated Modelling & Analysis Suite
		ITB	Internal transport barrier
		ITER	International Thermonuclear Experimental Reactor

JET	Joint European Torus
JT-60SA	Japan Tokamak-60 Super Advanced
J-TEXT	Joint TEXT
KSTAR	Korea Superconducting Tokamak Advanced Research
LCFS	Last closed flux surface
LHD	Large helical device
LNA	Low-noise amplifier
LO	Local oscillator
MAST-U	Mega Ampere Spherical Tokamak—Upgrade
MCF	Magnetic confinement fusion
MHD	Magnetohydrodynamics
MIR	Microwave imaging reflectometry
NBI	Neutral beam injection
NIF	National Ignition Facility
NTM	Neoclassical tearing mode
PCR	Poloidal correlation reflectometry
PLL	Phase-locked loop
PPR	Plasma position reflectometry
QCM	Quasi-coherent mode
RCR	Radial correlation reflectometry
RMP	Resonant magnetic perturbation
RTP	Rijnhuizen Tokamak Project
SAMI	Synthetic Aperture Microwave Imaging
SNR	Signal-to-noise ratio
SoC	System-on-chip
SOL	Scrape-off layer
SPARC	Smallest Possible ARC (affordable, robust, compact)
SST-1	Steady State Superconducting Tokamak
TAEs	Toroidal Alfvén eigenmodes
TCV	Tokamak à Configuration Variable
TEXTOR	Torus Experiment for Technology Oriented Research
TEXT-U	Texas Experimental Tokamak Upgrade
TFR	Tokamak de Fontenay-aux-Roses
TJ-II	Toro de la Junta de Energía Nuclear—II
TST-2	Tokyo Spherical Tokamak 2
W7-AS	Wendelstein 7-Advanced Stellarator
W7-X	Wendelstein 7-X
WCM	Weakly coherent mode
WEST	Tungsten (W) Environment in Steady-state Tokamak
YIG	Yttrium iron garnet

I. INTRODUCTION

More than 100 years ago, Sir Arthur Eddington predicted that the sun is powered by subatomic processes turning hydrogen into helium and continued that “*we sometimes dream that man will one day learn to release it [the sun’s energy source] and use it for his service.*”¹ Today, realizing controlled fusion is no longer just a dream:^{2,3} fusion research has reached a point where not only publicly funded projects like International Thermonuclear Experimental Reactor (ITER)⁴ are being built aiming at achieving a Q -value (Q is the ratio of fusion power released to auxiliary heating power) larger than one, or having achieved it already in the case of National Ignition Facility (NIF),^{5,6} if comparing instead the energy being coupled into the vacuum chamber

with the released energy. Also, privately funded fusion projects have gained impressive momentum over the last few years, with some of them currently assembling devices that are designed for a Q -value larger than one.⁷

Electromagnetic waves in the microwave frequency range (also referred to as *millimeter-waves* for the higher frequency values in this range) play an indispensable role in magnetic confinement fusion (MCF) plasma experiments for heating^{8,9} and diagnostic purpose^{10,11} due to the characteristic frequencies (i.e., cutoffs and resonances), which are functions of plasma density and background magnetic field. An advantage of microwave systems is the small space requirements for in-vessel components (e.g., emitting and receiving antennas, reflecting and polarizing mirrors) compared to other heating or diagnostic systems. This is of special importance in a potential fusion power plant where the in-vessel wall will be covered with Tritium-breeding blankets.¹² The requirement of having a Tritium-breeding ratio larger than 1 strongly limits the space available for plasma diagnostics: slightly less than 1 % of the vessel wall is available for diagnostics in a DEMO-type device,¹³ compared to approximately 20 % in ITER. The diagnostic components are, on the other hand, large enough with not too strong demands on mechanical precision of their respective surfaces such that small imperfections caused by the harsh environment around a fusion plasma do not degrade the components’ performance significantly.

The most advanced MCF concepts are tokamak and stellarator,¹⁴ whose successful operation relies heavily on microwave plasma diagnostics. These diagnostics can be sorted into two groups: *active* and *passive* diagnostics. The group of active diagnostics encompasses *interferometry*, *polarimetry*, *reflectometry*, and *wave scattering*. Passive diagnostics include *electron cyclotron emission* (ECE) and *electron Bernstein wave emission* (EBE). While all of those were in the early days of fusion research situated in the microwave range of frequencies, this is no longer the case for interferometry¹⁵ and polarimetry¹⁶ which have moved into the infrared range in modern fusion devices. We will therefore not discuss them further. Scattering diagnostics¹⁷ will also be omitted as they are not set up as imaging diagnostics (see further below for a discussion about imaging diagnostics). Hence, only the cases of reflectometry and electron cyclotron and electron Bernstein wave emission will be discussed in this paper. The dielectric properties of a plasma are mainly determined by its electrons; thus, information on their properties is primarily obtained through these diagnostics. Active and passive diagnostics are both important as they are capable of probing the electron species with a high spatial and temporal resolution.

Small-scale turbulence is responsible for a majority of the observed radial heat and particle transport in MCF plasmas, which is highlighted by large-scale numerical models.^{18–24} Validation of the simulations’ results by experimental data is a crucial factor in the trustworthiness of the models themselves²⁵ and thus also for the predictions and extrapolations made with these models for future fusion devices. For these validations, it is crucial to not only investigate the temporal behavior of the electron plasma density and temperature along a line of sight and thus only obtain 1D measurements. Instead, the spatial extent in the full poloidal cross section is required. This has been made possible with *microwave imaging diagnostics*, which correspond basically to a microwave camera obtaining 2D images with a high temporal resolution in a poloidal cross section. Outside of fusion, microwave imaging diagnostics also play an important role in medical

applications,^{26–29} security screening,³⁰ and synthetic aperture radar systems.³¹ For a general overview, the interested reader is referred to the book of Pasterino.³²

From the large number of plasma diagnostics developed over the last 70 years,^{33–35} microwave-based diagnostics together with neutron diagnostics are considered to be the most (and probably the only ones) compatible with the harsh environment in high-performance future fusion reactors.³⁶ A potential fusion power plant differs significantly from fusion experiments currently in operation or under construction. The role of the diagnostics is no longer to study and investigate plasma physics processes but rather to protect the machine and ensure operation at the optimum conditions^{37,38} (i.e., control, not research-driven investigation).

Microwave diagnostics do not only play an indispensable role in conventional tokamaks and stellarators; they also play a major role in spherical tokamaks, like ST40 being operated by Tokamak Energy,³⁹ in the field-reversed configuration device C-2W from TAE Technologies,⁴⁰ or in the high-field and more compact tokamak SPARC from CFS, which is currently under construction.⁴¹

The intention of this review is not to cover all aspects of plasma microwave diagnostics. For this purpose, the interested reader is referred to the textbooks by Heald and Wharton⁴² and by Hartfuß and Geist,¹¹ and to a number of review or overview papers.^{10,43–45} The present review seeks to give an overview of microwave imaging diagnostics, including recent findings and results, developments, and advances, and also a perspective of what to expect in the future. To get a better understanding of the general capabilities of reflectometry and emission diagnostics, we do not restrict ourselves to their imaging versions but also give a brief description and overview of their 1D implementations. Let it be noted that several decades of research with microwave diagnostics have formed the basis for this work.^{46–49}

This paper begins with an overview of waves in plasmas in Sec. II, followed by a discussion of electron cyclotron emission diagnostics in Sec. III. Electron Bernstein wave emission is described in Sec. IV, after which reflectometry is discussed in Sec. V. A summary and conclusion in Sec. VI closes the paper.

II. WAVES IN PLASMAS

This article does not intend to give a thorough introduction into the fascinating and wide field of waves in plasmas. Instead, a brief overview with the most important fundamentals will be presented, providing the reader with the necessary background for the following chapters. For a comprehensive work on waves in plasmas, we refer the interested reader to one of the seminal textbooks in this field.^{50–53}

Burning plasmas, as well as hot plasmas from existing devices, require a relativistic treatment to fully cover the behavior of waves in plasmas. To understand the basic principles of the microwave diagnostics, however, a cold plasma description is sufficient. Assuming a plane wave with an angular frequency ω_0 propagating at an angle θ with respect to the background magnetic field \mathbf{B}_0 , and the wave vector \mathbf{k} being oriented along the z axis in a Cartesian coordinate system, the index of refraction N is given by the *Appleton–Hartree* equation,³⁵ which was originally introduced to describe the propagation of radio waves in the ionosphere:⁵⁴

$$N^2 = 1 - \frac{2X(1-X)}{2(1-X) - Y^2 \sin^2 \theta \pm \sqrt{Y^4 \sin^4 \theta + 4Y^2(1-X)^2 \cos^2 \theta}}, \quad (1)$$

with the commonly used abbreviations $X = \omega_{pe}^2/\omega_0^2$ and $Y = \omega_{ce}/\omega_0$, where ω_{pe} and ω_{ce} correspond to the electron plasma and cyclotron frequencies, respectively. The plus and the minus sign in the denominator of Eq. (1) refer to the *ordinary mode* (O-mode) and the *extraordinary mode* (X-mode).

Cutoffs and resonances are found by solving Eq. (1) for $N \rightarrow 0$ and $N \rightarrow \infty$, respectively

$$\omega_{\text{cut}1} = \omega_{pe}, \quad \omega_{\text{cut}2,3} = \pm \omega_{ce}/2 + \sqrt{\omega_{ce}^2/4 + \omega_{pe}^2}, \quad (2)$$

$$\omega_{\text{res}1,2}^2 = \frac{\omega_{ce}^2 + \omega_{pe}^2}{2} \pm \sqrt{\left(\frac{\omega_{ce}^2 + \omega_{pe}^2}{2}\right)^2 - \omega_{ce}^2 \omega_{pe}^2 \cos^2 \theta}. \quad (3)$$

For the often applied case of propagation perpendicular to the background magnetic field, $\theta = 90^\circ$, the dispersion relations of O- and X-mode simplify to

$$N_O^2 = 1 - X = 1 - \frac{\omega_{pe}^2}{\omega_0^2}, \quad (4)$$

$$N_X^2 = 1 - \frac{X(1-X)}{1-X-Y^2} = 1 - \frac{\omega_{pe}^2(\omega_0^2 - \omega_{pe}^2)}{\omega_0^2(\omega_0^2 - \omega_{pe}^2 - \omega_{ce}^2)}. \quad (5)$$

The O-mode exhibits a cutoff at the electron plasma frequency, as already shown in Eq. (2). For the X-mode, two cutoffs are found, as can also be seen in Eq. (2), referred to as the *right-hand cutoff* for the + sign and the *left-hand cutoff* for the – sign. Only the X-mode experiences a resonance, which simplifies from Eq. (3) to

$$\omega^2 = \omega_{UH}^2 = \omega_{pe}^2 + \omega_{ce}^2, \quad (6)$$

denoted as *upper-hybrid resonance*. These characteristic frequencies define the accessible region for electromagnetic waves, as they can freely propagate only if there is no cutoff or resonance. Figure 1 shows the characteristic frequencies in a plasma corresponding to an ITER reference case⁵⁵ as a function of the radial coordinate in a poloidal cross section. As can be seen, all characteristic frequencies lie within the microwave range, which is usually defined as^{56,57} ranging from 300 MHz to 300 GHz, corresponding to wavelengths of 1 m and 1 mm, respectively.

As shown in Fig. 1, typical electron temperatures in ITER are expected to be around $T_e \leq 20$ keV. At these values, relativistic effects start to play a role. An effective electron mass can be used to take these effects into account:⁵⁸

$$m_e = m_{e0} \sqrt{1 + 5/\mu}, \quad (7)$$

with m_{e0} the electron rest mass and $\mu = m_{e0}c^2/T_e$ with T_e in units of J. The cutoff frequencies are reduced by relativistic effects, as can be seen in Fig. 1. Using the effective electron mass, the resulting cutoff frequencies and refractive indices were shown to be in good agreement with a fully relativistic computation.⁵⁸

III. ELECTRON CYCLOTRON EMISSION

In magnetized plasmas, charged particles gyrate around magnetic field lines, emitting radiation at their respective cyclotron frequency and its harmonics. The electron cyclotron frequency reads³⁵

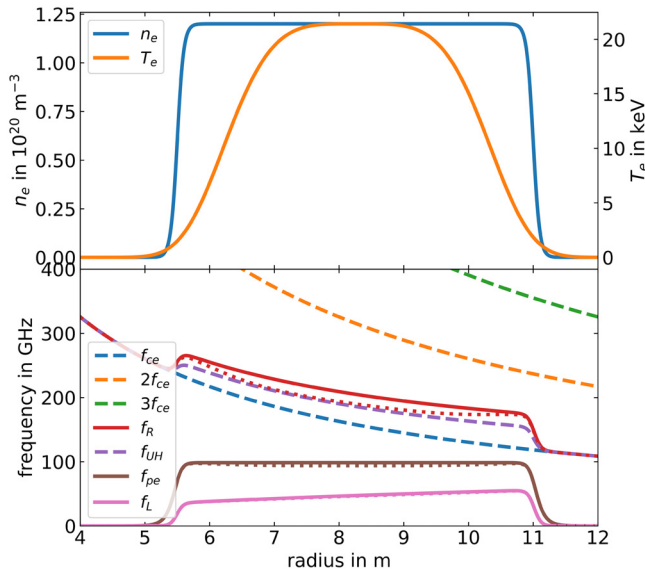


FIG. 1. (Top) Radial profiles of electron density and electron temperature and (bottom) characteristic frequencies, see Eqs. (2) and (3), as a function of radius for parameters corresponding to an ITER reference case.⁵⁵ The effect of taking into account relativistic corrections is indicated for the cutoff frequencies by the respective dotted lines.

$$\omega_{ce} = n \frac{eB}{\gamma m_e}, \quad (8)$$

with n the harmonic number, e the electron charge, B the magnetic field strength, $\gamma = (1 - v^2/c_0^2)^{-1/2}$ the relativistic Lorentz factor, and m_e the electron mass. Assuming $\gamma = 1$, Eq. (8) can be translated to $f_{ce} = \omega_{ce}/(2\pi) \approx 28 \text{ GHz/T}$ for the fundamental ($n = 1$). A magnetic field strength of 5 T yields therefore a cyclotron frequency of $f_{ce} = 140 \text{ GHz}$, lying in the microwave frequency range.

If the plasma density and temperature are sufficiently high, the plasma becomes optically thick. The intensity of the electron cyclotron emission (ECE) radiation at a certain frequency is then given within the Rayleigh–Jeans law by¹¹

$$I(\omega) = \frac{\omega^2 k_B T_e}{8\pi^3 c_0^2}, \quad (9)$$

describing black-body radiation where the radiation intensity I is proportional to the electron temperature T_e , $I \propto T_e$. Since the magnetic field strength along a radial cut in a tokamak poloidal cross section varies with radius,

$$B(R) = \frac{B_0 R_0}{R}, \quad (10)$$

with B_0 the field on axis and R_0 the major radius, and thus also the electron cyclotron frequency f_{ce} , a frequency-resolved measurement of the ECE intensity yields a 1D radial profile of the electron temperature. For Eq. (9) to hold, the *optical thickness* τ (corresponding to the strength of absorption) has been assumed to be large. If this is not the case, the dependency of I on τ needs to be taken into account, and Eq. (9) changes to¹⁰

$$I(\omega) = \frac{\omega^2 k_B T_e}{8\pi^3 c_0^2} \frac{1 - e^{-\tau}}{1 - \rho_{\text{refl}} \cdot e^{-\tau}}, \quad (11)$$

with ρ_{refl} accounting for reflections from the inner vessel wall having values between 0 and 1, where for metal wall surfaces values close to 1 are approached.⁵⁹ Note that for large values of τ , Eq. (11) approaches Eq. (9).

The optical thickness τ , sometimes also referred to as *optical depth*, is the integral absorption by the plasma, described by the quantity α , along a ray path s , $\tau = \int \alpha ds$, and is a function of n_e , T_e , B_0 , and the harmonics number. Figure 2 shows τ for O- and X-mode up to harmonics of $n = 3$ obtained using the formulas derived by Bornatici *et al.*⁶⁰ for the ITER reference case as shown in Fig. 1. One can clearly see the optical thickness at the second harmonic of the X-mode τ_{X2} being the largest everywhere with values well above 1, i.e., having the highest absorption. Note that τ_{O1} , τ_{X1} , and τ_{X3} are all also well above 1, τ_{O2} on the other hand might need a more careful treatment here. In particular, at the edge, the optical depth can be close to 1 or even below, no longer fulfilling the condition for a blackbody, meaning that the radiation temperature is no longer equal to the local electron temperature but instead dominated by higher values from further inside where the plasma still acts as a blackbody. This is referred to as *shine-through* and requires forward modeling to include the plasma edge in the data analysis process.^{61–63} Likewise, non-thermal electron components spoil the ECE signal and need to be taken into account in the forward model.⁶⁴ Note that also very hot plasmas with a bulk electron temperature of $T_e > 5 \text{ keV}$, require a dedicated forward model.⁶⁵

The sensitive receiver frequency range of ECE diagnostics often includes the frequency range of high-power microwave heating sources, the gyrotrons.⁶⁶ To protect these sensitive diagnostics from stray radiation due to non-absorbed power, notch filters are an essential part of it. They exist in different implementations^{67–70} and are very narrow band-stop filters with a width of $\approx 2 \text{ GHz}$ and an attenuation of typically more than 50 dB.

The ECE spectrum is usually measured in discrete frequency channels to ideally cover the full radius, where each channel allows for

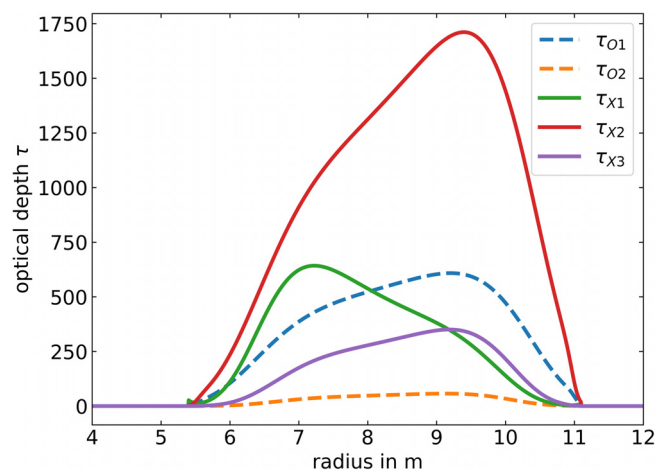


FIG. 2. Optical depths as a function of radius for parameters corresponding to an ITER reference case,⁵⁵ see Fig. 1, calculated using the formulas provided by Bornatici *et al.*⁶⁰

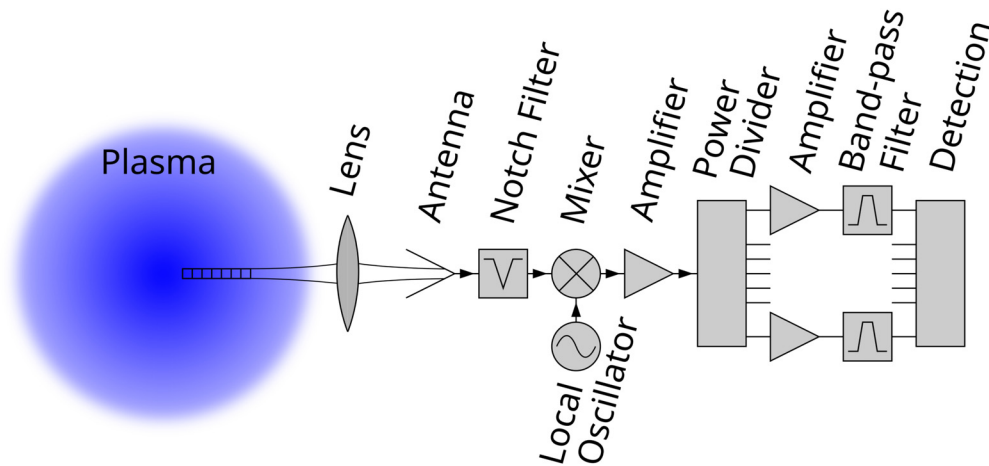


FIG. 3. Schematic diagram of a typical multi-channel heterodyne ECE radiometer system. Note that the optical path is usually more complicated than illustrated here.

a high enough data acquisition rate to investigate the plasma dynamics. To obtain a full 1D profile at once, the ECE signal is, after passing the notch filter, first down-converted to an intermediate frequency (IF) and then amplified by a broadband amplifier. As illustrated in Fig. 3, a power divider then divides the signal into separate channels, each of which is equipped with a bandpass filter, selecting a different part of the spectrum and feeding it to a data acquisition system.⁷¹ The width of the filters and the distance of their central frequency define the radial resolution of the resulting T_e profile. Selecting the bandwidth of the filter constitutes a compromise between spatial resolution and signal-to-noise ratio (SNR): a smaller bandwidth allows for better spatial resolution but reduces the SNR. In tokamaks, the ECE radiometer typically measures in the equatorial plane across the poloidal cross section.

To ensure accurate absolute measurements of the electron temperature, the ECE diagnostic system must be absolutely calibrated. This is usually done by employing a large-aperture black-body radiation source of known temperature, e.g., a heated glass ceramic and liquid nitrogen-cooled absorber plates.^{71,72} For improved SNR, the usage of silicon carbide plates, allowing very high temperatures up to 600 °C, is currently explored.⁷³ Instead of using such a hot/cold calibration, it is also possible to use a hot calibration source only, which is capable of operation at different temperatures, as successfully demonstrated on the tokamaks Tore Supra,⁷⁴ K-STAR,⁷⁵ or EAST.⁷⁶ The calibration is a challenging task due to the necessary extrapolation from a measurement at a few hundred degrees to millions of degrees in the plasma. The linearity of the amplifiers must thus be very good, and a cross-calibration with other diagnostics measuring T_e is recommended.^{76,77} If only the relative fluctuation level $\delta T_e/T_e$ is of interest, an absolute calibration is not necessary and might just be omitted.⁷⁸ Note that T_e in this case should be understood as the radiation temperature $T_{e,\text{rad}}$, and $\delta T_e/T_e = \delta T_{e,\text{rad}}/T_{e,\text{rad}}$.

While ECE radiometers are fast enough to investigate turbulent electron temperature fluctuations extending up to the MHz range of frequencies, thermal noise, inherent to ECE radiation, is typically on the order of 5% making it impossible to resolve small-scale and small-amplitude fluctuations of the electron temperature.^{45,79} However,

measuring and understanding the behavior of these fluctuations is considered to be of major importance when it comes to correctly describing turbulent (also referred to as *anomalous*) transport losses.^{80–82} In particular, toward the plasma center, the fluctuation amplitude becomes small,⁴⁵ on the order of 0.1%, making it impossible to measure them with conventional ECE. To overcome this limitation, correlation techniques can be used, based on the idea that thermal noise exhibits no correlation features, in contrast to the thermal T_e fluctuations.⁷⁹ Cross correlating signals from either two separate radiometers⁸³ or from neighboring channels^{84,85} thus yields the fluctuations δT_e , while suppressing the noise (assuming that the structures are larger than the corresponding spatial channel separation). This technique is known as *correlation electron cyclotron emission (CECE)* and is (or was) employed on many fusion devices around the world: Tore Supra,⁸⁶ DIII-D,⁸⁷ Alcator C-Mod,^{88,89} AUG,⁹⁰ TCV,⁹¹ and J-TEXT.⁹² As will be briefly shown in Sec. III A, CECE plays an important role in turbulent transport studies.

For plasmas with low optical depth of $\tau \leq 4$, electron temperature fluctuations measured by CECE are affected by contamination from electron plasma density fluctuations.^{93,94} Their contribution to the CECE signal can be quantitatively accounted for, provided that the electron plasma density fluctuations are known, for example, obtained from another diagnostics.

In the remaining part of this section, a brief overview of the 1D ECE diagnostic system will be given in Sec. III A to understand the capabilities and limitations of the 1D diagnostics and to better comprehend and put into perspective those of the 2D electron cyclotron emission imaging (ECEI) system, which is discussed in Sec. III B.

A. 1D electron cyclotron emission diagnostics

ECE has been first applied as a diagnostics in 1974 at the CLEO tokamak,⁵⁹ and is nowadays considered a standard diagnostics for MCF devices. For a detailed description of the challenges that needed to be solved and pushed the development of the ECE diagnostics forward, we refer the interested reader to the comprehensive overview by Costley.⁹⁵ As indicated in Table I, ECE is installed on basically all major MCF devices. It is the primary diagnostic technique for

TABLE I. ECE diagnostics on the upper part and CECE diagnostics on the bottom part of the table (separated by the blank row) installed on various fusion experiments in operation.

Device	Frequency in GHz	Mode	Channels	Comment	References
AUG	85...185	X2	60	Profile ECE ⁶⁵	96
	132.5...147.5	X2	6	Inline ECE	97
DIII-D	83...130	X2	40		98,99
EAST	97...167	X2	56		100
LHD	50...150	X2	14 + 32		101,102
	34...65	X2	32	Low- B_0	103
KSTAR	110...162	X2	40		104
	163...196	X2	8		105
SST1	74...86	X2	8		106
TCV	66...114	X2	48		107
	78...148	O2, X2	24	Vertical ECE	108
TJ-II	50...60	X2	16		109
W7-X	126...162	X2	32, 16		110
AUG	105...125	X2	30		111
	105...113	X2	24		112
DIII-D	72...108	X2	8	CECE8	113
	92...106	X2	2	CECE2	87
EAST	104...132	X2	8		100
TCV	67...100	X2	6		107

obtaining electron temperature measurements in future fusion devices like ITER,^{114,115} the EU DEMO,³⁸ or the proposed CFETR.¹¹⁶

1. Fusion devices in operation

The conventional ECE diagnostics does not only play an important role in obtaining the equilibrium profile of the electron temperature, but, by combining spatial and temporal resolution, it can provide important information on the localization of magnetic islands. These are formed when a neoclassical tearing mode (NTM) is growing, an instability that significantly reduces confinement and can trigger a disruption.¹¹⁷ The diagnostics might thus offer vital information on where to drive current by localized microwave heating to stabilize these instabilities.^{118,119} Having the ECE diagnostics and the electron cyclotron resonance heating (ECRH) antenna usually positioned at different toroidal positions, additional equilibrium reconstruction and mapping of the ECE port onto the ECRH port are required. This step can be overcome by *inline ECE*,^{120,121} where the ECRH system and the ECE diagnostics share the antenna and thus have the same line of sight. Such a system was installed at AUG,⁹⁷ allowing for direct feedback experiments for stabilizing NTMs.¹²² A bidirectional diplexer, referred to as a fast directional switch (FADIS),¹²³ developed originally for fast-switching between two launcher positions, was installed for this purpose behind the launcher to connect the ECE radiometer and ECRH source to the same antenna (in principle, the diplexer is used as a frequency filter). As illustrated in Fig. 4, FADIS acts as a ring resonator with two fixed corrugated mirrors and two focusing mirrors of which one is movable to adjust the resonator frequency. For a given input port, one of the output ports has a peak in the transmission frequency,

while the other output port exhibits a notch filter characteristic and is referred to as a non-resonant output port. Tuning the resonance frequency of FADIS to the ECRH frequency, the ECRH power is passed to the plasma and suppressed at the ECE port, while the radiation coming from the plasma is passed directly to the ECE port. Further suppression of the signal is needed, as the power reaching the radiometer should typically not exceed 1 mW. This is achieved by an oversized Mach-Zehnder interferometer,¹²⁴ a notch filter based on a waveguide Bragg reflector,¹²⁵ and a PIN switch.⁹⁷ A quasi-inline configuration, where ECE and ECRH systems share the same toroidal position but a different poloidal position, has been successfully tested at TCV.¹²⁶

Another implementation to detect NTMs has been suggested^{127,128} and successfully tested in DIII-D recently.¹²⁹ Using a tunable yttrium iron garnet (YIG) bandpass filter in the IF section of the radiometer allows one to either acquire a radial T_e profile with using only one channel or, without requiring an absolute calibration, estimate the T_e gradient scale length $L_{T_e} = T_e/|\nabla T_e|$ in real time. Varying the frequency, the measured intensity variation is proportional to the variation of $T_e(r)$ and thus a fast frequency scan yields an estimation of $L_{T_e}(r)$ which can then be used to localize NTMs. This technique has also been suggested recently for the upgraded CECE diagnostics on EAST.¹⁰⁰

Another method to determine L_{T_e} has been implemented¹³⁰ in DIII-D: channels from two CECE diagnostics, CECE8¹¹³ and CECE2,⁸⁷ were correlated to estimate the radial correlation length to $L_{T_e} \approx 10\rho_s$, with ρ_s the ion Larmor radius calculated using the electron temperature.

Upgraded CECE diagnostics on AUG¹¹¹ and DIII-D⁹⁹ enable measurements of $\delta T_e/T_e$ with spatial resolutions of a few millimeters

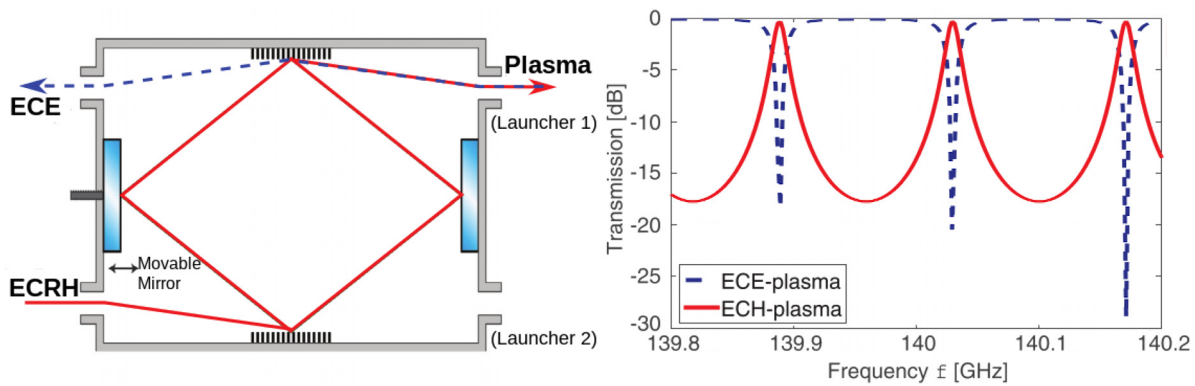


FIG. 4. Schematic of the bidirectional diplexer FADIS as used in AUG with the paths traveled by ECE and ECRH indicated in blue and red, respectively, with the transmission as a function of the frequency as shown on the right. When in resonance, as for the ECRH beam, FADIS transmits a narrow frequency band via the top right port, while when being out of resonance, as is the case for the broad frequency spectrum of the ECE signal, it is directly reflected out of the diplexer, here via the top left port, into the radiometer. Adapted with permission from Van Den Brand, "Modelling and measurements for control of magnetic instabilities in tokamak plasmas," Ph.D. thesis (Technische Universiteit Eindhoven, 2016).⁴⁹⁶ Copyright Van Den Brand.

only. This allows for quantitative comparison of numerical approaches to simulate plasma turbulence with actual experimental data, yielding¹³¹ good agreement for $L_{T_e}(r)$ but revealing an overestimation in the simulations of $\delta T_e/T_e$ by roughly a factor of 2. Such validation studies are of particular importance on the path to a better understanding of the turbulence-driven heat flux in MCF experiments, considered to be the major loss channel in tokamaks.¹³²

Understanding the physics of the transition from *low-* to *high-confinement* mode (from L- to H-mode), in particular of the observed variation of the heating power threshold (to enter the H-mode) with magnetic configuration, was the subject of recent studies in AUG:¹³³ fluctuation amplitudes of the electron temperature at the edge obtained from CECE measurements were found to be larger in less favorable magnetic configurations prior to the transition, accompanied by a larger power threshold, in agreement with an observed reduced shear layer (playing an important role in the H-mode as it suppresses turbulence at the edge¹³⁴).

An important characteristic of the H-mode is the formation of a transport barrier at the edge leading to steep plasma pressure profiles and the formation of a pedestal. The pedestal is, however, unstable and collapses more or less periodically with the release of substantial heat and particles, imposing a risk for the divertor. These periodic events are referred to as *edge-localized mode (ELM)*.¹³⁵ Combining and correlating the CECE diagnostics with other diagnostics installed on EAST, it could be shown that boron powder injection resulted in a suppression of ELMs accompanied by the onset of edge harmonic oscillations (EHO), avoiding impurity accumulation.¹³⁶

A promising and often applied technique to suppress ELMs involves generating a stochastic magnetic field at the plasma edge, a method known as resonant magnetic perturbation (RMP).¹³⁷ CECE diagnostics in DIII-D enabled measurements showing that the electron temperature fluctuations increase after successful transition to ELM suppression triggered by RMPs,¹³⁸ indicating increased gradient-driven turbulent transport as a mechanism to enable H-mode operation without ELMs.

A regime between L- and H-mode is the *I-mode*, which is characterized by L-mode-like particle transport (i.e., exhibiting no particle transport barrier) but reduced, H-mode-like, heat transport,¹³⁹ making

it an interesting scenario for a future fusion reactor (since it is an ELM-free regime). An edge instability, referred to as *weakly coherent mode (WCM)*, is thought to be responsible for the comparably strong particle transport in the I-mode.¹⁴⁰ CECE measurement in AUG showed that the WCM has its origin in the L-mode and that a continuous increase in frequency is seen when going from L- to I-mode.¹⁴¹ With two toroidally separated CECE diagnostics, it could be shown that the WCM features long toroidal correlation lengths, hence low toroidal mode numbers.¹¹²

The *enhanced H-mode* is a confinement regime free of ELMs but still exhibiting very good confinement.¹⁴² A *quasi-coherent mode (QCM)* is thought to regulate transport and thus keep the pedestal stable. The absence of the dangerous type-I ELMs (dangerous due to their violent impact on the divertor¹⁴³) makes this scenario an interesting candidate for fusion experiments. Similar to the WCM in the I-mode regime, the QCM is localized at the plasma edge. This was recently confirmed¹⁴⁴ in AUG with the CECE diagnostics, where the radial position of maximum mode amplitude was found to be correlated with the position of maximum T_e gradient. Strong fluctuation levels of $\delta T_e/T_e \approx 7\%$ were found, although care has to be taken with these absolute values due to the relatively low optical depth at these positions.¹⁴⁵ The combination of the CECE diagnostics and the profile ECE system allowed tracing the origin of the QCM back to the core regions of the plasma.

A modification of the CECE diagnostics in DIII-D enabled the first measurement of electron temperature fluctuations on the high magnetic field side via fundamental O-mode emission.⁹⁴ Investigating fluctuations on both low- and high-field sides allowed studies of poloidal asymmetries in turbulence. Fluctuation levels of $\delta T_e/T_e \approx 0.9 \dots 1.7\%$ were found, where the large span was due to the relatively low optical depth of $\tau_e^0 \approx 2.7$, resulting in a noticeable influence of plasma density fluctuations on the optical depth and thus on the measurement of the temperature fluctuation.

In a recent study in DIII-D, the temporal resolution of the ECE system allowed the investigation of the broadening of an ECRH microwave beam due to turbulent plasma density fluctuations at the edge. A deposition profile broadened by up to 150% was found to be correlated with the fluctuation level of edge density turbulence by

conducting microwave heat pulse propagation experiments¹⁴⁶ where transport analysis of the electron temperature response to the ECRH power modulation yields the deposition profile. The experimentally deduced broadening was found to be in good agreement with full-wave simulations.¹⁴⁷ A novel approach to determine the deposition profile of NBI has been developed¹⁴⁸ using coherently averaged ECE data based on different time scales of the respective terms in the equations for the local power and particle balance.

Recently, negative triangularity plasmas have raised much interest due to their improved confinement properties without ELM activities, making it a promising candidate for a reactor configuration.¹⁴⁹ The triangularity δ refers to the shape of the poloidal cross section, more precisely of the last closed flux surface (LCFS). The CECE diagnostics was one of the diagnostics involved, showing DIII-D is able to sustain a negative triangularity plasma at reactor-relevant parameters.¹⁵⁰ The tokamak TCV offers great flexibility in the configuration of the background magnetic field, making it an ideal candidate to investigate the influence of triangularity on plasma turbulence. With the CECE diagnostics, it was found that negative triangularity leads to an increasingly narrower turbulence frequency range⁹¹ and that the fluctuation level decreases when going from $+\delta$ to $-\delta$ plasmas,^{91,151} as shown in Fig. 5.

In a study combining the ECE diagnostics with an interferometer, Langmuir probe arrays in the vicinity of the divertor, and an infrared camera looking at the divertor, the heat flux onto the divertor was studied in dependence of the edge turbulence.¹⁵² Both particle and heat flux were found to increase with an increase in amplitude of coherent modes in the pedestal, driven by plasma pressure gradients. Correlating the CECE diagnostics with a reflectometer in AUG allowed to deduce the cross-phase between density and temperature fluctuations aiming for a better understanding of the nature of the underlying instabilities¹⁵³ (a technique that has been used before in different experiments^{154–156}).

The turbulent electron heat transport, determined by fluctuations of n_e and T_e and their respective phase,¹⁵⁵ is of particular interest as the majority of the heating power in a fusion device goes directly to the

electrons and only indirectly to the ions via collisions. With the CECE diagnostics on EAST, a degradation of energy confinement time was shown¹⁵⁷ to be correlated with an increase in $\delta T_e/T_e$.

Fast-ion populations in the core of fusion plasmas are known to drive *toroidal Alfvén eigenmodes* (TAEs), resulting in an overall performance reduction and imposing a threat to the first wall by fast-ion transport losses.¹⁵⁸ In a recent study¹⁵⁹ in KSTAR, TAE was studied, with their footprint in the T_e spectra being used to spatially localize them. ECCD was shown to mitigate the TAE, thus increasing fast-ion confinement. The mode structure of TAE was reconstructed from ECE measurements in TCV,¹⁶⁰ yielding good agreement with computations, putting the conclusions drawn from these computations on solid ground.

In contrast to tokamaks, stellarators have a more complicated, 3D structure of the background magnetic field: in large helical device (LHD), the ECE diagnostics is installed at the horizontal port, where the magnetic field features a maximum in the plasma center, which requires having two antenna systems to obtain a full profile, one located at the inboard side and one at the outboard side. The diagnostics played an important role in studying the dynamics of an internal transport barrier (ITB),⁷² the formation of magnetic islands,^{161,162} and the collapse of magnetohydrodynamics (MHD) modes.¹⁶³ Two new radiometers have been developed recently at LHD,¹⁰³ tailored for investigating plasmas with lower background magnetic fields.

A novel approach for the absolute calibration of ECE diagnostics based on the hot/cold method has been employed on W7-X.¹⁶⁴ A forward model was developed evaluating not just the reference temperatures of the calibration sources but also taking into account intermediate effective temperatures caused by the finite width of the microwave beam and thus providing a measurement for the beam width. A Bayesian analysis for this model was implemented within the Minerva framework, which is used at several fusion experiments across the world.^{165,166} This approach allows a much faster calibration, which might become mandatory for the envisaged long-pulse operation of W7-X, where noticeable drifts in the ECE signals are expected, requiring regular calibrations.¹¹⁰ In a recent work, the responses of the individual components in the transmission line have been treated separately in the calibration process, allowing for enhanced the understanding of the overall signal quality and thus also proposing potential improvements.¹⁶⁷

The ECE diagnostics in W7-X played a crucial role in heat pulse experiments, where ∇T_e and the spatiotemporal evolution of T_e is used to estimate the electron heat flux by solving a heat transport equation.¹⁶⁸ It was found that the observed electron heat transport is larger than the neoclassical transport, thereby confirming one of the design criteria of W7-X, exhibiting reduced neoclassical transport.

Temporal and spatial measurements of T_e performed with the ECE diagnostics played furthermore a crucial role in recent studies in W7-X, where periodic crashes of the central electron temperature (similar to sawtooth crashes in tokamaks) were observed in current drive experiments.¹⁶⁹ In a very recent set of experiments, ELM-like events were observed after the build-up of a pedestal in the T_e profile.¹⁷⁰ For the high-density operation planned in W7-X, X2 radiation would be in cutoff, and the possibility of using X3 instead is currently explored.¹⁷¹

2. Future fusion devices

COMPASS Upgrade is a tokamak with a major and minor radius of $R = 0.894$ m and $a = 0.27$ m, respectively, and a magnetic field

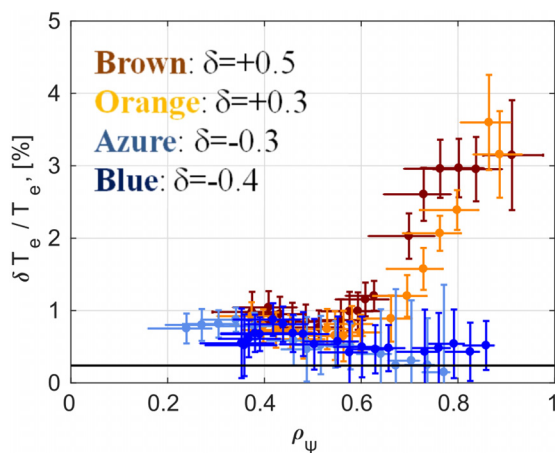


FIG. 5. Relative electron temperature fluctuation amplitude as a function of the radial coordinate for varying triangularity δ as obtained from the CECE diagnostics in TCV. Adapted with permission from Fontana *et al.*, *Rev. Sci. Instrum.* **88**, 083506 (2017). Copyright 2017 AIP Publishing LLC.⁹¹

strength of $B_{\text{tor}} \leq 5$ T. It is currently under construction in Prague, addressing among other topics, advanced confinement scenarios and power exhaust. An ECE system will be available from the beginning of the operation.¹⁷² In addition to the perpendicular view to obtain T_e and $\delta T_e/T_e$ profiles, an additional oblique view, 12° from perpendicular view, is planned to be used for non-thermal electron investigations. Two radiometers with 40 channels each have been designed for X2-mode operation, one for full magnetic field operation covering $f = 215\text{--}306$ GHz and the other for low magnetic field operation covering $f = 105\text{--}160$ GHz.

Another tokamak currently under construction is Divertor Tokamak Test facility (DTT), which is a major radius of $R = 2.2$ m larger than COMPASS Upgrade. It is located in Frascati (near Rome) and dedicated to divertor studies. Two ECE systems are planned to be implemented:¹⁷³ one system in O1-mode is capable of measuring a full radial profile with a frequency range of $f = 130\text{--}250$ GHz. The second system is in X2-mode configuration, able to perform measurements from the low-field side up to the center, and is sensitive to radiation with a frequency of $f = 260\text{--}380$ GHz. The transmission line is currently planned to primarily consist of waveguides.

The ECE diagnostics for the ITER tokamak, currently under construction in Cadarache (France), has two primary purposes: deliver radial T_e profiles from the plasma core together with the Thomson scattering system¹⁷⁴ and provide information on fluctuations δT_e which are associated with NTMs^{175,176} in order to stabilize them with localized microwave heating and subsequent current drive.^{177–179} In addition, the diagnostics is foreseen¹¹⁵ for contributing to measurements of the edge T_e profile, of fluctuations δT_e related to Alfvénic activities, of the stored energy in the plasma, of the power being radiated in the frequency range to which the ECE radiometer is sensitive, of runaway electrons, and of the existence of the H-mode and accompanying ELMs. Two lines of sight will be available: a radial and an oblique view, which both yield T_e profiles in the absence of non-thermal electron components. Non-thermal distortions in the bulk electron distribution would spoil the oblique view. The combination of the two views, however, allows to reconstruct a two-temperature bulk distribution.¹⁸⁰

Essential for a reliable operation of the full diagnostic system, which is foreseen to operate for up to 30 years over the lifetime of ITER, is the construction and intensive testing of prototypes of the various components. Status updates of the ECE system, including the status of the prototype testings, are regularly published,^{115,181–183} making it easy for the community to follow the progress and also allowing to review certain aspects where necessary. The diagnostic setup includes four transmission lines: a polarization splitter divides the two lines of sight into four beams, selecting O- and X-mode for each line of sight. The transmission lines have a length of 43 m each, connecting the front end at the ITER vacuum vessel with the ECE diagnostic room. Circular waveguides with smooth inner walls will be used, as they have been found^{115,184} to yield the lowest transmission losses over the full frequency operational range of $70\text{--}1000$ GHz. Microwaves over such a wide frequency range suffer from a few resonant absorption lines in the atmosphere, mostly due to water vapor.¹⁸⁵ As using evacuated waveguides for the transmission line would add a significant risk of failure to the whole system (due to the large number of potential vacuum leakages), it was decided to use compressed air/dry N_2 purged transmission lines instead.¹⁸⁶ A hot calibration source will be used,

which is capable of operation at different temperatures. In the traditional hot-cold calibration, as previously described, a microwave absorber cooled with liquid nitrogen to 77 K is used as a cold source. However, the use of cryogenic fluids is typically not permitted for in-vessel calibrations in fusion devices.¹⁸⁷ Using a hot source instead simplifies the calibration setup. Moreover, performing the calibration over a broader temperature range and incorporating multiple calibration points, yields a more reliable calibration. The harsh environment in ITER together with the requirement of long-term reliability makes the development of a hot source a non-trivial challenge,¹⁸⁸ with the outcome of favoring an emitter made of SiC after promising tests of a prototype.¹⁸⁹

Although the JT-60SA tokamak is already operational,¹⁹⁰ it remains at an early stage of its commissioning and is therefore included in this section on future fusion devices. A vertical ECE diagnostics is considered to be installed in JT-60SA, aiming to investigate high-energy, non-thermal electrons.¹⁹¹ The general idea is that high-energy electrons lead to a downshift of the frequency due to the relativistic mass increase, see Eq. (8). By collecting the ECE radiation along a vertical line of sight with $|\mathbf{B}| = \text{const.}$, harmonic overlap is avoided, and emissions from small populations of high-energy electrons accumulate and are thus easier to observe.^{192,193}

B. 2D electron cyclotron emission imaging diagnostics

The fundamental enhancement of the electron cyclotron emission imaging (ECEI) diagnostics, compared to conventional ECE, is due to the usage of large-aperture optics, which focuses a vertically extended region onto an array of detectors (an imaging array). As indicated in Fig. 6, this allows to obtain a 2D image in a poloidal cross section to investigate the spatial and temporal behavior of small-scale structures in the T_e profile. The development of this diagnostics is generally considered a breakthrough,^{46,49,195} which enabled a series of investigations not possible otherwise:

- The study of NTM suppression in great detail on TEXTOR using 2D T_e profiles to track the dynamical behavior of magnetic islands and the effect of localized microwave heating on them in comparison with theoretical models.¹⁹⁶
- Significant enhancement of a model for sawtooth oscillations and crashes by obtaining 2D images of δT_e in the core of TEXTOR.¹⁹⁷
- The 2D visualization of the full lifetime cycle of ELMs in KSTAR.¹⁹⁸
- Push forward the understanding of Alfvén instabilities with detailed measurements of the 2D poloidal structure of Alfvén eigenmodes in AUG¹⁹⁹ and DIII-D.^{200,201}
- Study of the interplay of ELMs and plasma turbulence by analyzing their spatial structure and temporal behavior in KSTAR.²⁰²
- Detailed observation of fishbone instabilities driven by energetic electrons in HL-2A.²⁰³

This list is, of course, not complete, and we would like to refer the interested reader to previous review papers on ECEI diagnostics.^{46,48,195,204}

The concept of the ECEI diagnostics has been developed and operated for the first time at the TEXT-U tokamak,^{205,206} followed by the tokamaks RTP^{207,208} and TEXTOR.^{209,210} Figure 6 shows as an example the implementation of an ECEI diagnostics in AUG. The

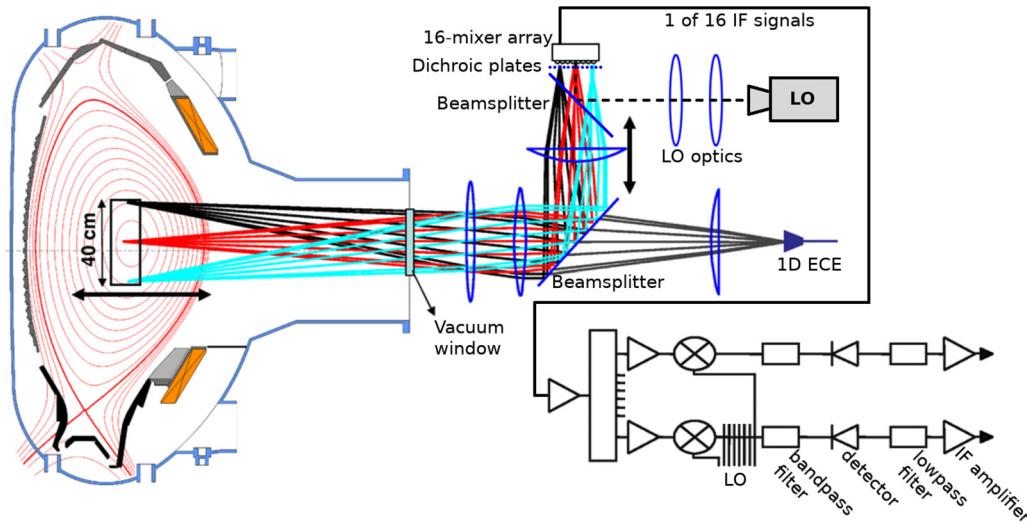


FIG. 6. Overview of the ECE and ECEI diagnostics installed on AUG. As can be seen, the systems share two lenses (made of HDPE) and are separated by a beam splitter. A movable lens in the ECEI system allows to radially shift the diagnosed plane. The LO is fed into the beam path via another beam splitter, dichroic plates are used as a high-pass filter before the signal is mixed the first time to the IF range. Each of the 16 (vertically separated in the plasma) channels is then split up into 8 channels, each of which is further down-converted and then bandpass-filtered with slightly different central frequencies, providing the radial resolution in the plasma. Adapted with permission from Classen *et al.*, *Rev. Sci. Instrum.* **81**, 10D929 (2010). Copyright 2010 AIP Publishing LLC.¹⁹⁴

imaging optics, located just outside of the vacuum, can be clearly identified, followed by the first local oscillator (LO) to mix the signal down to the IF range. After the power divider (to achieve spatial resolution), a second LO and mixer arrangement is used. An overview of ECEI systems on current MCF devices is given in Table II. In the following, a brief overview of some important recent ECEI experiments and the respective findings will be given, followed by a discussion of the technical advances.

ELM crashes are usually preceded by so-called inter-ELM modes observed over a broad spectral range.²¹⁹ ECEI observations in AUG, including a forward model to account for the effect of edge density fluctuations on the comparably low optical depth at the plasma edge, allowed to characterize these inter-ELM modes in great detail:²²⁰ a low-frequency mode with a frequency on the order of 10 kHz, correlated with high-frequency magnetic fluctuations on the order of 200 kHz, was identified in the upper part of the steep gradient with a toroidal mode number of 13–14. In a recent study,²²¹ the frequency was found to decrease with increasing toroidal rotation velocity

(modified by NBI). The CECE diagnostics were used for localizing the structures, while ECEI delivered the poloidal velocity and the mode structure. Figure 7 shows as an example time-resolved 2D snapshots of the plasma edge region in AUG obtained from the ECEI diagnostics. The coherent, mode-like structure of the electron temperature fluctuations can clearly be seen, propagating in an upward direction with a velocity corresponding approximately to the $E \times B$ velocity, inferred from measurements of the radial electric field.²²¹

The so-called *quiescent H-mode*²²² is a promising candidate for future large-scale fusion devices as it features no ELMs. Enhanced transport, as found in DIII-D via CECE measurements,²²³ due to edge harmonic oscillations²²⁴ or QCMs²²⁵ allows for sustaining a stable pedestal. ECEI diagnostics aiming at improving the physics understanding of these MHD modes were recently conducted on DIII-D,²²⁶ requiring forward modeling of the ECE radiation due to the plasma at the edge, which is not necessarily optically thick. It was demonstrated how MHD fluctuations at the pedestal cause fluctuations of the radiation temperature in the pedestal and scrape-off layer (SOL). The

TABLE II. ECEI diagnostics installed in fusion experiments currently in operation.

Device	Frequency in GHz	Mode	Number of channels (vertical × horizontal)	References
AUG	90...140	X2	16 × 8 + 20 × 8	194 and 211
DIII-D	75...140	X2	2 × (20 × 8)	212
EAST	90...140	X2	24 × 16	213
HL-2A	60...135	X2	24 × 8	214
J-TEXT	90...140	X2	2 × (16 × 8)	215
LHD	50...57	X2	8 × 8	216
	35...42	X2	8 × 8	217
KSTAR	80...140	X2/O1	2 × (24 × 8)	218

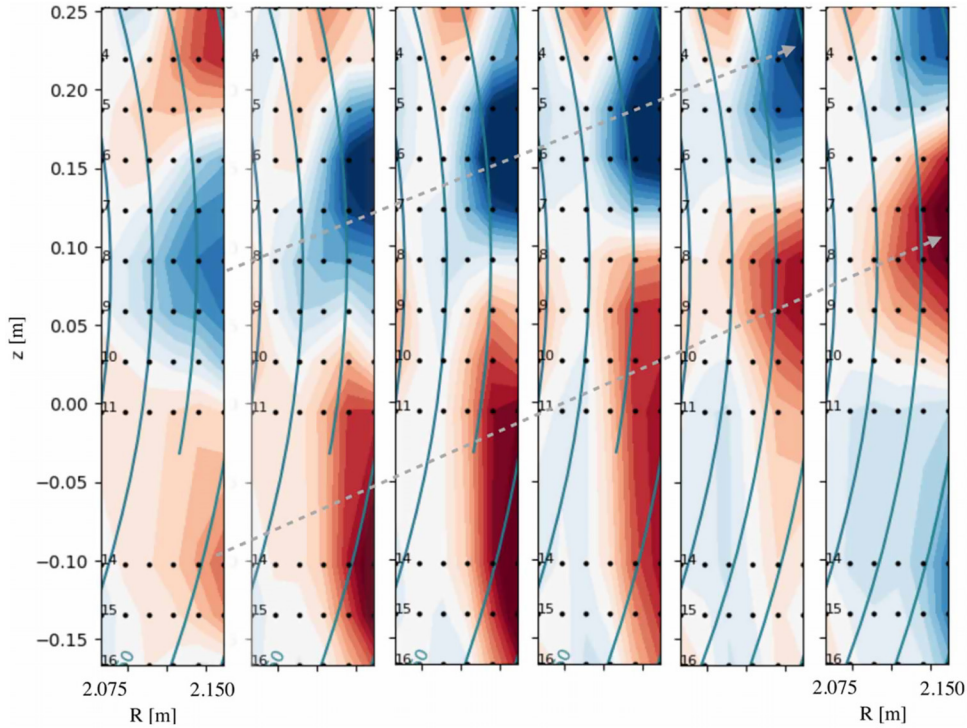


FIG. 7. Successive snapshots in time, covering a time span of $50 \mu\text{s}$, of the radiative temperature fluctuation level, with red indicating positive and blue negative values, respectively, in a poloidal cross section in AUG as obtained from the ECEI diagnostics. The solid curved lines indicate flux surfaces, and the dots indicate the position of the measurements. The gray arrows are included as a visual guide to follow the evolution of minimum and maximum values over time. Adapted with permission from Vanovac *et al.*, Plasma Phys. Controlled Fusion **65**, 095011 (2023). Copyright 2023 IOP Publishing.²²¹

radiation in the SOL was found to be very sensitive to radial displacements of the separatrix caused by MHD activities and thus provides a measure of this displacement, which is important to accurately predict the wetted area in the divertor (i.e., the area onto which the plasma flows).

Disruptions describe the sudden, uncontrolled, and catastrophic loss of plasma control resulting in large amounts of power and destructive forces on the structural components surrounding the plasma.²²⁷ A deep convolutional neural network has been applied to predict disruptions in DIII-D using data from the ECEI diagnostics only. Based on a dataset of 2747 shots, the neural network achieved an accuracy slightly above 90% in predicting whether a shot will disrupt or not,²²⁸ demonstrating that the ECEI diagnostics alone is a useful tool for disruption prediction.

Significant noise suppression of ECEI data was achieved in DIII-D by using short time intervals of 1 ms and average spatially localized ensembles.²²⁹ Only channels on the same flux surface exhibit high coherence, yielding frequency and radial structures of MHD modes. Using this technique, TAE can be clearly seen in the ECEI data, see Fig. 8.

In recent studies in DIII-D, finite- n interchange modes were observed with the ECEI diagnostics in the edge of negative triangularity plasmas.²³⁰ Combined with simulations, a low- n pressure-driven resistive ballooning mode at the plasma edge was concluded to be responsible for the absence of an H-mode during negative triangularity plasmas.

In a so-called *hybrid scenario* the plasma current is driven by a combination of inductive and non-inductive current.²³¹ It features a different q -profile, with q being the safety factor, than the standard H-mode. This prevents sawtooth activities in the core and also

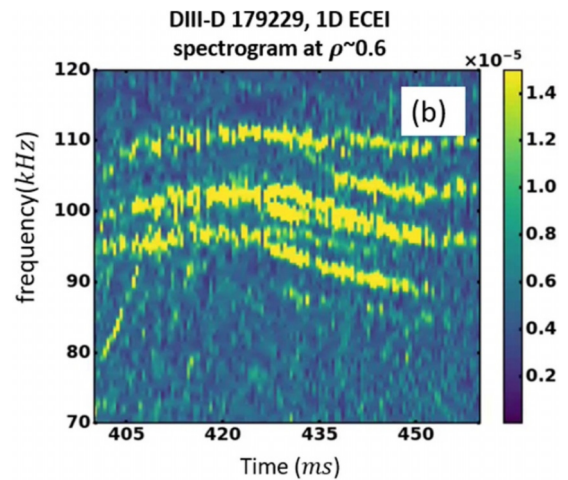


FIG. 8. Spectrogram of the radiative temperature fluctuation obtained from the ECEI diagnostics on DIII-D using a dedicated noise suppression analysis yielding clear Alfvén eigenmodes. Reproduced with permission from Yu *et al.*, Plasma Phys. Controlled Fusion **63**, 055001 (2021). Copyright 2021 IOP Publishing.²²⁹

prevents triggering large NTMs, resulting in a relatively large normalized plasma beta of $\beta_N \approx 3$. The improved stability makes this scenario attractive for fusion experiments, and it has therefore been implemented at various fusion devices. In a recent study in KSTAR,²³² a coherent edge-localized mode was identified in this scenario as being related to the presence of a broader and heightened pedestal and a reduced pressure gradient. This mode was observed between ELM crashes and leads to a somewhat increased particle and heat transport likely related to the aforementioned edge properties and thus to the good confinement.

Using two toroidally separated ECEI diagnostics allows to study variation and correlations along the toroidal direction. Such a 3D imaging diagnostics has been implemented on KSTAR,²¹⁸ which allowed to track and visualize the evolution of MHD instabilities in 3D, as shown in Fig. 9.

ELMs, a “side effect of the H-mode,”²³³ can be mitigated and suppressed using RMPs, as described in Sec. III A. The interplay of stochastic magnetic fields and plasma turbulence is an active area of research, where KSTAR has recently performed an interesting set of experiments,²³⁴ applying a statistical method known as *complexity-entropy analysis*. It is a useful method to characterize the state of plasma turbulence and quantify the predictability of time series. Using the ECEI diagnostics to observe fluctuations at the plasma edge, it was found that the ELM suppression phase due to RMP reduces the chaotic nature of the observed turbulence, thus indicating a fundamental change in the dynamics.

The existing ECEI systems installed at KSTAR are currently upgraded to realize higher data acquisition rates allowing the investigation of ion cyclotron waves and harmonics.²³⁵ After successful numerical design and optimization studies, the upgraded system is scheduled to be in operation for the next experimental campaign.

C. Technological advances of ECE

One of the most important technological developments in recent years is probably the *system-on-chip* (SoC) technology from the University of California Davis:^{236,237} instead of a quasi-optical Schottky diode mixer with planar antenna arrays in microstrip technology, a double-balanced down-converting mixer, a $\times 4$ multiplier, and a preceding low-noise amplifier (LNA) have all been integrated into a single receiver chip, as illustrated in Fig. 10. A strong improvement in sensitivity of at least a factor of 20 is achieved²³⁶ (mostly due to the preceding LNA). Furthermore, manufacturing large quantities of the chips is possible, reducing the overall costs. In the design usually followed, see e.g., Fig. 6, the LO signal is fed into the beam path via quasi-optical coupling structures. The new approach uses an internal $\times 8$ multiplier chain which reduces the LO frequency to below 12 GHz, thereby replacing the large-aperture optics with coaxial connectors and allowing for a much more compact design, see Fig. 10. After a first successful proof-of-principle setup,⁷⁸ this concept has been installed and used on the ECEI diagnostics at DIII-D.²³⁶ As a next step, chips based on the wide-bandgap semiconductor GaN are currently explored^{238,239} due to their promising resilience against the harsh conditions in burning fusion plasmas.²⁴⁰

The ECEI radiometer in KSTAR has been recently updated²⁴¹ by a modular antenna/detector array, as shown in Fig. 11. The modular character of the array allows single channels to be easily replaced in the case of a failure, instead of replacing the whole array. In addition, the upgraded antenna/detector modules provide an increased gain of 10–20 dB compared to the previously used conventional antenna/detector array.

Modern ECRH systems often make use not only of high-power but also of multi-frequency gyrotrons.⁶⁶ For the ECE diagnostics, this means the necessity of notch filters to effectively suppress more than

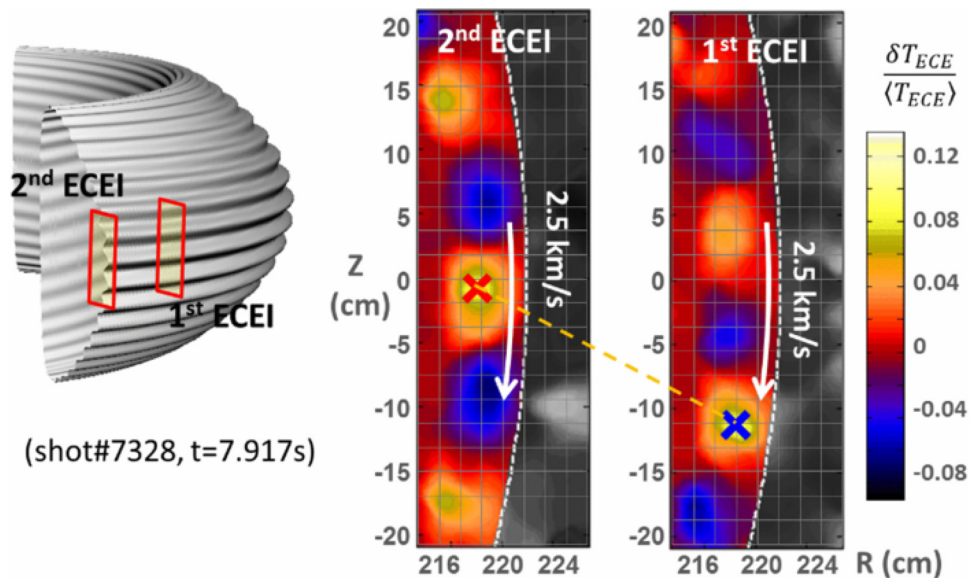


FIG. 9. Quasi 3D image of an ELM obtained from two toroidally separated ECEI diagnostics in KSTAR. The color scale represents normalized fluctuation amplitude of the emission temperature, with a value of 1 corresponding to 100%. Adapted with permission from Yun *et al.*, Rev. Sci. Instrum. **85**, 11D820 (2014). Copyright 2014 AIP Publishing LLC.²¹⁸

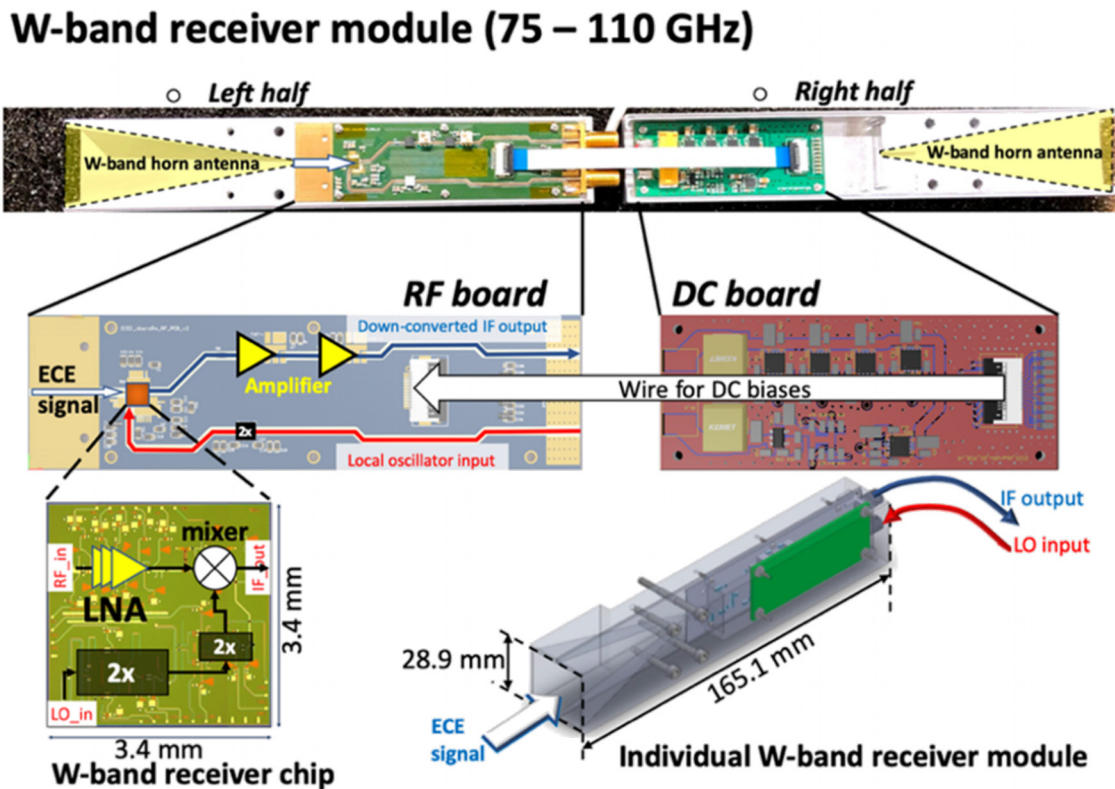


FIG. 10. Single receiver module for the ECEI diagnostics in DIII-D, sensitive to $f = 75\text{--}110$ GHz, based on the SOC technology. The module, shown at the top, consists of an RF board and DC board inside of a shielding housing. The pyramidal horn antenna receives the ECE radiation, which is fed via a waveguide-to-microstrip transition directly to a broadband LNA, see the chip at the bottom of the figure, then to a down-converting mixer, followed by two IF amplifiers. The LO is provided via an external coaxial connector, as indicated at the bottom right. Adapted with permission from Zhu *et al.*, *Rev. Sci. Instrum.* **91**, 093504 (2020). Copyright 2020 AIP Publishing LLC.²³⁶

one frequency. This has been realized at AUG and W7-X by so-called *Bragg reflectors*, which are based on circular oversized waveguides with a corrugation whose periodic structure satisfies the Bragg condition.¹²⁵ These components have the disadvantage of being expensive to manufacture due to their complex structure. A simpler and more compact approach has been recently proposed and successfully tested:⁷⁰ coupled waveguide resonators with varying rectangular cross sections were shown to suppress the typical gyrotron frequencies of 105 and 140 GHz by approximately 90 dB. Figure 12 shows simulations for these filters performed with the mode matching method, illustrating the strong suppression of the aforementioned frequencies. In contrast to notch filters realized as coupled cavities, this method also suppresses higher-order modes²⁴² being potentially excited due to the usage of oversized waveguides in the transmission line.

A somewhat similar approach is investigated at DIII-D: a waveguide with resonant cavities of cylindrical shape has been numerically designed²⁴³ and shown to suppress the resonant frequency, here 140 GHz, by 90 dB.

When designing new optics systems, it is important to properly evaluate the overall performance of the new system before actually building it. To this end, using synthetic diagnostics is mandatory, including not only the wave path through the optics but also the actual plasma response.²⁴⁴ Only then it is possible to elaborate the design

properly. As an example, Fig. 13 shows the complete set of imaging optics guiding the emission from the plasma to the antenna array for a newly designed ECEI diagnostics in HL-2M included in simulations using a diffractive optical simulation module.²⁴⁵ Also, for existing ECE diagnostics, the development of a synthetic ECE can be helpful in the interpretation of the acquired data.⁶³

Tunable yttrium iron garnet (YIG) filters have been added to a number of recently updated radiometers.^{91,129,246} Traditional radiometers employ bandpass filters with fixed frequencies in the IF section, thereby binding a frequency channel to a certain radial position. As the center frequency of a YIG bandpass filter can be tuned, adjustments of the corresponding radial position can be easily performed.²⁴⁷ Since each of these filters can be adjusted individually, a great degree of flexibility is gained. Note that such adjustments can even be performed during a discharge, thus allowing an ECE channel to keep its view onto a certain flux surface instead of a fixed radial position, which might enable further insights into plasma dynamics.²⁴⁷

Increasing the duration of plasma discharges in modern devices does not only constitute a challenge for plasma-facing components but also for data acquisition and handling. The amount of acquired data per year from the ECEI diagnostics alone has, for example, been estimated to be on the order of several hundred terabytes for KSTAR

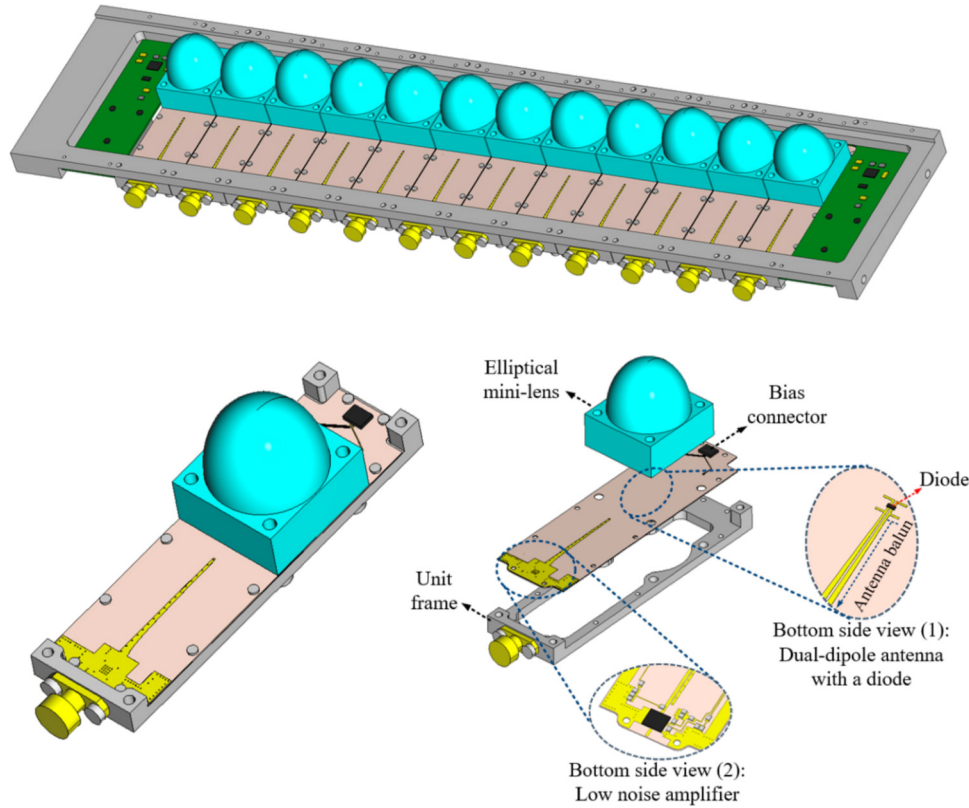


FIG. 11. Modular antenna/detector proposed for KSTAR at the top, single-unit antenna/detector module at the bottom, consisting of an elliptical lens, a dual-dipole antenna with a Schottky diode, where the signal from the plasma is mixed with an LO signal fed into the optical path via a beam splitter, an antenna balun, a low-noise amplifier, and a frame. Adapted with permission from Lee *et al.*, *Appl. Sci.* **12**, 2431 (2022). Copyright 2022 Authors, licensed under a Creative Commons Attribution 4.0 License.²⁴¹

when going to long-pulse discharges.²⁴⁸ A new procedure for filtering and cleaning the acquired ECEI data prior to storing it has been developed at EAST.²⁴⁹ Machine learning techniques are applied to identify saturated, weak, and zero signals in the raw data to ease the data

analysis and also save computational resources. A similar approach is pursued at the J-TEXT tokamak.²⁵⁰

Another machine learning approach is used at EAST to support data analysis:²⁵¹ pattern recognition is used to identify spatiotemporal structures of δT_e in a 2D plane obtained with the ECEI diagnostics. A method based on spectral clustering was shown to achieve successful recognition of sawtooth patterns with a success rate between 90% and 97%.

IV. ELECTRON BERNSTEIN WAVE EMISSION

If the electron plasma frequency exceeds the electron cyclotron frequency, a plasma is referred to as *over-dense*.^{252–255} Microwave heating at the electron cyclotron resonance layer is then no longer possible. This can be overcome by heating at harmonics of the electron cyclotron frequency but requires high electron temperatures to be efficient⁶⁰ and is generally not performed for harmonic numbers larger than three^{256–259} due to the increasingly strong dependence of the absorption on the electron temperature. The electron *Bernstein wave (EBW)*²⁶⁰ provides an alternative as it propagates in plasma densities exceeding the corresponding cutoff density of a given wave frequency. It is an electrostatic wave that is very well absorbed (and emitted) at the electron cyclotron resonance and its harmonics. The optical depth for EBWs significantly exceeds that of the O- and X-mode. While conventional tokamaks are usually not operated in over-dense regimes,

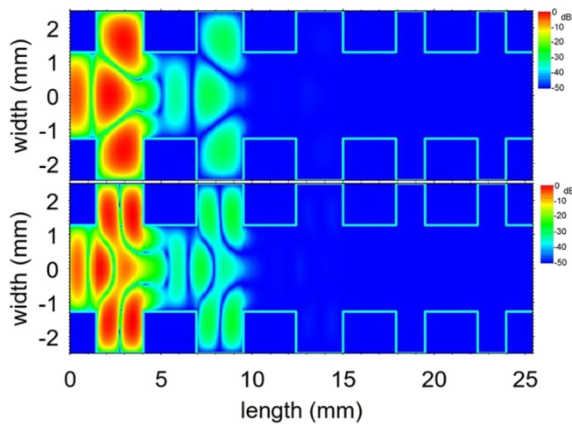


FIG. 12. Normalized intensity distribution along a 105/140 GHz notch filter based on coupled waveguide resonators for 105 GHz (top) and 140 GHz (bottom). Reprinted with permission from Wagner *et al.*, *IEEE Trans. Microwave Theory Tech.* **71**, 2558–2566 (2023). Copyright 2023 IEEE.⁷⁰

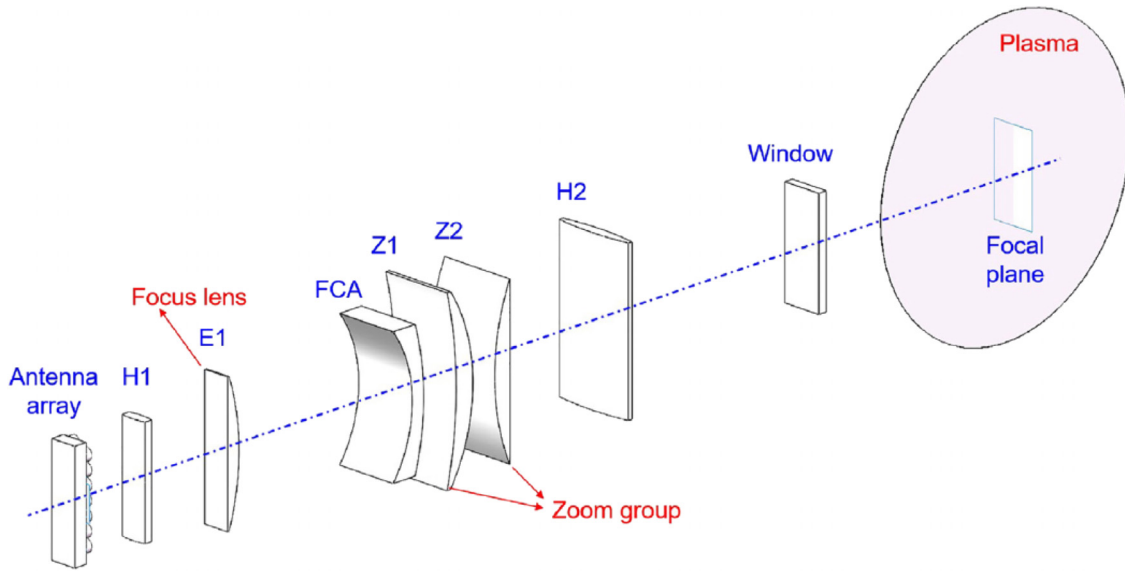


FIG. 13. Arrangement of the imaging optics of the newly designed ECEI diagnostics considered for HL-2M. The complete set of imaging optics is included in simulations, resulting in a synthetic ECEI diagnostics. Adapted with permission from Jiang *et al.*, Fusion Eng. Des. 191, 113570 (2023). Copyright 2023 Elsevier.²⁴⁵

other MCF configurations like stellarators, spherical tokamaks, or reversed field pinches can very well be operated in such regimes.

Because of their electrostatic nature, EBWs must be coupled to electromagnetic waves at the plasma boundary via mode conversion processes. Describing the mode coupling processes from a heating perspective, two processes are possible: the first and more common is the O–X–B conversion.²⁶¹ As illustrated in Fig. 14, an O-mode is injected at an optimum angle with respect to the background magnetic field into the plasma. In the vicinity of the plasma frequency layer, O- and X-mode degenerate, their polarization coincides, and the O-mode couples to the X-mode, which continues to propagate slightly further into regions of higher plasma density until it is reflected at the so-called turning point.²⁶² The X-mode propagates outwards, and upon approaching the upper-hybrid resonance layer, it becomes increasingly electrostatic until it can couple to the backwards propagating EBW. The optimum injection angle of the O-mode depends on the normalized plasma density gradient length $k_0 L_n = k_0 n / |\nabla n|$, with k_0 the

vacuum wavenumber of the microwave, and on the normalized background magnetic field $Y = \omega_{ce} / \omega_0$. The overall coupling efficiency is dominated by the O–X coupling, which is best²⁶³ approximated by²⁶⁴

$$\eta_{OX} = \exp \left\{ -\pi k_0 L_n \sqrt{Y/2} [2(1+Y)(N_z - N_{z,opt})^2 + N_y^2] \right\}, \quad (12)$$

where N_z and N_y are the refractive index components in the z (along \mathbf{B}_0) and y (perpendicular to \mathbf{B}_0 and ∇n) directions, respectively, and $N_{z,opt}$ refers to the optimum injection angle given by

$$N_{z,opt}^2 = \frac{Y}{1+Y}. \quad (13)$$

Collisional damping²⁶⁵ in the vicinity of the upper-hybrid resonance or non-linear effects²⁶⁶ can reduce the X–B coupling efficiency, which is otherwise usually assumed to be perfect.

For very steep density profiles with values of $k_0 L_n < 5$, the X-mode can tunnel through the evanescent layer defined by upper-hybrid resonance and right-hand cutoff layer and leave the plasma. This reduces the overall conversion efficiency, and another coupling process becomes more suitable, the so-called *direct X–B coupling*: an X-mode is injected perpendicularly onto the right-hand cutoff layer, where it can tunnel through the evanescent layer as just described. In the triplet of left-hand cutoff, upper-hybrid resonance, and right-hand cutoff, EBWs can then be excited.²⁶⁷

Both processes are reciprocal, i.e., EBWs being generated by coherent electron motion inside of the plasma can couple to electromagnetic waves at the plasma boundary and thus carry information about the electron temperature to a receiving antenna and a subsequent radiometer, which can be identical to those used in ECE systems. Such a diagnostics is referred to as *electron Bernstein wave emission (EBE) diagnostics*. Localized T_e measurements can be performed even in cold plasmas, due to the large optical depth of EBWs. Additional ray tracing calculations are, however, required to determine the exact

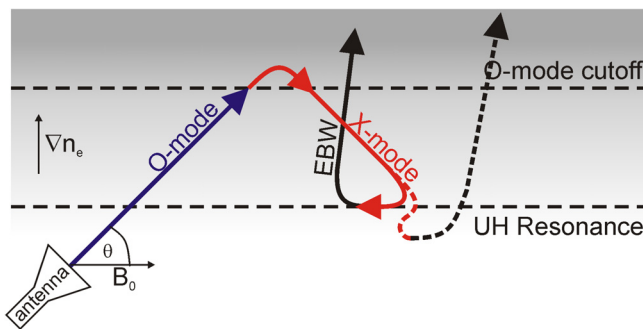


FIG. 14. Illustration of the O–X–B mode conversion process for fundamental heating (solid line) and second harmonic heating (short-dashed line).

location where the emission originated from due to the dependence of the EBW's wavenumber on local background magnetic field and electron plasma density.

EBE diagnostics have been successfully operated at the stellarators W7-AS,²⁶⁸ TJ-II,²⁶⁹ WEGA,²⁷⁰ and Heliotron J,²⁷¹ at the spherical tokamaks MAST,²⁵⁵ NSTX,²⁶⁵ CDX-U,²⁷² and TST-2,²⁷³ at the tokamaks COMPASS²⁷⁴ and TCV,²⁷⁵ and at the reversed field pinch MST²⁷⁶ among others.

Modern or future tokamaks designed for actual fusion experiments will not be operated in over-dense regimes. Stellarators can be operated at higher densities, but with large magnetic field strengths of several Tesla, EBE is not attractive as a core diagnostics: with increasing magnetic field strength, and thus increasing electron cyclotron frequency, the parameter $k_0 L_n$ becomes very large, reaching values of $k_0 L_n > 100$, which reduces the width of the angular window for efficient O-X coupling to values below 1 degree.²⁷⁷

Spherical tokamaks are operated at lower magnetic field strengths and therefore have lower electron cyclotron frequencies, resulting typically in values of $k_0 L_n \leq 20$ which are more suitable for efficient coupling. At MAST-U, for example, a high-power EBW heating system is presently under construction.²⁷⁸ A novel approach for an EBE imaging diagnostics had been developed and implemented at the MAST tokamak:^{279,280} the concept of interferometric imaging, well known in radio astronomy,²⁸¹ was adopted to an EBE radiometer with the advantage of no longer requiring large optical components like mirrors and lenses to focus the radiation onto the antenna plane. Instead, the phase and amplitude of the signal are recorded at each antenna, allowing to "sweep" the imaging microwave beam by adjusting the phase at each antenna by subsequent data processing. This diagnostics, referred to as Synthetic Aperture Microwave Imaging (SAMI), operates in the 10...40 GHz frequency range, using eight antipodal Vivaldi antennas²⁷⁹ (see Fig. 15). SAMI corresponds to a phased-array antenna,

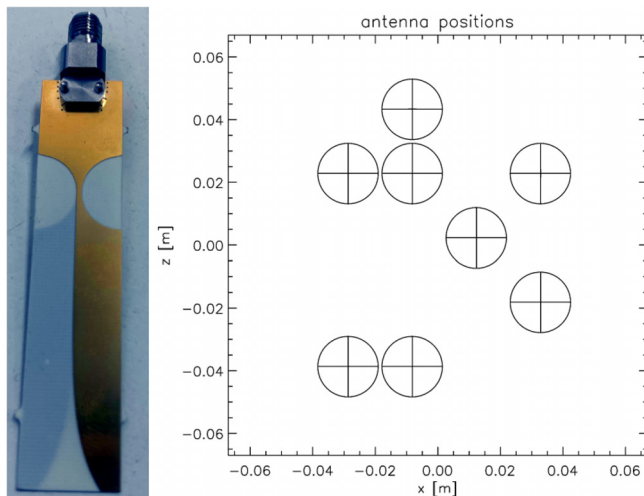


FIG. 15. (Left) Photo of an antipodal Vivaldi antenna realized in microstrip technology as used in the SAMI diagnostics, overall length is 66 mm. (Right) Arrangement of eight such antennas in the diagnostics, as derived from an optimization algorithm. Adapted with permission from S. Freethy, "Synthetic aperture imaging of B-X-O mode conversion," Ph.D. thesis (University of York, 2012). Copyright 2012 Author, licensed under a Creative Commons Attribution-NonCommercial-NoDerivs 2.5 International License.²⁸²

where careful spatial arrangement of the individual antennas is important,²⁸² illustrated in Fig. 15, as the image is reconstructed from cross correlating the antennas and multiple measurements of the same sample in Fourier space should be avoided. On the other hand, grating lobes, which occur when antenna spacing is larger than half the wavelength, should be minimized. An optimization algorithm is used to find the best antenna positions as a compromise between the aforementioned criteria. The digitizer of the radiometer was realized by a customized FPGA.²⁸³ A similar approach is pursued at the spherical tokamak QUEST, where an array antenna without lenses is designed to collect EBE and, via a subsequent data analysis obtain the direction from which the radiation originates.²⁸⁴

Figure 16 shows the mode conversion efficiency obtained from the SAMI diagnostics on MAST compared with analytical estimations. Excellent qualitative agreement is found while the two mode conversion windows do not agree quantitatively well with each other. The inclination between the two conversion windows corresponds to the inclination of the magnetic field line at the mode conversion layer and allows thus, in principle, to estimate the current density in the pedestal,²⁷⁹ an important parameter to better understand the physics in the pedestal. A diagnostics like SAMI might therefore not only be useful in devices with lower magnetic fields but could also play an important role in diagnosing the divertor region of conventional tokamaks and stellarators.

V. REFLECTOMETRY

Reflectometry is based on the principle of radar,²⁸⁶ where an electromagnetic wave of relatively low power is launched toward an object and its reflected part is then detected by a receiving antenna. Reflectometry has been first applied to the ionosphere in the 1930s²⁸⁷ to measure its height distribution, a technique also referred to as *ionosonde*, and proposed to be used in the laboratory in 1961.²⁸⁸ More than two decades later, in 1985, the first plasma density profile was successfully measured by means of reflectometry in the Tokamak de Fontenay-aux-Roses (TFR),²⁸⁹ only to be quickly used thereafter as a standard diagnostics in magnetic confinement experiments (see, e.g., Refs. 290 and 291, and the references listed therein). In-depth discussions on the basics of reflectometry can be found, e.g., in Ref. 291, whereas here we will restrict ourselves to the general concepts and focus more on the diagnosed plasma physics.

If an electromagnetic wave is launched into a plasma, it can propagate as long as the corresponding refractive index, see Eq. (1), is larger than zero, $N > 0$. For $N = 0$, the wave encounters a cutoff and is reflected, as illustrated in Fig. 17. The position of this cutoff layer depends only on electron density in the case of the O-mode and on electron density and background magnetic field (via the electron cyclotron frequency ω_{ce}) in the case of the X-mode, see Eq. (2). While propagating through the plasma, the wave experiences a phase shift ϕ depending on the local index of refraction. After being reflected at the cutoff layer and reaching the receiving antenna, the wave will thus have accumulated a total phase shift ϕ which reads²⁹⁰

$$\phi = 2 \frac{\omega}{c_0} \int_{r_{\text{cutoff}}}^{r_{\text{edge}}} N(r) dr - \frac{\pi}{2}, \quad (14)$$

with r_{cutoff} and r_{edge} the radial positions of the cutoff layer and plasma edge, respectively (and assuming $r_{\text{cutoff}} > r_{\text{edge}}$), the additional phase of $\pi/2$ due to reflection at the cutoff layer, and the factor 2 due to

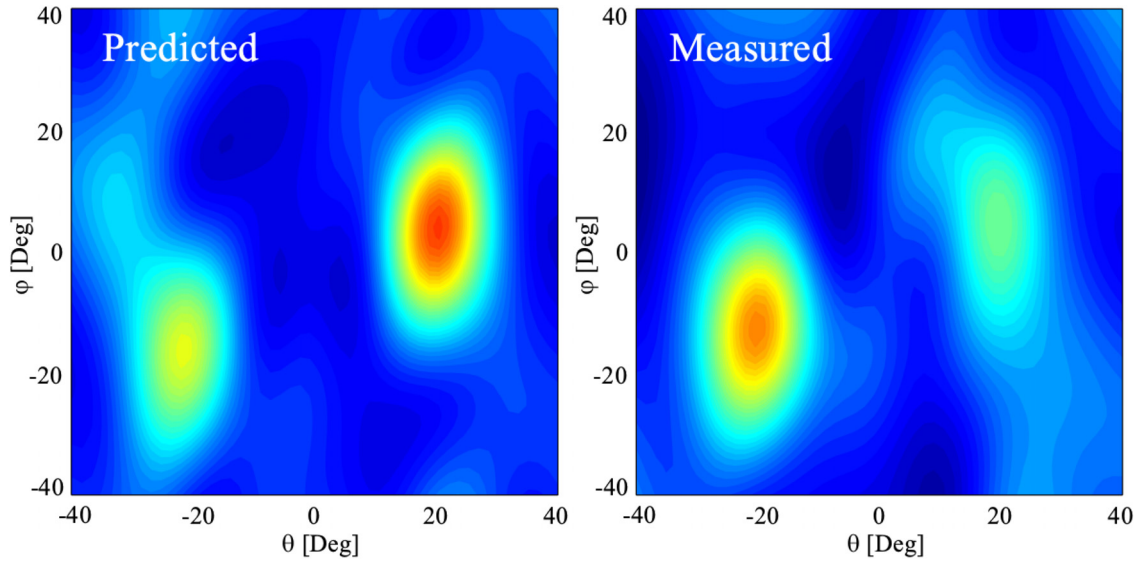


FIG. 16. O–X–B mode conversion efficiency as a function of poloidal and toroidal injection angle as obtained from (left) analytical estimations using Eq. (12) and (right) from measurements with the SAMI diagnostics at MAST. Reproduced with permission from Freethy *et al.*, Plasma Phys. Controlled Fusion 55, 124010 (2013). Copyright 2013 IOP Publishing.²⁸⁵

propagating forth and back. Equation (14) is valid under the conditions of geometric optics, i.e., assuming that the refractive index variation is small within one wavelength.⁵⁰

Figure 17 illustrates the basic principles of a reflectometer with two antennas, one for transmitting and one for receiving the microwave, referred to as a *bistatic* configuration (in contrast to *monostatic* configurations, where a single antenna is used for both transmitting and receiving the signal). The illustrated setup features homodyne detection, in which the mixer inputs are at the same frequency. As a result, after low-pass filtering, the output contains information on both, amplitude and phase. While the phase, being caused by the plasma, is the main quantity of interest (after removing contributions

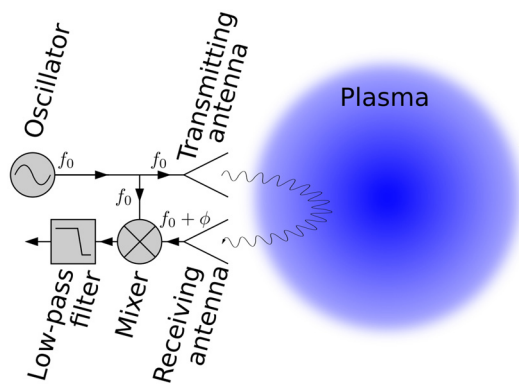


FIG. 17. Schematic diagram of a typical homodyne and bistatic reflectometry system. Note that the sine wave serves just as an illustration to distinguish transmitting and receiving antennas and is not intended to indicate the actual physical path of the wave.

from the microwave circuit and from waveguide dispersion via calibration measurements), amplitude fluctuations are also present in the extracted signal. In a heterodyne detector,⁷¹ the frequency inputs at the mixer would be slightly different, either by two oscillators kept at a small, constant frequency difference [often by a *phase-locked loop (PLL)*²⁹² or one oscillator and a frequency-shifting component. The signal at the mixer output, the IF, retains spectral information within a chosen band centered at the frequency difference between the two inputs and also preserves the phase relation (heterodyne detectors are also referred to as *coherent detectors*.¹¹). A heterodyne detector works around a predefined center frequency, which facilitates the signal conditioning (filtering and amplification) and can later go through an I/Q demodulator tuned for the predefined center frequency.⁷¹ The I/Q demodulation allows for isolated measurement of the phase and amplitude, which allows for a more precise interpretation of each quantity unaffected by the other.

The phase shift ϕ in Eq. (14) can be measured directly (instantaneous phase) and put into the equation, but it often has a relatively high noise level as it takes into account all frequency components. Alternatively, a spectrogram of the signal can be calculated, and only the contribution from the reflection at the plasma cutoff can be extracted (the maximum of the spectrogram is a good starting point). This technique allows stacking spectrograms from multiple sweeps to significantly reduce the contribution of spurious reflections and emphasize the plasma reflection.²⁹³ The beat frequency f_{beat} , resulting from the interference of the reflected signal with a reference signal, can be extracted from the spectrogram and translated into phase increments. This is achieved by first dividing by the frequency sweep rate $S_r = df/dt$, followed by integrating over the probing frequency:²⁹⁴ $d\phi/df = 2\pi \cdot f_{\text{beat}}/S_r$. The phase increments for each probing frequency increment allow to determine the position of the cutoff layer after applying inversion methods²⁹⁵ (analytically for the O-mode²⁸⁹

and numerically for the X-mode^{294,295}) and thus retrieve a radial electron plasma density profile, hence the expression *profile reflectometry*. To actually obtain these profiles, different measurement techniques exist, which will be briefly described in the following. For typical ITER parameters, relativistic effects should be taken into account, changing the spatial position of the cutoff layers, as illustrated in Fig. 1. Neglecting these effects can lead to errors as high as 35 % for density profile reconstruction in ITER plasmas.²⁹⁶ In some cases, the downshift of the cutoff frequency can even lead to hollow profiles, thus limiting access to the plasma core.²⁹⁷

An emitted pulse with a central frequency ω_0 offers the opportunity to probe a large part of the electron plasma density profile at once due to its range of Fourier components, each being reflected at different locations of the profile, resulting in a range of time delays. This technique is referred to as *pulse radar reflectometry* and has been used, for example, at TEXTOR²⁹⁸ or LHD.²⁹⁹ It can be further separated into *short pulse reflectometry*³⁰⁰ and *ultrashort pulse reflectometry*.³⁰¹ In the first case, the pulses are not too short such that a single pulse covers only a limited radial region, whereas the latter employs ultrashort pulses spanning a larger radial area due to the wider spectrum, thereby requiring in principle only a single pulse for profile reconstruction at the plasma edge. A recent example for the implementation of a short pulse reflectometer is provided by TCV.³⁰² An ultrashort pulse reflectometer has recently been developed and successfully tested at EAST.³⁰³ A disadvantage of pulse radar reflectometry is that the pulse can be significantly broadened,³⁰⁴ as different frequency components experience different refractive indices. This can lead to errors in the measured propagation time and, consequently, in the inferred spatial position of the respective cutoff layer. In general, pulse radar reflectometry is not too common, which is also due to the required broadband microwave components and high-speed digitizers.

Applying *amplitude modulation (AM)* is another technique, used for example in the W7-AS stellarator,³⁰⁵ the Alcator C-Mod tokamak³⁰⁶ or in the TJ-II stellarator³⁰⁷ and the HL-2A tokamak.³⁰⁸ The amplitude of the probing wave is modulated with frequencies on the order of 100 MHz and instead of the phase delay, the group delay is measured in this case. More common³⁰⁹ are profile reflectometry systems based on *frequency modulation (FM)*, also commonly referred to as *frequency-modulated continuous-wave (FMCW)* reflectometry, where the launched frequency is swept on time scales below the lifetime of plasma density fluctuations. While sweeping times were some tens of microseconds in early implementations,³¹⁰ times as fast as 1 μ s have been demonstrated already a few years ago.³¹¹ FM profile reflectometry was applied on a variety of devices, e.g., on JET,³¹² COMPASS,³¹³ or Tore Supra³¹⁴ and is used on, e.g., EAST,^{315,316} HL-2A,³¹⁷ J-TEXT,³¹⁸ AUG,³¹⁹ KSTAR,³²⁰ and DIII-D,³²¹ to name just a few. It is furthermore under consideration for ITER,³²² MAST-U,³²³ COMPASS Upgrade,³²⁴ or the high-field tokamak SPARC.³²⁵ A detailed overview of different profile reflectometry systems can be found, e.g., in Refs. 10,290, and 326.

Instead of obtaining just a single radial profile of the electron plasma density, profile reflectometry is considered to be important in future fusion devices for monitoring the plasma position and shape via multiple viewing chords. This technique is referred to as *plasma position reflectometry (PPR)*. It has been successfully demonstrated for a single line of sight on AUG³²⁷ and COMPASS,³²⁸ and for multiple chords on the reversed field pinch device RFX-mod2.³²⁹ PPR

will be installed on DTT³³⁰ and is considered for the EU DEMO^{38,331} and CFETR.^{332,333}

Obtaining background electron plasma density profiles is only one application of reflectometry. The second application consists of extracting plasma dynamics like turbulent plasma density fluctuations or MHD modes. This is, in principle, possible with the techniques described so far, although only within some simplifying assumptions,³³⁴ as outlined in Sec. V A. More suitable methods are *correlation reflectometry* and *Doppler reflectometry (DR)*, which will both be discussed briefly in Secs. V A and V B. *Microwave imaging reflectometry (MIR)* is a third method, which will be described in more detail afterwards.

A. Correlation reflectometry

Profile reflectometry needs to ensure that the measurements are performed on time scales faster than the propagation speed of plasma density structures, approximately given by the electron diamagnetic drift velocity as a general upper limit,³³⁵ such that the diagnosed plasma density profile does not vary during the measurement. The presence of turbulent plasma density fluctuations leads otherwise to a broadening of the spectrum of the reflected wave due to the variation and movement of the reflective layer with a strong weighting of the fluctuations in the vicinity of the cutoff layer.⁴⁶ A technique aimed at determining the spatial size of the density variations is *correlation reflectometry*.^{336–338} If two (or more) waves with slightly different frequencies are used, such that the corresponding reflection points are slightly separated, see Fig. 18, the method is referred to as *radial correlation reflectometry (RCR)*. In *poloidal correlation reflectometry (PCR)*, only one wave is injected, but multiple receiving antennas, distributed poloidally, are used, as illustrated in Fig. 18. The spatial separation of the reflection points needs to be on spatial scales below the size of the coherent density structures. The cross correlation of the two signals allows them to estimate the structure sizes or the poloidal propagation speed of density fluctuations from which the radial electric field E_r can be derived, linked via the $E_r \times B$ drift.

Correlation reflectometry has been studied numerically,^{339,340} and used in the past at the ATF stellarator,³⁴¹ at TEXTOR,^{342,343} the T-10 tokamak,³⁴⁴ JT-60U,³⁴⁵ and JET.^{346,347} A list of current experiments equipped with correlation reflectometry diagnostics is given in Table III.

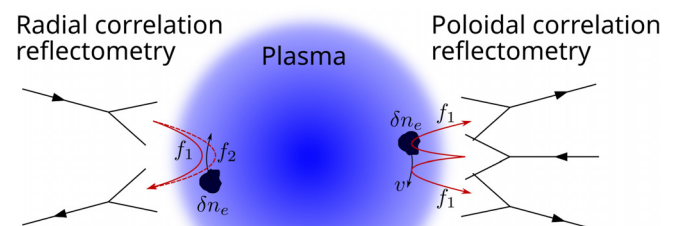


FIG. 18. Illustration of (left) radial correlation reflectometry where two (or more) probing frequencies are used corresponding to different radial positions of the reflective layer and (right) poloidal correlation reflectometry where the reflected microwave beam is collected at two (or more) poloidally separated positions.

TABLE III. Correlation reflectometry diagnostics currently in operation.

Device	Frequency in GHz	Mode	Channels		References
			Radial	pol. \times tor.	
AUG	24...37, 40...57	O	2	2×2	348
EAST	20.4...40	O	4	2×1	349
	40...60	O	4	2×1	350
	61.2...73.6	O	4	2×1	351
W7-X	79.2...96	X	4	2×1	352
	22...40, 40...60	O	1	2×2	353

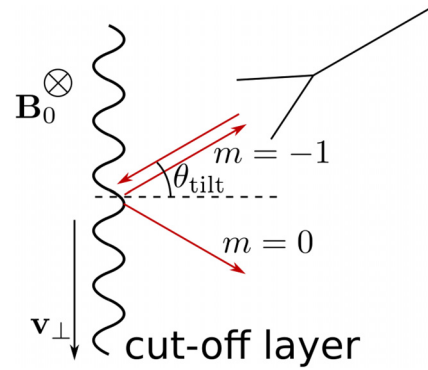
A set of experiments at TEXTOR enabled the first experimental investigations of long-range correlations of plasma density fluctuations along magnetic field lines with correlation reflectometry.³⁵⁴ This was done previously mostly with Langmuir probes, which are restricted in fusion experiments to a very small radial region at the plasma boundary.^{355,356}

On DIII-D, a correlation reflectometer allowed to compare the radial correlation length L_{\perp} of plasma density fluctuations in L-mode discharges with analytical predictions and values deduced from gyrokinetic simulations.³⁵⁷ An experimentally obtained value of $L_{\perp} \approx 5...10\rho_s$, where ρ_s is the ion Larmor radius evaluated using the electron temperature, showed good agreement with predictions and marked an important milestone in experiment–simulation comparisons.

In a series of experiments on W7-X, a PCR diagnostics³⁵³ was used to investigate the shear layer at the plasma edge by monitoring the poloidal velocity of density structures and thus determining the transition into the SOL by a change in sign of the rotation velocity.³⁵⁸ Very recently, using the same diagnostics, it was possible to detect a QCM on W7-X for the first time.³⁵⁹ It was observed in the plasma core, found to be of electrostatic nature, and its frequency and velocity were found to depend on the injected ECRH power.

The poloidal correlation reflectometer on AUG, consisting of four receiving antennas, was recently upgraded to inject two frequencies simultaneously, thus providing an additional radial channel.³⁴⁸ This allows to differentiate between perpendicular and radial correlation length, L_{\perp} and L_{rad} , of the turbulent electron plasma density fluctuations. Furthermore, the velocity v_{\perp} and the dissipation time τ_d can be obtained from the diagnostics. The importance of correctly accounting for the influence of the local fluctuation level by a weighting function was clearly shown, leading to an overestimation of the correlation length up to a factor of 4 otherwise.³⁴⁸

EAST is currently equipped with four separate PCR diagnostics, see Table III. This enables investigation of plasma dynamics from the edge to the core. In particular, the formation of an *internal transport barrier* (ITB) in EAST was studied with these diagnostics. The onset of an ITB in a plasma results in a reduction of heat transport, driven by small-scale turbulence, and thus an increase in temperature and density in the plasma core.³⁶⁰ The turbulent plasma density fluctuations in the core of EAST could be observed during the formation of an ITB with one of the PCR systems, where it was found that the turbulence inside of the ITB is not completely suppressed.³⁶¹ Interestingly, an increase could even be observed in a later stage, which was attributed to the occurrence of reversed shear Alfvén eigenmodes.


FIG. 19. Illustration of Doppler reflectometry.

B. Doppler reflectometry

In the reflectometry techniques described so far, a wave is injected normal to the flux surfaces, or rather along the density gradient to be more precise, and, interpreting the cutoff layer as a diffraction grating, its 0th order reflection is analyzed. These schemes are often referred to as *conventional reflectometry*. If, instead, the injection happens at an angle θ_{tilt} with respect to the normal of the reflecting layer, the -1 order of diffraction is scattered back to the antenna, as illustrated in Fig. 19, reducing the 0th order in the acquired signal. A poloidally moving perturbation at the reflecting layer then causes a Doppler shift in the frequency of the reflected signal,³⁶² hence the name *Doppler reflectometry* (DR) or *Doppler backscattering* (DBS).³⁶³ The Doppler shift is proportional to the velocity of the perturbation and thereby also to the radial electric field³⁶⁴ (assuming that the phase velocity of the perturbation is small compared to the plasma flow caused by the $E_r \times B$ drift³⁶⁵). The perturbations in the reflecting layer can be interpreted as a thin phase grating. Assuming the perturbation to be of sinusoidal shape with a wavelength of λ_{\perp} , for the injected wave to return to the antenna, i.e., for the -1 order of the diffraction pattern, the Bragg condition requires

$$k_{\perp} = 2k_0 \sin \theta_{\text{tilt}}, \quad (15)$$

with k_{\perp} the wavenumber of the perturbation and k_0 the wavenumber of the probing wave. Different injection angles θ_{tilt} allow thus to probe different fluctuation wavenumbers. For low turbulence levels, the power S of the backscattered microwave is furthermore proportional to the square of the density fluctuation amplitude, $S \propto |\delta n_e|$, and allows thus to also probe the fluctuation strength.^{366,367}

DR has been first used in 1999 at the W7-AS stellarator,³⁶⁸ followed by the Tore Supra tokamak.^{369,370} It is nowadays considered a standard diagnostics for studying the perpendicular velocity v_{\perp} of electron plasma density fluctuations,^{364,371,372} the spectrum of the perpendicular wavenumber of these fluctuations,³⁷³ their radial correlation length³⁷⁴ and fluctuation levels,³¹⁰ and the radial electric field E_r .³⁷⁵ It is thus installed on many MCF devices currently in operation, see Table IV (and was also installed in some devices no longer in operation, like JET³⁹⁷ and JT-60U,³⁴⁵ the spherical tokamak Globus-M³⁹⁸ or the C-2 field-reversed configuration³⁹⁹). In Sec. V B 1, we will elaborate further on a few of those devices, followed by a brief discussion on future implementation.

TABLE IV. Doppler reflectometry diagnostics currently in operation.

Device	Frequency in GHz	Mode	Injection angle	References
AUG	75...110	O/X	-14°...16°	376
DIII-D	55...75	O/X	-15°...20° (pol.) -10°...10° (tor.)	377
	55...75	O/X	0°...15°	378
	60...90	O/X	-18°...0° (pol.) -7°...0° (tor.)	379
EAST	60...90	X	-10°...20°	380
	55...75	X	5°...12°	381
	80.4...96.4	X	-4°...12°	382
Globus-M2	20...48	O	0°...15° (pol.)	383
			0°...8° (tor.)	
Heliotron J	26.5...40	O	Fixed	384
	33...50	X	Fixed	385
	26...40	O	Fixed	386
HL-2A	34...48	X	Fixed	387
	52.5...75	X	Fixed	387
HL-3	34...48	X	Fixed	388
JTEXT	50...75	X	Fixed	389
LHD	26...40	O/X	Fixed	390
	26...40	O/X	Fixed	391
MAST-U	32.5...50	O/X	0°...10.6°	392
	34...67.5	X	0°...12°	393
TCV	40...75	O/X	10°...58° (pol.)	394
			-180°...180° (tor.)	
TJ-II	33...50	X	±20°	371
TUMAN-3M	18...26	O	±10°	395
W7-X	50...75	O	Fixed	396

1. Doppler reflectometry in operating fusion devices

To obtain radially resolved measurements of turbulent plasma density structures with a DR diagnostics, a set of frequencies should ideally be injected simultaneously into the plasma (frequency hopping, where the probing frequency is scanned, is an alternative solution with the drawback of the long time needed to perform a full scan). In AUG, a novel method to create such a frequency comb has been implemented in a DR diagnostics, allowing to freely tune remotely both the center frequency and the difference between the frequencies by using a three-tone signal put into a frequency multiplier.³⁷⁶ In most existing DR diagnostics with a frequency comb, their center frequency and frequency difference are fixed.^{378,381,401-403} After successful testing in the laboratory, first data have been obtained, monitoring the transition from L- to H-mode, thus illustrating the reliability of the novel technique.

Sometimes, experimentally obtained spectra of the wavenumber of the density fluctuations are found to disagree with spectra from corresponding density turbulence simulations. At AUG, full-wave simulations of the DR diagnostics using realistic plasma density turbulence data generated by turbulence codes showed clearly how the spectrum obtained from the diagnostics was different from the underlying

spectrum of the density fluctuations, caused by a non-linear saturation at low-to-intermediate wavenumbers and a superlinear signal enhancement at larger wavenumbers.⁴⁰⁴ Such simulations are thus important to guide the interpretation of obtained spectra from DR diagnostics in certain scenarios.

The Doppler reflectometry diagnostics installed on W7-X showed a clear dependence of the velocity shear layer near the separatrix and of the radial electric field E_r in the SOL on the injected heating power and on plasma density.³⁹⁶ In a recent set of experiments, the diagnostics was used to perform systematic studies of ion-scale plasma density fluctuations in the core, providing evidence that microscale turbulence and not neoclassical losses is the main mechanism limiting the ion confinement in W7-X, thereby proving the optimization of W7-X a success.⁴⁰⁵ A scaling of the amplitude of the turbulence with the ratio of density to temperature gradient was also found (as expected for ion temperature gradient-driven instabilities), allowing the increase the global confinement time by reducing that ratio.⁴⁰⁶

In 2022, the first detailed comparisons on DIII-D between the DR diagnostics and the *charge-exchange recombination (CER)* diagnostics were performed⁴⁰⁷ to infer the toroidal angular velocity $\omega_{E \times B} = E_r / (RB_\theta)$. CER measures ions undergoing charge-exchange reactions with neutrals provided by a neutral beam injection system. Despite the different underlying physics, the two diagnostics showed good agreement at different strengths of torque applied by the neutral beam injection.

A preceding paper from DIII-D studied a predator-prey-like relationship between plasma density turbulence acting as a predator of profile gradients via turbulent transport, and then as prey to the $E \times B$ shear flow, deduced from DR measurements.⁴⁰⁸ Such a cycle can regulate transport and may thus contribute to the development of ELM-free plasma scenarios. In particular, the role of these predator-prey dynamics in sustaining a quiescent H-mode was a central focus of the studies.⁴⁰⁹

In a recent paper, a novel synthetic DR diagnostics applied to DIII-D was reported:⁴¹⁰ a beam-tracing code, called *Scotty*, to calculate the weighting function along the injected microwave beam, using a model for the turbulent plasma density fluctuation spectrum obtained from a quasi-linear code, was used to calculate the electron density fluctuation spectrum from the backscattered power spectrum measured with the DR diagnostics. *Scotty*⁴¹¹ has been developed to bridge the gap between fast but simplifying ray tracing calculations⁴¹² and more rigorous but computationally heavy full-wave simulations.⁴¹³

The same code was used to show the importance of toroidal wave vector matching: the reflected power was found to decrease exponentially with toroidal angular mismatch.⁴¹⁴ This makes measurements of large poloidal wavenumbers k_θ challenging. Using a toroidally steerable antenna of one of the DR diagnostics installed at DIII-D, it could be shown that high wavenumbers up to $k_\theta \leq 20 \text{ cm}^{-1}$ are accessible when trying to take care that the toroidal launch angle is perpendicular to the magnetic field line of interest.⁴¹⁵

A novel DR diagnostics has been installed in 2023 at DIII-D, operating from 60...90 GHz, see Table IV. It has the unique ability to investigate not only electron plasma density fluctuations up to a few MHz, but also in the Alfvénic range at 6.5 MHz, the ion cyclotron frequency range of around 20 MHz, and fluctuations around 476 MHz driven by externally injected helicon waves.³⁷⁹ This diagnostics will play an important role in studying helicon wave propagation, absorption, and net toroidal current drive.

A new DR diagnostics is planned to be installed by the end of 2024 on DIII-D,⁴¹⁶ aiming to investigate the pedestal and the SOL, regions that are important for transport studies and validation of transport models. The system will encompass a frequency range of 33...50 GHz, and it will be integrated into one of the existing DR systems by modifying the quasi-optical setup such that it can be used for both systems. A full-scale mockup has been successfully tested in the laboratory.⁴¹⁶

EAST is equipped with three DR diagnostics, see Table IV, all of them capable of measuring simultaneously at different radial positions by injecting multiple frequencies provided by a comb generator. Using two poloidally separated DR diagnostics, it was possible to observe a *geodesic acoustic mode (GAM)*⁴¹⁷ and its interaction with the background turbulence. A GAM is basically a transient branch of a zonal flow and thought to play an important role in the transition from low- to high-confinement mode.³⁶⁵

A new DR diagnostics has been recently installed on the MAST-U spherical tokamak.³⁹³ It operates over a rather large frequency range, see Table IV, encompassing the Q- and the V-band. While separate microwave sources are used for each band, they share the quasi-optical system, consisting of a focusing lens made of high-density polyethylene (HDPE) and a fixed and rotatable mirror. First experiments were performed, where the diagnostics has been successfully benchmarked against another, well-established DR diagnostics on MAST-U.³⁹² This DR, which had been previously installed in 2022, is special due to its capability of operating in both O- and X-mode by a large-scale polarizer, part of the quasi-optical transmission system, and a system of waveguide switches.³⁹² The system can also operate at different launching and receiving polarizations, allowing to perform so-called *cross polarization scattering* for probing magnetic field fluctuations.⁴¹⁸

Injecting pellets into the core of MCF devices is often accompanied by improved plasma performance.^{419–421} Recently, such an improvement has also been observed in the TJ-II stellarator.⁴²² The DR diagnostics showed a more negative radial electric field, together with a reduction of the plasma density fluctuation level, in regions of strong density gradient.

LHD is equipped with two DR diagnostics, see Table IV, being installed at different toroidal positions, which enables toroidal correlation studies. Both systems generate a series of frequencies via a comb generator to allow for radially resolved measurements. Only recently, a design for one of the systems has been developed using an arrangement of multiple mixers to reduce the intermediate frequency³⁹¹ and thus make data acquisition less challenging compared to the previous implementation.³⁹⁰

2. Doppler reflectometry in future fusion devices

Reflectometry in ITER will play an important role in measuring the plasma density profile during long-pulse discharges.⁴²³ Two lines of sight for a DR diagnostics are foreseen to be installed together with the profile reflectometry diagnostics. While the general design of the reflectometry diagnostics is set to a frequency range of 30...165 GHz, supporting both O- and X-mode, details for the DR system are still in an early stage of development.⁴²⁴

Although JT-60SA is already operational, it remains at an early stage of its commissioning and is therefore included in this section on future fusion devices. A feasibility study has been performed,⁴²⁵

showing that a DR diagnostics would play an important role in accomplishing the envisaged scientific program of JT-60SA.

C. Microwave imaging reflectometry

Assuming 1D plasma density fluctuations, where the cutoff layer moves forth and back in the frame of the wave results in variations of the phase of the reflected wave. Measuring these phase changes allows thus to deduce the plasma density fluctuations in the vicinity of the cutoff layer. Magnetically confined plasmas exhibit, however, plasma density fluctuations that are 2D in nature, leading to a corrugated cutoff layer that reflects an incoming wave into multiple directions and not only back to the antenna.^{46,334} The detection antenna will therefore see a complicated interference pattern, and the simple relation between phase and δn_e is no longer true. As Hutchinson states in his text book,³⁵ “*Fluctuation measurements in the plasma interior using reflectometry are relatively straightforward to perform but rather hard to interpret.*”

To overcome this problem, the concept of *microwave imaging reflectometry (MIR)* has been developed: as illustrated in Fig. 20, the reflective cutoff layer is illuminated by a beam, covering a poloidal area as large as possible. A beam splitter, built for example of Teflon, Mylar, or Plexiglas,⁴²⁶ is used to separate injected and reflected microwave beam. Using large-aperture optics, the rays reflected from the corrugated cutoff layer are collected simultaneously at an image plane by a series of antennas, allowing the reconstruction the spatial shape of the density structures. Care has to be taken that the wavefront curvature of the microwave beam matches the curvature of the cutoff layer. Additional radial resolution is achieved by using multiple frequencies simultaneously, as seen in Fig. 20. The principle of MIR has been confirmed first by numerical studies⁴²⁷ and shown experimentally in a proof-of-principle experiment on TEXTOR,⁴²⁸ following a systematic study in the laboratory (not at the tokamak) using a corrugated reflecting target to simulate a fluctuating reflection layer in the plasma.⁴²⁹

Since ECEI and MIR diagnostics can share the imaging optics, they can, in principle be installed in parallel. Due to being more challenging to operate, though, MIR diagnostics are only installed on a few devices,^{430,431} see Table V.

At DIII-D, a MIR diagnostics was successfully commissioned in 2014.⁴³² The optics transmission system was realized by a combination of large-aperture HDPE lenses and one beam-forming mirror, as well as a mini-lens array detector collecting the reflected signal. This design was chosen to reduce problems encountered on TEXTOR, where a set of tilted curved mirrors resulted in asymmetrical aberration in the beam and the planar antenna array with a large substrate lens in front introduced significant spherical aberration in the focal plane.^{432,439} Before installation at DIII-D, the full MIR diagnostics was thoroughly tested in the laboratory and compared with Gaussian beam propagation calculations, yielding excellent agreement.⁴³²

As illustrated in Fig. 21, the MIR diagnostics at DIII-D enabled studies of edge harmonic oscillation (EHO) in quiescent H-mode regimes,⁴⁴¹ where they are thought to play an important role in avoiding the necessity for ELMs due to providing a continuous, instead of intermittent and thus more violent, flux of particles and energy across the edge. In a combined study of experimental data and results from modeling, it was found that EHO can be destabilized by plasma rotation or rotational shear.⁴⁴² The importance of a synthetic diagnostics

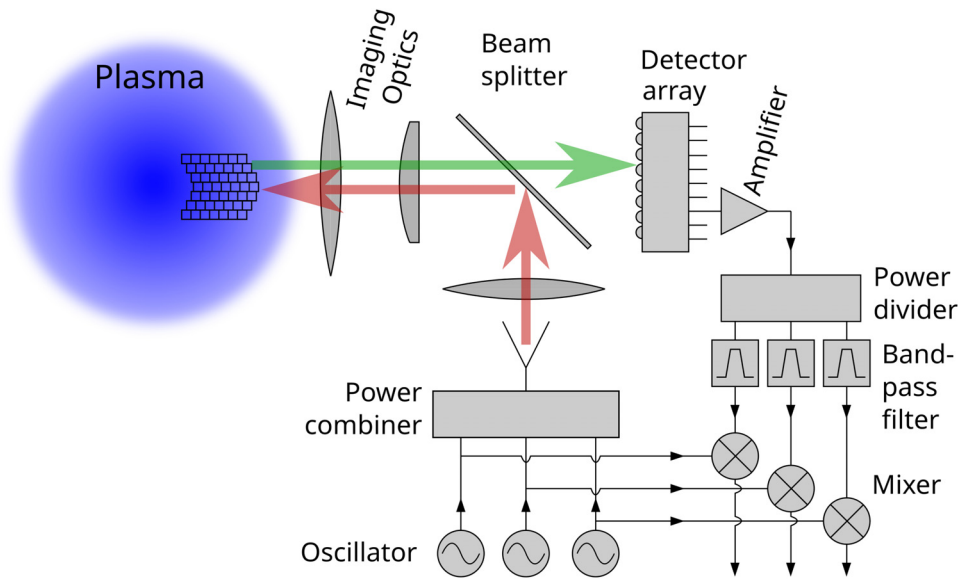


FIG. 20. Principle of a microwave imaging reflectometry diagnostics illustrated. Multiple lines of sight are imaged from the 2D sampling volume, indicated in the plasma by the grid, onto a 1D array of detectors. Note that the optical path is usually more complicated than illustrated here.

TABLE V. MIR diagnostics installed on various fusion experiments in operation, upper part of the table, and MIR diagnostics that have been operated in the past, bottom part of the table.

Device	Frequency in GHz	Mode	Channels		References
			Radial	pol. × tor.	
DIII-D	56...74	X	4	12 × 1	432
EAST	75...105	X	8	12 × 1	433 and 434
HL-2A	32...38	O/X	4	8 × 2	308
KSTAR	78...96	X	4	16 × 1	435
TST-2	23...32	O	2	6 × 6	436
LHD	60.41...64.61	X	4	7 × 7	437
	26...34	O	4	8 × 8	438
TEXTOR	88	X	1	16 × 1	428

to correctly interpret the experimental data was highlighted and is investigated in more detail in another study.⁴⁴⁰

The MIR diagnostics at KSTAR has received an upgrade in 2018, with the resulting parameters given in Table V. Among other things, the imaging optics have been upgraded to use mini-lenses in front of each individual antenna instead of a single, large substrate lens.⁴³⁵ The MIR diagnostics in KSTAR has been used intensively to study the occurrence of a QCM.⁴³⁵ In recent experiments, the complete life cycle of a QCM could be studied, as shown in Fig. 22. Starting from a coherent mode at around 40 kHz in the plasma core, excited by ECRH, a sudden transition into the QCM occurs at the same time when a sudden increase in plasma density is observed (not shown in the figure). With further increase in the plasma density, and thus also in collisionality, the QCM changes gradually into broadband turbulence, see

Fig. 22(b). The third transition, where the QCM is again present due to a decrease in plasma density, occurs suddenly when plasma current is ramping down and results in its complete disappearance.

The successful implementation of a combined ECEI and MIR diagnostics on EAST has been reported in 2023.⁴³⁴ The diagnostics share part of the imaging optics, specifically an HDPE lens (and the vacuum window), as can be seen in Fig. 23. A beam divider separates the beams of the two diagnostics, which do not overlap in frequency. Such a frequency-selective beam divider is realized via the *frequency-selective surface* method:⁴⁴⁵ thin periodic structures of 2D shape are printed onto a dielectric substrate, resulting either in transmission or reflection of the incoming wave, depending on if the incoming wave matches the resonant frequency of the structures.⁴⁴⁶ Preceding the installation on EAST, the diagnostics were intensively tested in the laboratory, including the usage of a rotating metal wheel with a sinusoidal corrugated surface to simulate a perturbed and poloidally moving cutoff layer⁴⁴⁷ and measurement of the wavefront curvature of emitting and receiving antenna, which needs to match the cutoff layer.⁴⁴⁸ In addition, a synthetic diagnostic suite has been developed to aid in the future interpretation and analysis of experimental data,⁴⁴⁹ with the MIR part based on a 2D full-wave model to propagate the microwave to the cutoff and back using the FDTD method.

As listed in Table V, the MIR system in HL-2A is a 64-channel diagnostics.³⁰⁸ It uses an adjustable antenna to match the wavefront of the diagnosing microwave as well as possible to the reflecting cutoff layer. This was realized by constructing the antenna as an array composed of 8 poloidal × 2 toroidal horn antennas, which can each individually be adjusted in vertical and horizontal direction.⁴²⁶

While, at the moment, there is no MIR diagnostics in operation on LHD, the focus is on the ECEI diagnostics; two systems have been operated in the past, see Table V. As these systems can, in principle, be reactivated, the diagnostics are included in our list of active experiments. Figure 24 illustrates the radiometer of the X-mode MIR

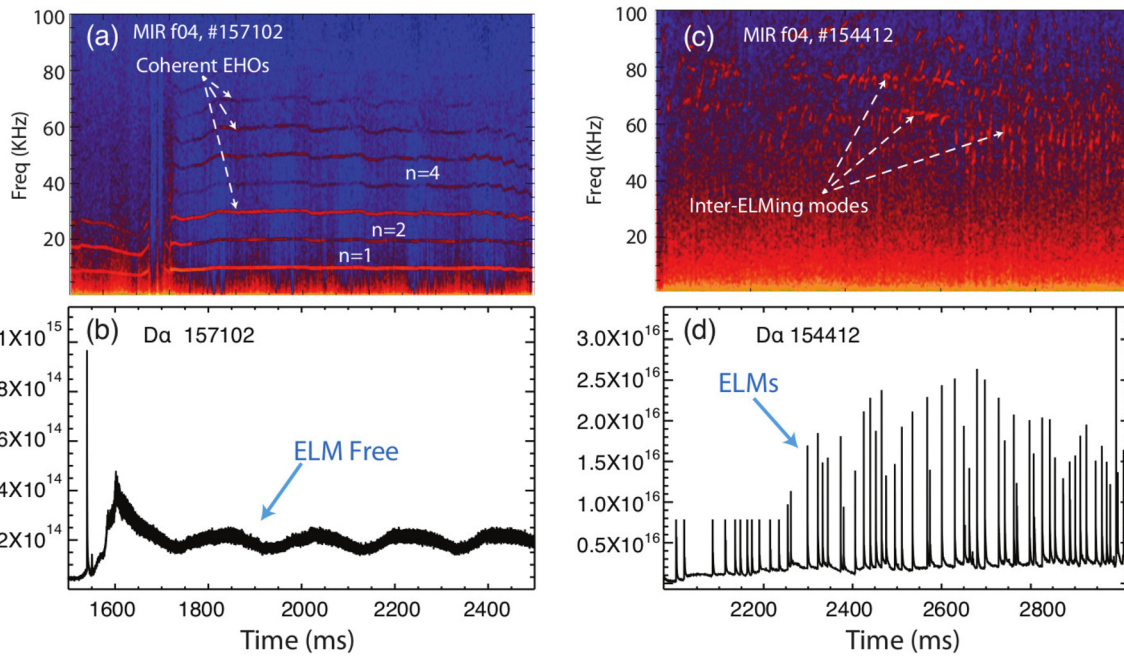


FIG. 21. Spectrograms acquired with the MIR diagnostics on DIII-D. The left column corresponds to a quiescent H-mode, while the right column corresponds to a conventional H-mode. The strong signal of the EHO during the quiescent H-mode can be clearly seen, while in the conventional H-mode, ELMs are frequently triggered. Adapted with permission from Ren *et al.*, *J. Instrum.* **10**, P10036 (2015). Copyright 2015 Authors, licensed under a Creative Commons Attribution 3.0 License.⁴⁴⁰

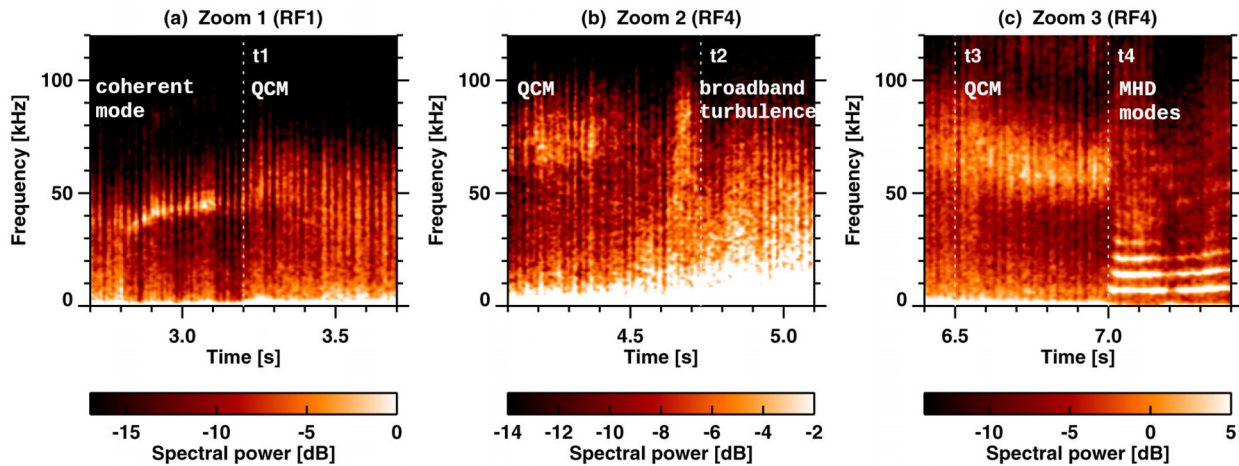


FIG. 22. Spectrograms acquired with the MIR diagnostics in KSTAR. Shown are three transitions of the QCM: (a) until $t_1 = 3.2$ s a coherent mode is dominant (exhibiting a narrow frequency band), followed by a sudden transition into a QCM (featuring a wider frequency band); (b) transition from a QCM into broadband turbulence at t_2 ; (c) suppression of the QCM at t_4 followed by the onset of an MHD mode and its harmonics. Adapted with permission from Lee *et al.*, *Nucl. Fusion* **61**, 016008 (2021). Copyright 2021 IAEA.⁴⁴³

diagnostics. The receiving antenna is realized as a stack of seven 7-channel horn antenna mixer arrays (a mixer is included on a thin printed circuit board (PCB) inside of each of the horns), resulting in a 2D imaging device. To investigate the performance of the optics setup, both the injected and reflected waves have been simulated using 2D FDTD simulations taking into account

all mirrors in the beam paths.⁴³⁷ As can be seen from Fig. 24, the mirrors act as intended, illuminating a specific position at the cutoff layer with the injected beam, and cover the antenna aperture of the receiving antenna. EHO was observed in LHD with this MIR diagnostics, appearing in medium-density plasmas but not in H-mode.

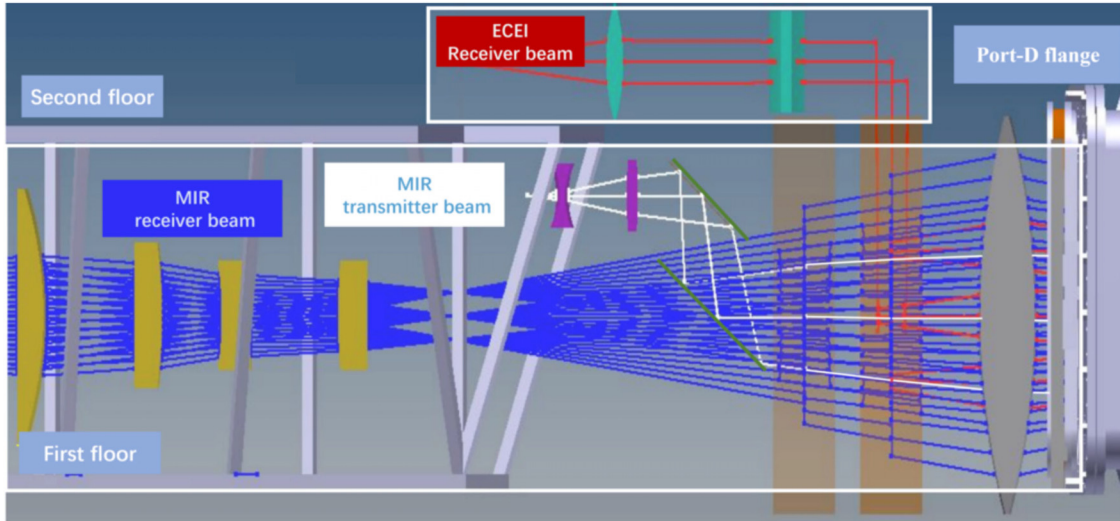


FIG. 23. The optics components of the MIR and ECEI diagnostics on EAST. It can be seen that both systems share the lens, made of HDPE, installed directly before the vacuum window (outside of the vacuum). Reproduced with permission from Zhang *et al.*, *J. Instrum.* **20**, T03008 (2025). Copyright 2025 IOP Publishing.⁴⁴⁴

A second MIR diagnostics at LHD had been subsequently operated. As listed in Table V, it was an O-mode system, which was used to diagnose electron plasma density fluctuations at the edge during H-mode operation.⁴³⁸ A major improvement was the implementation

of a horn antenna array: while in the previous version, the mixer included in the antenna array had to be irradiated with the LO signal, this is no longer necessary due to the inclusion of a quadrupler on the PCB.⁴⁵⁰ The quadrupler reduces the frequency of the LO by a factor of

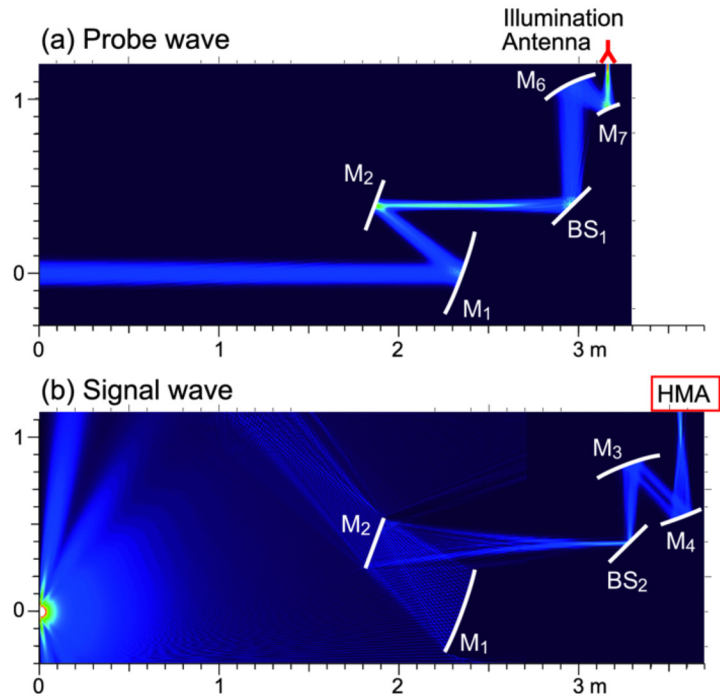
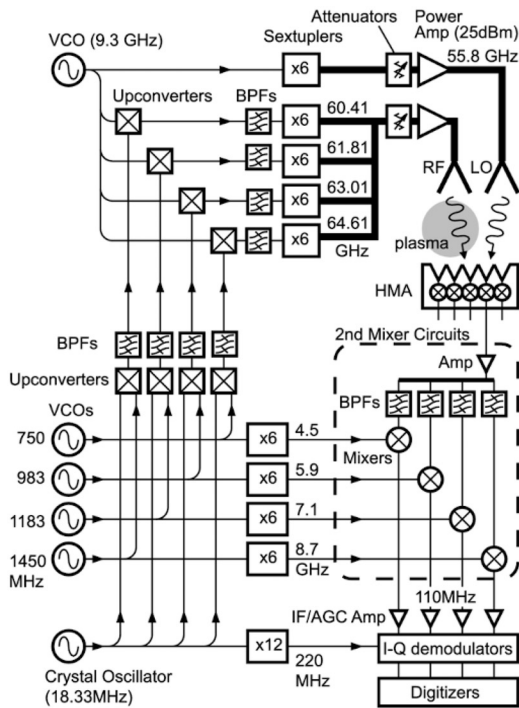


FIG. 24. (Left) Schematic of the radiometer setup for the (currently not operational) MIR diagnostics on LHD (HMA: horn-antenna mixer array). (Right) Full-wave simulations based on the FDTD method of (a) injected and (b) reflected waves with the plasma being located as a point source at position (0,0). Adapted with permission from Nagayama *et al.*, *Rev. Sci. Instrum.* **83**, 10E305 (2012). Copyright 2012 AIP Publishing LLC.⁴³⁷

26 March 2026 11:39:46

4, which can now directly be coupled by coaxial connectors without significant losses. This leads to a significant reduction of the overall size, as illumination optics to couple the LO into the mixers in the antenna array are no longer needed.⁴⁵¹

Some of the electronics from the O-mode MIR diagnostics in LHD, including the compact receiving antenna array, are reused in the recent MIR diagnostics in the TST-2 spherical tokamak.⁴³⁶ In a first series of experiments, it was possible to observe an internal reconnection event, which is somewhat similar to a disruption in a conventional tokamak but less severe since it only affects flux surfaces in a small, radially localized region.

D. Technological advances of reflectometry

Scanning the injection angle in DR corresponds to scanning the probed wavenumber of the turbulent plasma density fluctuations, see Eq. (15). Systems capable of scanning the injection angle achieve this usually by moving the plasma-facing mirror, as in the diagnostics listed in Table IV. An alternative method is provided by phased-array antennas. Not only does this remove the necessity of mechanically moving an in-vessel component, but it also allows for scanning the injection angle on much shorter time scales: oblique injection in this case is the result of a phase difference of neighboring channels from an array antenna. Such systems are well known from radar techniques used for weather or space observations.⁴⁵² Such an antenna prototype⁴⁵³ has been designed, manufactured, and successfully tested in W7-X,⁴⁵⁴ realized as a 32-element H-plane sector horn antenna array working in the frequency range of 75...110 GHz. A similar antenna has been designed for AUG.⁴⁵⁵ KSTAR has also recently designed and constructed a phased-array antenna prototype⁴⁵⁶ to be used as a DR diagnostics,⁴⁵⁷ scheduled to be installed in 2025. A promising approach to manufacturing such antenna arrays is 3D metal powder additive manufacturing, which has recently proved to be capable of producing prototype antennas.⁴⁵⁸ Metal additive manufacturing is a promising technological advancement for many microwave components, enabling quick and affordable manufacturing.

The SAMI diagnostics, discussed in Sec. IV, can not only be used as a passive antenna array but also as an active diagnostics. As such, it can also be used as a phased-array antenna for DR purposes, albeit via a different realization: an array of small Vivaldi antennas, built as printed circuit board devices, is used instead of the heavy antenna array discussed in the previous paragraph. Measurements in the spherical tokamaks MAST and NSTX-U have demonstrated the usefulness of this approach⁴⁵⁹ by successfully determining the pitch angle of the magnetic field line at the plasma boundary. An advanced version, SAMI-2, has been designed and constructed, featuring an array of dual-polarization sinuous antennas.⁴⁶⁰ SAMI-2 allows measuring a radial profile of the pitch angle and thus obtaining the edge current density profile. The diagnostics is now being commissioned at MAST-U.

MIR requires the phase front of the probing wave to match the cutoff layer, which is usually achieved by appropriate lenses. A lensless reconstruction employing a deep learning neural network based on convolutional neural networks was shown to work for scattering off simple geometrical objects.⁴⁶¹ Although a plasma density structure is more complicated in shape, the promising results from this proof-of-principle test justify a further investigation of this approach. The study also showed the importance of sufficient training data for the neural

network, which needs to be provided by proper simulations. To fully capture small-scale and large-amplitude effects, full-wave simulations are necessary instead. Such simulations are also important to develop synthetic diagnostics in order to assess the capabilities of already existing systems and guide the design of future systems.⁴⁶²

Like for the ECEI diagnostics, the most significant technological breakthrough for MIR and reflectometry in general is probably the SoC developments. In contrast to the passive ECEI system, reflectometry is an active diagnostics and requires therefore in addition a miniaturization of a transmitting module (and not only of the receiving module). This has been successfully reported⁴⁶³ for the V-band (55...75 GHz), with a transmitter being able to simultaneously emit eight tunable frequencies at an output power of approximately 1 mW (0 dBm). Using the wide-bandgap material GaN allows increasing the output power levels of up to 1 W while still maintaining a good SNR (note that the transmitting signal in an MIR diagnostics should not be too low due to the probing beam propagating through an optical system resulting in losses at each component⁴⁶). GaN has the further advantage of being able to operate in the harsher radiation environments.²³⁹ The SoC technology has the potential to greatly simplify and enhance the capability of reflectometry in general, and MIR systems in particular, as the technology is already enabling direct sampling in the GHz range⁴⁶⁴ and combining several functions into single components.

VI. SUMMARY, CONCLUSION, AND OUTLOOK

In the preceding pages, we gave a glimpse into the vast areas of plasma physics and fusion research that microwave-based diagnostics can contribute to. The 1D version of ECE and reflectometry has been crucial to enable physics understanding of various plasma dynamics processes. The next evolution of these diagnostics was the imaging diagnostic ECEI and MIR, which provide 2D images of plasma dynamics with high temporal and spatial resolution, thus significantly enhancing the understanding of particle and heat transport. Observations of confinement mode transitions, of amplitude and correlation lengths of electron temperature and electron density fluctuations, of MHD modes, and of plasma rotation and radial electric fields were all made possible with these diagnostics as described throughout the paper (note that this list is not exhaustive). While the first iterations of ECEI and MIR might have been bulky, their size could recently have been significantly reduced by the system-on-chip technology. This development not only reduces the size while maintaining a good signal-to-noise ratio, but it also reduces the power requirements, and all that at a lower cost. The latter fact eases maintenance, as entire diagnostic systems can be swapped in the case of a failure thereby increasing the uptime of a diagnostics and thus also of the fusion device. Furthermore, in the latest iteration, components are utilized that are resilient to the harsh environment of fusion reactors.

As outlined in the beginning of the paper, microwave diagnostics are one of the few diagnostics that can be operated in future fusion reactors. While their scope might shift from diagnosing plasma physics phenomena to controlling and monitoring purpose, their importance for safe operation is thereby increasing. Efficient use of the few available diagnostic ports in future devices⁴⁶⁵ requires diagnostics to share them, as for example, illustrated in Fig. 25 and also already realized in some experiments discussed above. Further integration with other diagnostics through multi-purpose ports will be necessary to make the best use of the limited available space. While this is relatively

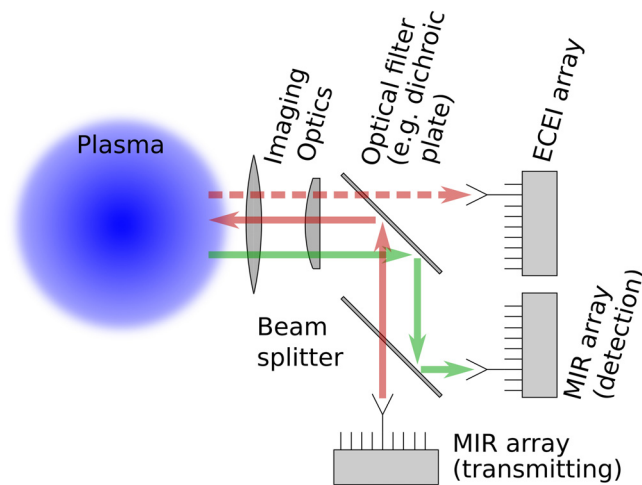


FIG. 25. Illustration of an ECEI and MIR diagnostics sharing part of the imaging optics, thereby making efficient usage of port space in fusion devices (which is generally limited). All components are simplified.

straightforward for microwave and optical diagnostics, it is more challenging when trying to combine microwave diagnostics with neutron diagnostics. Since the required optical components impose limitations on the overall size of the diagnostics, a potential next step to reduce their size involves using, for example, arrays of small lenses, as outlined in the ECEI section, or more compact implementations, where the lenses are directly integrated onto the circuit board.⁴⁶⁶ Alternatively, lenses could be eliminated altogether by reconstructing the signal from phase and amplitude using machine learning algorithms, an approach that is currently being explored. Neutrons, thermal and electromagnetic loads, long discharges, and structural challenges, all need to be addressed for the realization of the microwave diagnostics in ITER. Numerical studies, which simulate these loads on both individual components and the entire diagnostic system, play a key role in this process. In-vessel components, like mirrors for microwave diagnostics, require regular inspection, performing, for example calibration measurements. All this needs to be done remotely, as access to the vessel is no longer possible after a burning plasma. While the next-step devices, i.e., electricity-producing devices like DEMO, have in principle challenges similar to ITER, those are all on a much higher magnitude.⁴⁶⁷ Operating these diagnostics in ITER will therefore teach us valuable lessons to prepare them and adjust the designs where necessary for DEMO-like machines. A unique and essential opportunity to test the plasma-facing components of the diagnostics under neutron irradiation conditions expected in DEMO will be provided by the International Fusion Materials Irradiation Facility-DEMO Oriented Neutron Source (IFMIF-DONES), currently under construction in Granada, Spain.^{468,469}

Stray radiation from non-absorbed microwave heating will become significantly higher in future fusion devices due to the increased heating power, imposing a threat for the microwave diagnostics. While there exist promising solutions like the multi-frequency notch filters, as discussed, those solutions need to be tested in current devices like JT60-SA.⁴⁷⁰ Stray radiation needs to be monitored thoroughly,⁴⁷¹ such that shutters can react on short time scales, shielding

the microwave diagnostics from the hazardous power load.⁴⁷² Furthermore, for the long discharge times of future devices, care has to be taken that the frequency of the gyrotron is monitored, as it is known to drift, e.g., ± 250 MHz for a 140 GHz gyrotron.⁷⁰ This requires tunable notch filters, or filters with a sufficiently wide bandwidth. The frequency drift is most prominent in the first few seconds after turning on a gyrotron,⁴⁷³ when the acceleration voltage is still rising and the degree of ionization in the gyrotron's cavity is increasing. A second, slower drift, which can take several tens of seconds for the frequency to stabilize and reach its asymptotic value,^{474,475} it due to thermal effects and can vary strongly depending on the gyrotron manufacturer.

The development of synthetic diagnostics is becoming more and more important to model the experimental setup as close as possible and thus help with the correct interpretation of the acquired data.⁴⁷⁶ While the straightforward way might be to apply full-wave simulations,^{477–479} this is not always necessary and new numerical models might offer computationally less expensive alternatives with only little reduction in the physics captured.^{411,414} Combining several synthetic diagnostics for a multi-diagnostic inference is implemented in Integrated Modelling & Analysis Suite (IMAS) being developed for ITER⁴⁸⁰ but applicable to other machines as well.⁴⁸¹ Numerically designing the diagnostics and optimizing each of their components before actually constructing them is playing another important role.^{482,483} This is in particular, true for future machines, where diagnostics have to be reliable from the very first plasma. After extensive numerical tests of a diagnostics, the next step should always be a full setup of a prototype in the laboratory, trying to emulate plasma effects as closely as possible.

Machine learning is becoming more and more important in fusion research. In particular, deep learning and neural networks are already used for recognizing structures in experimental data, as described for the ECEI diagnostics in EAST. Another example is an ELM detecting neural network at DIII-D,⁴⁸⁴ or a discharge classification model based on deep convolutional neural networks applied to edge reflectometry data on KSTAR.⁴⁸⁵ With increasing discharge duration and increasing spatial and temporal resolution, data processing becomes a challenge.⁴⁸⁶ Machine learning can help here as well, to pre-analyze and then to clean the data prior to storing it, as already explored on a few devices.

The main author of this paper is working at a well-established and equipped university in Germany. Nonetheless, not all papers cited here were accessible from that university, and different ways to access them had to be found. Publishing open access should be mandatory to not exclude certain groups but instead try to include as many as possible, as this strongly increases the chances of getting a fusion reactor running within the next few decades. Not only results in the form of peer-reviewed papers should be openly available, but also codes for modeling and data analysis should be made available and released as open access. This will allow colleagues to cross-check, benchmark, and simply use each other's codes. Remote participation in experimental campaigns at large machines should be possible, and is for example foreseen for ITER,⁴⁸⁷ and acquired data should be made available (after an embargo period if necessary). From relatively early on, fusion was a collaborative effort, and the community should continue to openly discuss progress and challenges and try to continue to adapt the principles of open science⁴⁸⁸ to the benefit of the whole community and even beyond, as the openness is expected to boost knowledge transfer between publicly funded fusion research and private companies.⁴⁸⁹

This paper has hopefully convinced the reader of the usefulness of microwave diagnostics in general, and microwave imaging diagnostics in particular, by providing a few examples of the rich plasma physics phenomena that can be studied with them. The development of these diagnostics is progressing fast, adjusting to the needs of future fusion experiments. It can therefore be expected that they play an important role in advancing current, and developing new, plasma physics models to enable safe and efficient operation of a future fusion power plant.

ACKNOWLEDGMENTS

The authors would like to thank the editorial board, in particular Michael E. Mauel, for the kind invitation to contribute this review. We are also grateful to Thomas Klinger for his encouragement and support in the early stages of this work. Writing such a paper is not possible without the support of colleagues. In particular, we would like to thank (in no particular order) Terry Rhodes, Tokihiko Tokuzawa, Yasuto Kondo, Seong-Heon Seo, Chu Zhou, Andreas Krämer-Flecken, Carlo Sozzi, Dietmar Wagner, and Walter Kasperek for providing technical and operational details. Thanks to Eberhard Holzhauer for his diligent proofreading of this paper. This work has been part-funded by the EPSRC Energy Programme (Grant No. EP/W006839/1). The authors are indebted to the efforts of the open-source software community.

AUTHOR DECLARATIONS

Conflict of Interest

The authors have no conflicts to disclose.

Author Contributions

Alf Köhn-Seemann: Conceptualization (lead); Data curation (lead); Investigation (lead); Methodology (lead); Resources (lead); Visualization (lead); Writing – original draft (lead); Writing – review & editing (equal). **Rennan B. Morales:** Methodology (equal); Resources (equal); Writing – review & editing (equal).

DATA AVAILABILITY

Data sharing is not applicable to this article as no new data were created or analyzed in this study.

REFERENCES

- A. S. Eddington, “The internal constitution of the stars,” *Nature* **106**, 14–20 (1920).
- J. Ongena and Y. Ogawa, “Nuclear fusion: Status report and future prospects,” *Energy Policy* **96**, 770–778 (2016).
- A. Fasoli, “Essay: Overcoming the obstacles to a magnetic fusion power plant,” *Phys. Rev. Lett.* **130**, 220001 (2023).
- K. Ikeda, “Progress in the ITER physics basis,” *Nucl. Fusion* **47**, E01 (2007).
- J. Tollefson, “US nuclear-fusion lab enters new era: Achieving ‘ignition’ over and over,” *Nature* **625**, 11–12 (2024).
- H. Abu-Shawareb, and The Indirect Drive ICF Collaboration, “Achievement of target gain larger than unity in an inertial fusion experiment,” *Phys. Rev. Lett.* **132**, 065102 (2024).
- R. Pearson, “Preface to the Special Issue: The emergence of private fusion enterprises,” *J. Fusion Energy* **42**, 47 (2023).
- V. Erckmann and U. Gasparino, “Electron cyclotron resonance heating and current drive in toroidal fusion plasmas,” *Plasma Phys. Controlled Fusion* **36**, 1869–1962 (1994).
- R. Prater, “Heating and current drive by electron cyclotron waves,” *Phys. Plasmas* **11**, 2349 (2004).
- N. C. Luhmann, H. Bindslev, H. Park, J. Sánchez, G. Taylor, and C. X. Yu, “Chapter 3: Microwave diagnostics,” *Fusion Sci. Technol.* **53**, 335–396 (2008).
- H.-J. Hartfuß and T. Geist, *Fusion Plasma Diagnostics with Mm-Waves: An Introduction*, Physics Textbook (Wiley-VCH Verlag GmbH & Co. KGaA, Weinheim, Germany, 2013).
- C. L. Smith and S. Cowley, “The path to fusion power,” *Philos. Trans. R Soc. A* **368**, 1091–1108 (2010).
- T. N. Todd, “Diagnostic systems in DEMO: Engineering design issues,” in *FUSION REACTOR DIAGNOSTICS: Proceedings of the International Conference (AIP Conference Proceedings)* (Villa Monastero, Varenna (Lc), Italy, 2014), pp. 9–16.
- D. Meade, “50 years of fusion research,” *Nucl. Fusion* **50**, 014004 (2010).
- T. Akiyama, M. V. Zeeland, T. Carlstrom, R. Boivin, K. Brunner, J. Knauer, R. Yasuhara, K. Tanaka, H. Liu, Y. Zhou, N. Oyama, A. Sirinelli, K. Urabe, and N. Shirai, “Recent progress on dispersion interferometers for nuclear fusion and low-temperature plasmas,” *J. Instrum.* **15**, C01004 (2020).
- S. E. Segre, “A review of plasma polarimetry—Theory and methods,” *Plasma Phys. Controlled Fusion* **41**, R57–R100 (1999).
- S. K. Nielsen, P. K. Michelsen, S. K. Hansen, S. B. Korsholm, F. Leipold, J. Rasmussen, M. Salewski, M. Schubert, M. Stejner, J. Stober, and D. Wagner, “Recent development of collective Thomson scattering for magnetically confined fusion plasmas,” *Phys. Scr.* **92**, 024001 (2017).
- V. Grandgirard, Y. Sarazin, P. Angelino, A. Bottino, N. Crouseilles, G. Darmet, G. Dif-Pradalier, X. Garbet, P. Ghendrih, S. Jolliet, G. Latu, E. Sonnendrücker, and L. Villard, “Global full-*f* gyrokinetic simulations of plasma turbulence,” *Plasma Phys. Controlled Fusion* **49**, B173–B182 (2007).
- X. Garbet, Y. Idomura, L. Villard, and T. Watanabe, “Gyrokinetic simulations of turbulent transport,” *Nucl. Fusion* **50**, 043002 (2010).
- F. Jenko, D. Told, T. Görler, J. Citrin, A. Bañón Navarro, C. Bourdelle, S. Brunner, G. Conway, T. Dannert, H. Doerk, D. Hatch, J. Haverkort, J. Hobirk, G. Hogeweij, P. Mantica, M. Pueschel, O. Sauter, L. Villard, E. Wolfgram, and the ASDEX Upgrade Team, “Global and local gyrokinetic simulations of high-performance discharges in view of ITER,” *Nucl. Fusion* **53**, 073003 (2013).
- B. D. Dudley and J. Leddy, “Hermes: Global plasma edge fluid turbulence simulations,” *Plasma Phys. Controlled Fusion* **59**, 054010 (2017).
- J. B. Parker, L. L. LoDestro, D. Told, G. Merlo, L. F. Ricketson, A. Campos, F. Jenko, and J. A. Hittinger, “Bringing global gyrokinetic turbulence simulations to the transport timescale using a multiscale approach,” *Nucl. Fusion* **58**, 054004 (2018).
- A. Stegmeir, D. Coster, A. Ross, O. Maj, K. Lackner, and E. Poli, “GRILLIX: A 3D turbulence code based on the flux-coordinate independent approach,” *Plasma Phys. Controlled Fusion* **60**, 035005 (2018).
- M. Giacomini, P. Ricci, A. Corrado, G. Fourestey, D. Galassi, E. Lanti, D. Mancini, N. Richart, L. Stenger, and N. Varini, “The GBS code for the self-consistent simulation of plasma turbulence and kinetic neutral dynamics in the tokamak boundary,” *J. Comput. Phys.* **463**, 111294 (2022).
- J. P. Kleijnen, “Verification and validation of simulation models,” *Eur. J. Oper. Res.* **82**, 145–162 (1995).
- N. Nikolova, “Microwave imaging for breast cancer,” *IEEE Microwave Mag.* **12**, 78–94 (2011).
- An Introduction to Microwave Imaging for Breast Cancer Detection*, Biological and Medical Physics, Biomedical Engineering, edited by R. C. Conceição, J. J. Mohr, and M. O’Halloran (Springer International Publishing, Cham, 2016).
- C. Dachena, A. Fedeli, A. Fanti, M. B. Lodi, M. Pastorino, and A. Randazzo, “Microwave imaging for the diagnosis of cervical diseases: A feasibility analysis,” *IEEE J. Electromagn. RF Microwave Med. Biol.* **5**, 277–285 (2021).
- C. Dachena, A. Fedeli, A. Fanti, M. B. Lodi, G. Fumera, M. Pastorino, and A. Randazzo, “Initial experimental tests of an ANN-based microwave imaging technique for neck diagnostics,” *IEEE Microwave Wireless Compon. Lett.* **32**, 1495–1498 (2022).
- D. Sheen, D. McMakin, and T. Hall, “Three-dimensional millimeter-wave imaging for concealed weapon detection,” *IEEE Trans. Microwave Theory Tech.* **49**, 1581–1592 (2001).

- ³¹M. Dehmollaian and K. Sarabandi, "Refocusing through building walls using synthetic aperture radar," *IEEE Trans. Geosci. Remote Sens.* **46**, 1589–1599 (2008).
- ³²M. Pastorino, *Microwave Imaging*, 1st ed. (Wiley, 2010).
- ³³*Plasma Diagnostic Techniques*, Pure and Applied Physics, edited by R. H. Huddleston and S. L. Leonard (Academic Press, New York, 1965).
- ³⁴W. Lochte-Holtgreven, *Plasma Diagnostics* (North-Holland Publishing Company, 1968).
- ³⁵I. H. Hutchinson, *Principles of Plasma Diagnostics*, 2nd ed. (Cambridge University Press, Cambridge, 2002).
- ³⁶F. Volpe, "Prospects for a dominantly microwave-diagnosed magnetically confined fusion reactor," *J. Instrum.* **12**, C01094 (2017).
- ³⁷F. Orsitto, R. Villari, F. Moro, T. Todd, S. Lilley, I. Jenkins, R. Felton, W. Biel, A. Silva, M. Scholz, J. Rzadkiewicz, I. Duran, M. Tardocchi, G. Gorini, C. Morlock, G. Federici, and A. Litnovsky, "Diagnostics and control for the steady state and pulsed tokamak DEMO," *Nucl. Fusion* **56**, 026009 (2016).
- ³⁸W. Biel, R. Albanese, R. Ambrosino, M. Ariola, M. Berkel, I. Bolshakova, K. Brunner, R. Cavazzana, M. Ceconello, S. Conroy, A. Dinklage, I. Duran, R. Dux, T. Eade, S. Entler, G. Ericsson, E. Fable, D. Farina, L. Figini, C. Finotti, T. Franke, L. Giacomelli, L. Giannone, W. Gonzalez, A. Hjalmarsson, M. Hron, F. Janky, A. Kallenbach, J. Kogoj, R. König, O. Kudlacek, R. Luis, A. Malaquias, O. Marchuk, G. Marchiori, M. Mattei, F. Maviglia, G. De Masi, D. Mazon, H. Meister, K. Meyer, D. Micheletti, S. Nowak, C. Piron, A. Pironti, N. Rispoli, V. Rohde, G. Sergienko, S. El Shawish, M. Siccino, A. Silva, F. Da Silva, C. Sozzi, M. Tardocchi, M. Tokar, W. Treutterer, and H. Zohm, "Diagnostics for plasma control – From ITER to DEMO," *Fusion Eng. Des.* **146**, 465–472 (2019).
- ³⁹S. McNamara, O. Asunta, J. Bland, P. Buxton, C. Colgan, A. Dnestrovskii, M. Gemmell, M. Gryaznevich, D. Hoffman, F. Janky, J. Lister, H. Lowe, R. Mirfayzi, G. Naylor, V. Nemytov, J. Njau, T. Pyragius, A. Rengle, M. Romanelli, C. Romero, M. Sertoli, V. Shevchenko, J. Sinha, A. Sladkomedova, S. Sridhar, Y. Takase, P. Thomas, F. Varje, B. Vincent, H. Willett, J. Wood, D. Zakhar, D. Battaglia, S. Kaye, L. Delgado-Aparicio, R. Maingi, D. Mueller, M. Podesta, E. Delabie, B. Lomanowski, and O. Marchuk, "Achievement of ion temperatures in excess of 100 million degrees Kelvin in the compact high-field spherical tokamak ST40," *Nucl. Fusion* **63**, 054002 (2023).
- ⁴⁰L. Schmitz, B. Deng, M. Thompson, H. Gota, C. Lau, D. P. Fulton, Z. Lin, T. Tajima, M. Binderbauer, and TAE Team, "Combination Doppler backscattering/cross-polarization scattering diagnostic for the C-2W field-reversed configuration," *Rev. Sci. Instrum.* **89**, 10H116 (2018).
- ⁴¹M. L. Reinke, I. Abramovic, A. Albert, K. Asai, J. Ball, J. Batko, J. Brettingen, D. Brunner, M. Cario, J. Carmichael, C. Chrobak, A. Creely, D. Cykman, M. Dalla Rosa, E. Dubas, C. Downey, A. Ferrera, J. Frenje, E. Fox-Widdows, R. Gocht, G. Gorini, R. Granetz, M. Greenwald, A. Grieve, M. Hanson, J. Hawke, T. Henderson, S. Hicks, J. Hillesheim, A. Hoffmann, I. Holmes, N. Howard, A. Hubbard, J. W. Hughes, J. Ilagan, J. Irby, M. Jean, G. Kaur, R. Kennedy, E. Kowalski, A. Q. Kuang, R. Kulchy, M. LaCapra, C. Lafleur, M. Lagieski, R. Li, Y. Lin, T. Looby, R. Zubieta Lupo, S. Mackie, E. Marmor, S. McKanas, A. Moncada, R. Mumgaard, C. E. Myers, V. Nikolaeva, M. Nocente, S. Normile, C. Novoa, S. Ouellet, E. Panontin, C. Paz-Soldan, J. Pentecost, C. Perks, M. Petruzzo, M. Quinn, J. Raimond, P. Raj, M. Rebai, V. Riccardo, D. Rigamonti, J. E. Rice, A. Rosenthal, M. Safabakhsh, A. Saltos, J. Shanahan, M. Silva Sa, I. Song, J. Souza, B. Stein-Lubrano, I. G. Stewart, R. Sweeney, M. Tardocchi, A. Tinguely, D. Vezinet, X. Wang, and J. Witham, "Overview of the early campaign diagnostics for the SPARC tokamak (invited)," *Rev. Sci. Instrum.* **95**, 103518 (2024).
- ⁴²M. A. Heald and C. B. Wharton, *Plasma Diagnostics with Microwaves* (R. E. Krieger Pub. Co, Huntington, NY, 1978).
- ⁴³A. Krämer-Flecken, "Microwave and far infrared diagnostics," *Fusion Sci. Technol.* **45**, 418–425 (2004).
- ⁴⁴A. Mase, Y. Kogi, N. Ito, Y. Yokota, K. Akaki, K. Kawahata, Y. Nagayama, T. Tokuzawa, S. Yamaguchi, H. Hojo, N. Oyama, N. C. Luhmann, H. K. Park, and A. J. Donné, "Advancements of microwave diagnostics in magnetically confined plasmas," *Plasma Devices Oper.* **17**, 98–116 (2009).
- ⁴⁵H. J. Hartfuss, "Fusion plasma diagnostics with microwaves," in *2010 Conference Proceedings ICECom, 20th International Conference on Applied Electromagnetics and Communications* (IEEE, 2010), pp. 1–4.
- ⁴⁶H. Park, C. C. Chang, B. H. Deng, C. W. Domier, A. J. H. Donné, K. Kawahata, C. Liang, X. P. Liang, H. J. Lu, N. C. Luhmann, A. Mase, H. Matsuura, E. Mazzucato, A. Miura, K. Mizuno, T. Munsat, Y. Nagayama, M. J. Van De Pol, J. Wang, Z. G. Xia, and W.-K. Zhang, "Recent advancements in microwave imaging plasma diagnostics," *Rev. Sci. Instrum.* **74**, 4239–4262 (2003).
- ⁴⁷B. Tobias, N. C. Luhmann, Jr., C. W. Domier, X. Kong, T. Liang, S. Che, R. Nazikian, L. Chen, G. Yun, W. Lee, H. K. Park, I. G. Classen, J. E. Boom, A. J. Donné, M. A. V. Zeeland, R. Boivin, Y. Nagayama, T. Yoshinaga, D. Kuwahara, S. Yamaguchi, Y. Kogi, A. Mase, and T. L. Munsat, "Recent progress on microwave imaging technology and new physics results," *Plasma Fusion Res.* **6**, 2106042 (2011).
- ⁴⁸Y. Wang, B. Tobias, Y.-T. Chang, J.-H. Yu, M. Li, F. Hu, M. Chen, M. Mamidanna, T. Phan, A.-V. Pham, J. Gu, X. Liu, Y. Zhu, C. Domier, L. Shi, E. Valeo, G. Kramer, D. Kuwahara, Y. Nagayama, A. Mase, and N. Luhmann, "Millimeter-wave imaging of magnetic fusion plasmas: Technology innovations advancing physics understanding," *Nucl. Fusion* **57**, 072007 (2017).
- ⁴⁹Y. Zhu, J.-H. Yu, M. Chen, B. Tobias, and N. C. Luhmann, "New trends in microwave imaging diagnostics and application to burning plasma," *IEEE Trans. Plasma Sci.* **47**, 2110–2130 (2019).
- ⁵⁰V. L. Ginzburg, *The Propagation of Electromagnetic Waves in Plasmas* (Pergamon Press Inc, 1964).
- ⁵¹T. H. Stix, *Waves in Plasmas* (American Institute of Physics, New York, 1992).
- ⁵²M. Brambilla, *Kinetic Theory of Plasma Waves: Homogeneous Plasmas*, illustrated ed. (Oxford University Press, Oxford, 1998).
- ⁵³D. G. Swanson, *Plasma Waves*, 2nd ed., Series in Plasma Physics (Institute of Physics Pub, Bristol; Philadelphia, 2003).
- ⁵⁴E. Appleton, "Wireless studies of the ionosphere," *Inst. Electr. Eng.* **7**, 257–265 (1932).
- ⁵⁵M. Manso, D. Bartlett, L. Cupido, W. Kasperek, J. Sanchez, P. Stott, and D. Wagner, "Reflectometry for ITER density profiles," in *Diagnostics for Experimental Thermonuclear Fusion Reactors*, edited by P. E. Stott, G. Gorini, and E. Sindoni (Springer US, Boston, MA, 1996), pp. 133–142.
- ⁵⁶R. T. Hitchcock, "Radio-frequency and microwave radiation," in *Patty's Toxicology*, 1st ed., edited by E. Bingham, B. Cohnsen, and C. H. Powell (Wiley, 2012), pp. 133–168.
- ⁵⁷R. Sorrentino and G. Bianchi, *Microwave and RF Engineering*, 1st ed. (Wiley, 2010).
- ⁵⁸E. Mazzucato, "Relativistic effects on microwave reflectometry," *Phys. Fluids B* **4**, 3460–3461 (1992).
- ⁵⁹A. E. Costley, R. J. Hastie, J. W. M. Paul, and J. Chamberlain, "Electron cyclotron emission from a tokamak plasma: Experiment and theory," *Phys. Rev. Lett.* **33**, 758–761 (1974).
- ⁶⁰M. Bornatici, R. Cano, O. De Barbieri, and F. Engelmann, "Electron cyclotron emission and absorption in fusion plasmas," *Nucl. Fusion* **23**, 1153–1257 (1983).
- ⁶¹B. J. Tobias, M. E. Austin, J. E. Boom, K. H. Burrell, I. G. J. Classen, C. W. Domier, N. C. Luhmann, R. Nazikian, and P. B. Snyder, "ECE-imaging of the H-mode pedestal (invited)," *Rev. Sci. Instrum.* **83**, 10E329 (2012).
- ⁶²M. Willensdorfer, S. S. Denk, E. Strumberger, W. Suttrop, B. Vanovac, D. Brida, M. Cavedon, I. Classen, M. Dunne, S. Fietz, R. Fischer, A. Kirk, F. M. Lagner, Y. Q. Liu, T. Odstrčil, D. A. Ryan, E. Viezzer, H. Zohm, I. C. Luhmann, The ASDEX Upgrade Team, and The EUROfusion MST1 Team, "Plasma response measurements of external magnetic perturbations using electron cyclotron emission and comparisons to 3D ideal MHD equilibrium," *Plasma Phys. Controlled Fusion* **58**, 114004 (2016).
- ⁶³G. Yu, Y. Zhu, M. Austin, Y. Chen, J. Cao, A. Diallo, G. Kramer, Z. Li, X. Li, X. Liu, R. Nazikian, Y. Zheng, and N. C. Luhmann, Jr., "Diagnosing the pedestal magnetic field and magnetohydrodynamics radial structure with pedestal-scraper of layer electron cyclotron emission radiation inversion in H-mode plasma (invited)," *Rev. Sci. Instrum.* **93**, 103528 (2022).
- ⁶⁴S. Denk, R. Fischer, E. Poli, O. Maj, S. Nielsen, J. Rasmussen, M. Stejner, and M. Willensdorfer, "ECRad: An electron cyclotron radiation transport solver for advanced data analysis in thermal and non-thermal fusion plasmas," *Comput. Phys. Commun.* **253**, 107175 (2020).
- ⁶⁵S. S. Denk, R. Fischer, H. M. Smith, P. Helander, O. Maj, E. Poli, J. Stober, U. Stroth, W. Suttrop, E. Westerhof, M. Willensdorfer, and the ASDEX Upgrade

- Team, "Analysis of electron cyclotron emission with extended electron cyclotron forward modeling," *Plasma Phys. Controlled Fusion* **60**, 105010 (2018).
- ⁶⁶M. Thumm, G. Denisov, K. Sakamoto, and M. Tran, "High-power gyrotrons for electron cyclotron heating and current drive," *Nucl. Fusion* **59**, 073001 (2019).
- ⁶⁷Z. Shen, N. Ito, Y. Liang, L. Lin, C. W. Domier, M. Johnsaon, N. C. Luhmann, Jr., A. Mase, and E. Sakata, "Protection filters in ECEI systems for plasma diagnostics," *Plasma Fusion Res.* **2**, S1030 (2007).
- ⁶⁸J. Anderson, J. Doane, C. Moeller, H. Grunloh, R. O'Neill, M. Brookman, M. Smiley, and D. Su, "Design and performance of microwave components for ECH and ECE applications at general atomics," *EPJ Web Conf.* **203**, 04001 (2019).
- ⁶⁹D. Wagner, W. Kasperek, F. Leuterer, F. Monaco, T. Ruess, J. Stober, and M. Thumm, "A compact two-frequency notch filter for millimeter wave plasma diagnostics," *J. Infrared, Millimeter, Terahertz Waves* **41**, 741–749 (2020).
- ⁷⁰D. Wagner, W. Kasperek, F. Leuterer, F. Monaco, B. Plaum, T. Ruess, H. Schütz, J. Stober, and M. Thumm, "Single- and two-frequency sub-THz waveguide notch filters with rejection frequencies within and beyond the pass-band," *IEEE Trans. Microwave Theory Tech.* **71**, 2558–2566 (2023).
- ⁷¹H. J. Hartfuss, T. Geist, and M. Hirsch, "Heterodyne methods in millimeter wave plasma diagnostics with applications to ECE, interferometry and reflectometry," *Plasma Phys. Controlled Fusion* **39**, 1693–1769 (1997).
- ⁷²Y. Nagayama, K. Kawahata, S. Inagaki, S. Kubo, K. Narihara, N. Ohyabu, and T. L. Group, "Electron cyclotron emission diagnostics in the large helical device," *J. Plasma Fusion Res.* **79**, 601–607 (2003).
- ⁷³A. Sinha, D. Mohanta, N. Parmar, S. P. Pandya, and S. K. Pathak, "Design, development and characterization of indigenously developed high temperature black body source for calibration of ECE diagnostics," *EPJ Web Conf.* **313**, 03003 (2024).
- ⁷⁴J. L. Ségui, D. Molina, G. Giruzzi, M. Goniche, G. Huysmans, P. Maget, M. Ottaviani, and The Tore Supra Team, "An upgraded 32-channel heterodyne electron cyclotron emission radiometer on Tore Supra," *Rev. Sci. Instrum.* **76**, 123501 (2005).
- ⁷⁵Y. Kogi, S. H. Jeong, K. D. Lee, K. Akaki, A. Mase, D. Kuwahara, T. Yoshinaga, Y. Nagayama, M. Kwon, and K. Kawahata, "Calibration of electron cyclotron emission radiometer for KSTAR," *Rev. Sci. Instrum.* **81**, 10D916 (2010).
- ⁷⁶X. Liu, H. L. Zhao, Y. Liu, E. Z. Li, X. Han, C. W. Domier, N. C. Luhmann, A. Ti, L. Q. Hu, and X. D. Zhang, "Absolute intensity calibration of the 32-channel heterodyne radiometer on experimental advanced superconducting tokamak," *Rev. Sci. Instrum.* **85**, 093508 (2014).
- ⁷⁷K. D. Lee, J. H. Lee, Y. U. Nam, and S. Pyo, "Electron cyclotron emission calibration with Thomson scattering using a wide scan of toroidal magnetic field of KSTAR," *Rev. Sci. Instrum.* **95**, 083538 (2024).
- ⁷⁸Y. Zhu, Y. Ye, J.-H. Yu, B. Tobias, A.-V. Pham, Y. Wang, C. Luo, C. W. Domier, G. Kramer, Y. Ren, A. Diallo, R. Nazikian, M. Chen, G. Yu, and N. C. Luhmann, "Liquid crystal polymer receiver modules for electron cyclotron emission imaging on the DIII-D tokamak," *Rev. Sci. Instrum.* **89**, 10H120 (2018).
- ⁷⁹C. Watts, "A review of ECE correlation radiometry techniques for detection of core electron temperature fluctuations," *Fusion Sci. Technol.* **52**, 176–192 (2007).
- ⁸⁰P. C. Liewer, "Measurements of microturbulence in tokamaks and comparisons with theories of turbulence and anomalous transport," *Nucl. Fusion* **25**, 543–621 (1985).
- ⁸¹A. Fujisawa, "Turbulence in toroidal plasma," in *Proceedings of the 12th Asia Pacific Physics Conference (APPC12)* (Journal of the Physical Society of Japan, Makuhari, Japan, 2014).
- ⁸²A. Fujisawa, "Review of plasma turbulence experiments," *Proc. Jpn. Acad. Ser. B* **97**, 103–119 (2021).
- ⁸³S. Sattler and H. J. Hartfuss, "Experimental evidence for electron temperature fluctuations in the core plasma of the W7-AS stellarator," *Phys. Rev. Lett.* **72**, 653–656 (1994).
- ⁸⁴M. Kwon, R. F. Gandy, C. E. Thomas, and W. K. Lim, "Electron temperature fluctuation measurement from ECE on TEXT-U," *Rev. Sci. Instrum.* **63**, 4633–4635 (1992).
- ⁸⁵G. Cima, C. Watts, and R. F. Gandy, "Correlation radiometry of electron cyclotron radiation in TEXT-U (invited)," *Rev. Sci. Instrum.* **66**, 798–801 (1995).
- ⁸⁶V. S. Udintsev, M. Goniche, J. L. Ségui, G. Giruzzi, D. Molina, F. Turco, G. T. A. Huysmans, P. Maget, T. S. Team, and A. Krämer-Flecken, "First results of correlation electron cyclotron emission on Tore Supra," *Fusion Sci. Technol.* **50**, 508–520 (2006).
- ⁸⁷A. E. White, L. Schmitz, W. A. Peebles, T. A. Carter, T. L. Rhodes, E. J. Doyle, P. A. Gourdain, J. C. Hillesheim, G. Wang, C. Holland, G. R. Tynan, M. E. Austin, G. R. McKee, M. W. Shafer, K. H. Burrell, J. Candy, J. C. DeBoo, R. Prater, G. M. Staebler, R. E. Waltz, and M. A. Makowski, "A correlation electron cyclotron emission diagnostic and the importance of multifield fluctuation measurements for testing nonlinear gyrokinetic turbulence simulations," *Rev. Sci. Instrum.* **79**, 103505 (2008).
- ⁸⁸C. Sung, A. White, N. Howard, C. Oi, J. Rice, C. Gao, P. Ennever, M. Porkolab, F. Parra, D. Mikkelsen, D. Ernst, J. Walk, J. Hughes, J. Irby, C. Kasten, A. Hubbard, M. Greenwald, and the Alcator C-Mod Team, "Changes in core electron temperature fluctuations across the ohmic energy confinement transition in Alcator C-Mod plasmas," *Nucl. Fusion* **53**, 083010 (2013).
- ⁸⁹N. T. Howard, C. Sung, and A. E. White, "Measurement of multifield fluctuation fluctuations using a tunable correlation electron cyclotron emission system on Alcator C-Mod," *Rev. Sci. Instrum.* **85**, 11D811 (2014).
- ⁹⁰S. J. Freethy, G. D. Conway, I. Classen, A. J. Creely, T. Happel, A. Köhn, B. Vanovac, and A. E. White, "Measurement of turbulent electron temperature fluctuations on the ASDEX Upgrade tokamak using correlated electron cyclotron emission," *Rev. Sci. Instrum.* **87**, 11E102 (2016).
- ⁹¹M. Fontana, L. Porte, and P. Molina Cabrera, "Correlation electron cyclotron emission diagnostic in TCV," *Rev. Sci. Instrum.* **88**, 083506 (2017).
- ⁹²H. Zhou, Z. J. Yang, X. L. Xie, C. Zhang, X. M. Pan, Q. X. Cai, and B. W. Ruan, "Measurement of electron temperature fluctuations on J-TEXT via correlation ECE," *Rev. Sci. Instrum.* **89**, 10H105 (2018).
- ⁹³T. D. Rempel, R. F. Gandy, and A. J. Wootton, "Density fluctuation effects on electron cyclotron emission correlation measurements in optically gray plasmas," *Rev. Sci. Instrum.* **65**, 2044–2048 (1994).
- ⁹⁴C. Sung, T. L. Rhodes, and W. A. Peebles, "Turbulence measurements on the high and low magnetic field side of the DIII-D tokamak," *Rev. Sci. Instrum.* **89**, 10H106 (2018).
- ⁹⁵A. E. Costley, "50 years of electron cyclotron emission research," *Fusion Sci. Technol.* **55**, 1–15 (2009).
- ⁹⁶S. K. Rathgeber, L. Barrera, T. Eich, R. Fischer, B. Nold, W. Suttrop, M. Willensdorfer, E. Wolftrum, and the ASDEX Upgrade Team, "Estimation of edge electron temperature profiles via forward modelling of the electron cyclotron radiation transport at ASDEX Upgrade," *Plasma Phys. Controlled Fusion* **55**, 025004 (2013).
- ⁹⁷H. Van Den Brand, W. Bongers, J. Stober, W. Kasperek, D. Wagner, N. Doelman, W. Klop, L. Giannone, M. Reich, E. Westerhof, M. De Baar, The ASDEX Upgrade Team, and The EUROfusion MST1 Team, "Inline ECE measurements for NTM control on ASDEX Upgrade," *Nucl. Fusion* **59**, 016013 (2019).
- ⁹⁸M. E. Austin and J. Lohr, "Electron cyclotron emission radiometer upgrade on the DIII-D tokamak," *Rev. Sci. Instrum.* **74**, 1457–1459 (2003).
- ⁹⁹D. D. Truong and M. E. Austin, "High spatial resolution upgrade of the electron cyclotron emission radiometer for the DIII-D tokamak," *Rev. Sci. Instrum.* **85**, 11D814 (2014).
- ¹⁰⁰H. Zhao, A. Ti, T. Zhou, Z. Zhu, Y. Liu, B. Ling, Q. Zang, J. Huang, and X. Gong, "Current status of ECE system on EAST tokamak," *EPJ Web Conf.* **277**, 03007 (2023).
- ¹⁰¹Y. Nagayama, K. Kawahata, A. England, Y. Ito, N. Bretz, M. McCarthy, G. Taylor, J. Doane, H. Ikezi, T. Edlington, and J. Tomas, "Electron cyclotron emission diagnostics on the large helical device," *Rev. Sci. Instrum.* **70**, 1021–1024 (1999).
- ¹⁰²S. Sudo, Y. Nagayama, M. Emoto, M. Goto, Y. Hamada, K. Ida, T. Ido, H. Iguchi, S. Inagaki, M. Isobe, K. Kawahata, K. Khlopenkov, S. Masuzaki, T. Minami, S. Morita, S. Muto, H. Nakanishi, K. Narihara, A. Nishizawa, S. Ohdachi, M. Osakabe, T. Ozaki, B. J. Peterson, S. Sakakibara, M. Sasao, K. Sato, M. Shoji, K. Tanaka, K. Toi, T. Tokuzawa, K. Watanabe, T. Watanabe, I. Yamada, N. Ashikawa, T. Kobuchi, Y. Liang, N. Tamura, H. Sasao, A. Ejiri, S.

- Okajima, A. Mase, S. Tsuji-Iio, T. Akiyama, V. Zanza, G. Bracco, A. Sibio, B. Tilia, A. V. Krasilnikov, J. F. Lyon, L. N. Vyacheslavov, G. A. Wurden, and LHD Team, "Overview of large helical device diagnostics (invited)," *Rev. Sci. Instrum.* **72**, 483–491 (2001).
- ¹⁰³T. Tokuzawa, Y. Goto, D. Kuwahara, M. Nishiura, and T. Shimizu, "New Q and V-band ECE radiometer for low magnetic field operation on LHD," *EPJ Web Conf.* **277**, 03008 (2023).
- ¹⁰⁴S. H. Jeong, K. D. Lee, Y. Kogi, K. Kawahata, Y. Nagayama, A. Mase, and M. Kwon, "Electron cyclotron emission diagnostics on KSTAR tokamak," *Rev. Sci. Instrum.* **81**, 10D922 (2010).
- ¹⁰⁵K. Kawahata, Y. Nagayama, H. Tsuchiya, A. Mase, Y. Kogi, S. H. Jeong, K.-D. Lee, and R. J. Wylde, "Broadband multichannel radiometer for ECE measurements on KSTAR," *Plasma Fusion Res.* **6**, 2402094 (2011).
- ¹⁰⁶V. Siju, D. Kumar, P. Shukla, and S. K. Pathak, "Characterization and calibration of 8-channel E-band heterodyne radiometer system for SST-1 tokamak," *Rev. Sci. Instrum.* **85**, 053503 (2014).
- ¹⁰⁷M. Fontana, L. Porte, and P. Marmillod, "Electron cyclotron emission (ECE) and correlation ECE diagnostics on TCV," *EPJ Web Conf.* **147**, 02005 (2017).
- ¹⁰⁸A. Tema Biwole, L. Porte, S. Coda, A. Fasoli, and TCV Team, "Vertical electron cyclotron emission diagnostic on the tokamak à configuration variable," *Rev. Sci. Instrum.* **94**, 103504 (2023).
- ¹⁰⁹E. De La Luna, I. García-Cortés, V. Tribaldos, F. Tabarés, J. Jiménez, T. Estrada, E. Ascasibar, A. Cappa, F. Castejón, A. Fernández, J. Herranz, K. Likin, A. López-Fraguas, R. Martín, K. McCarthy, I. Pastor, J. Sánchez, D. Tafalla, and B. Zurro, "Electron cyclotron emission measurements on TJ-II stellarator plasmas," *Fusion Eng. Des.* **53**, 147–151 (2001).
- ¹¹⁰M. Hirsch, U. Höfel, J. W. Oosterbeek, N. Chaudhary, J. Geiger, H.-J. Hartfuss, W. Kasperek, N. Maruschchenko, B. Van Milligen, B. Plaum, T. Stange, J. Svensson, H. Tsuchiya, D. Wagner, G. McWeir, R. Wolf, and W7-X Team, "ECE diagnostic for the initial operation of Wendelstein 7-X," *EPJ Web Conf.* **203**, 03007 (2019).
- ¹¹¹A. J. Creely, S. J. Freethy, W. M. Burke, G. D. Conway, R. Leccacorvi, W. C. Parkin, D. R. Terry, and A. E. White, "Correlation electron cyclotron emission diagnostic and improved calculation of turbulent temperature fluctuation levels on ASDEX Upgrade," *Rev. Sci. Instrum.* **89**, 053503 (2018).
- ¹¹²R. Bielajew, G. D. Conway, T. Happel, K. Höfler, P. A. M. Cabrera, U. Plank, P. Rodriguez-Fernandez, D. Silvagni, B. Vanovac, C. Yoo, A. White, and The ASDEX Upgrade Team, "Electron temperature fluctuation measurements with correlation electron cyclotron emission in L-mode and I-mode plasmas at ASDEX Upgrade," *EPJ Web Conf.* **277**, 03002 (2023).
- ¹¹³C. Sung, W. A. Peebles, C. Wannberg, T. L. Rhodes, X. Nguyen, R. Lantsov, and L. Bardóczy, "A frequency tunable, eight-channel correlation ECE system for electron temperature turbulence measurements on the DIII-D tokamak," *Rev. Sci. Instrum.* **87**, 11E123 (2016).
- ¹¹⁴A. Donné, A. Costley, R. Barnsley, H. Bindslev, R. Boivin, G. Conway, R. Fisher, R. Giannella, H. Hartfuss, M. V. Hellermann, E. Hodgson, L. Ingesson, K. Itami, D. Johnson, Y. Kawano, T. Kondoh, A. Krasilnikov, Y. Kusama, A. Litnovsky, P. Lotte, P. Nielsen, T. Nishitani, F. Orsitto, B. Peterson, G. Razdobarin, J. Sanchez, M. Sasao, T. Sugie, G. Vayakis, V. Voitsenya, K. Vukolov, C. Walker, K. Young, and T. I. T. G. O. Diagnostics, "Chapter 7: Diagnostics," *Nucl. Fusion* **47**, S337–S384 (2007).
- ¹¹⁵Y. Liu, V. Udintsev, S. Danani, G. Paraiso, G. Taylor, M. Austin, A. Basile, J. Beno, B. Bunkowski, R. Feder, T. Giacomini, J. Guirao, S. Houshmandyar, H. Huang, A. Hubbard, S. Hughes, S. Jha, A. Khodak, R. Kumar, S. Kumar, V. Kumar, P. Maquet, C. Nazare, H. Neilson, A. Ouroua, S. Pak, H. Pandya, C. Penney, P. Phillips, S. Pish, J. Poissy, W. Rowan, A. Saxena, M. Schneider, S. Strank, S. Thomas, G. Vayakis, F. Waelbroeck, M. Walsh, and L. Worth, "Progress in ITER ECE diagnostic design and integration," *J. Instrum.* **17**, C04019 (2022).
- ¹¹⁶Y. Yang, G. Li, Y. Wang, T. Ming, X. Han, S. Liu, E. Wang, W. Yang, H. Liu, Z. Zou, W. Li, H. Qu, Y. Liu, G. Li, Q. Hu, X. Gao, J. Li, and Y. Wan, "Progress of concept design for CFETR diagnostic system," *IEEE Trans. Plasma Sci.* **46**, 1361–1365 (2018).
- ¹¹⁷R. J. La Haye, "Neoclassical tearing modes and their control," *Phys. Plasmas* **13**, 055501 (2006).
- ¹¹⁸M. Maraschek, G. Gantenbein, Q. Yu, H. Zohm, S. Günter, F. Leuterer, and A. Manini, "Enhancement of the stabilization efficiency of a neoclassical magnetic island by modulated electron cyclotron current drive in the ASDEX Upgrade tokamak," *Phys. Rev. Lett.* **98**, 025005 (2007).
- ¹¹⁹E. Kolemen, A. Welander, R. La Haye, N. Eidietis, D. Humphreys, J. Lohr, V. Noraky, B. Penaflor, R. Prater, and F. Turco, "State-of-the-art neoclassical tearing mode control in DIII-D using real-time steerable electron cyclotron current drive launchers," *Nucl. Fusion* **54**, 073020 (2014).
- ¹²⁰J. W. Oosterbeek, A. Bürger, E. Westerhof, M. R. De Baar, M. A. Van Den Berg, W. A. Bongers, M. F. Graswinckel, B. A. Hennen, O. G. Kruijt, J. Thoen, R. Heidinger, S. B. Korsholm, F. Leipold, and S. K. Nielsen, "A line-of-sight electron cyclotron emission receiver for electron cyclotron resonance heating feedback control of tearing modes," *Rev. Sci. Instrum.* **79**, 093503 (2008).
- ¹²¹E. Westerhof, S. K. Nielsen, J. W. Oosterbeek, M. Salewski, M. R. De Baar, W. A. Bongers, A. Bürger, B. A. Hennen, S. B. Korsholm, F. Leipold, D. Moseev, M. Stejner, and D. J. Thoen, "Strong scattering of high power millimeter waves in tokamak plasmas with tearing modes," *Phys. Rev. Lett.* **103**, 125001 (2009).
- ¹²²W. A. Bongers, A. P. H. Goede, E. Westerhof, J. W. Oosterbeek, N. J. Doelman, F. C. Schüller, M. R. De Baar, W. Kasperek, W. Wubie, D. Wagner, J. Stober, and Textor Team, "Magnetic island localization for NTM control by ECE viewed along the same optical path of the ECCD beam," *Fusion Sci. Technol.* **55**, 188–203 (2009).
- ¹²³W. Kasperek, R. Van Den Braber, N. Doelman, E. Fritz, V. Erckmann, F. Hollmann, G. Michel, F. Noke, F. Purps, W. Bongers, B. Krüger, M. Petelin, L. Lubyako, A. Bruschi, and ECRH Groups at IPP Greifswald and IPF Stuttgart, "High-power performance of a resonant diplexer for advanced ECRH," *Fusion Sci. Technol.* **59**, 729–741 (2011).
- ¹²⁴W. Bongers, W. Kasperek, N. Doelman, R. Van Den Braber, H. Van Den Brand, F. Meo, M. De Baar, F. Amerongen, A. Donné, B. Elzendoorn, V. Erckmann, A. Goede, L. Giannone, G. Grünwald, F. Hollman, G. Kaas, B. Krijger, G. Michel, L. Lubyako, F. Monaco, F. Noke, M. Petelin, B. Plaum, F. Purps, J. Ten Pierik, C. Schüller, J. Slob, J. Stober, H. Schütz, D. Wagner, E. Westerhof, and D. Ronden, teams at the contributing institutes, and the ASDEX Upgrade Team, "Commissioning of inline ECE system within waveguide based ECRH transmission systems on ASDEX upgrade," *EPJ Web Conf.* **32**, 03006 (2012).
- ¹²⁵D. Wagner, W. Bongers, W. Kasperek, F. Leuterer, F. Monaco, M. München, H. Schütz, J. Stober, M. Thumm, and H. V. Brand, "A multifrequency notch filter for millimeter wave plasma diagnostics based on photonic bandgaps in corrugated circular waveguides," *EPJ Web Conf.* **87**, 04012 (2015).
- ¹²⁶N. Rispoli, C. Sozzi, L. Figini, D. Micheletti, C. Galperti, M. Fontana, E. Alessi, S. Coda, S. Garavaglia, T. Goodman, M. Kong, M. Maraschek, A. Moro, L. Porte, O. Sauter, U. Sheikh, and D. Testa, "Tracking of neoclassical tearing modes in TCV using the electron cyclotron emission diagnostics in quasi-inline configuration," *Fusion Eng. Des.* **146**, 666–670 (2019).
- ¹²⁷S. Houshmandyar, Z. J. Yang, P. E. Phillips, W. L. Rowan, A. E. Hubbard, J. E. Rice, J. W. Hughes, and S. M. Wolfe, "Temperature gradient scale length measurement: A high accuracy application of electron cyclotron emission without calibration," *Rev. Sci. Instrum.* **87**, 11E101 (2016).
- ¹²⁸S. Houshmandyar, M. E. Austin, M. W. Brookman, Y. Liu, W. L. Rowan, and H. Zhao, "Variable location channels to improve efficiency and precision for direct ∇T_e measurements and high spatial resolution T_e -profile measurements using electron cyclotron emission," *Rev. Sci. Instrum.* **89**, 10H109 (2018).
- ¹²⁹S. Houshmandyar, R. Xie, M. E. Austin, W. L. Rowan, and H. Zhao, "Fast modulating electron cyclotron emission (FMECE) diagnostic for tokamaks," *Rev. Sci. Instrum.* **92**, 033510 (2021).
- ¹³⁰G. Wang, T. L. Rhodes, and W. A. Peebles, "Analysis method for calculating radial correlation length of electron temperature turbulence from correlation electron cyclotron emission radiometer," *Rev. Sci. Instrum.* **93**, 113511 (2022).
- ¹³¹S. J. Freethy, T. Görler, A. J. Creely, G. D. Conway, S. S. Denk, T. Happel, C. Koenen, P. Hennequin, A. E. White, and ASDEX Upgrade Team, "Validation of gyrokinetic simulations with measurements of electron temperature fluctuations and density-temperature phase angles on ASDEX Upgrade," *Phys. Plasmas* **25**, 055903 (2018).
- ¹³²W. Horton, *Turbulent Transport in Magnetized Plasmas*, 2nd ed. (World Scientific, 2017).
- ¹³³R. Bielajew, U. Plank, G. Conway, A. Hubbard, P. Rodriguez-Fernandez, B. Vanovac, C. Yoo, A. White, and the ASDEX Upgrade Team, "Edge radiated temperature fluctuations across confinement regime transitions in favorable

- and unfavorable drift configurations at ASDEX Upgrade,” *Nucl. Fusion* **63**, 126022 (2023).
- ¹³⁴H. Biglari, P. H. Diamond, and P. W. Terry, “Influence of sheared poloidal rotation on edge turbulence,” *Phys. Fluids B* **2**, 1–4 (1990).
- ¹³⁵H. Zohm, “Edge localized modes (ELMs),” *Plasma Phys. Controlled Fusion* **38**, 105–128 (1996).
- ¹³⁶Z. Sun, A. Diallo, R. Maingi, Y. Qian, K. Tritz, Y. Wang, Y. Wang, A. Bortolon, A. Nagy, L. Zhang, Y. Duan, Y. Ye, H. Zhao, H. Wang, X. Gu, G. Zuo, W. Xu, M. Huang, C. Li, X. Meng, C. Zhou, H. Liu, Q. Zang, L. Wang, J. Qian, G. Xu, X. Gong, J. Hu, and E. Team, “Suppression of edge localized modes with real-time boron injection using the tungsten divertor in EAST,” *Nucl. Fusion* **61**, 014002 (2021).
- ¹³⁷T. E. Evans, R. A. Moyer, K. H. Burrell, M. E. Fenstermacher, I. Joseph, A. W. Leonard, T. H. Osborne, G. D. Porter, M. J. Schaffer, P. B. Snyder, P. R. Thomas, J. G. Watkins, and W. P. West, “Edge stability and transport control with resonant magnetic perturbations in collisionless tokamak plasmas,” *Nat. Phys.* **2**, 419–423 (2006).
- ¹³⁸C. Sung, G. Wang, T. L. Rhodes, S. P. Smith, T. H. Osborne, M. Ono, G. R. McKee, Z. Yan, R. J. Groebner, E. M. Davis, L. Zeng, W. A. Peebles, and T. E. Evans, “Increased electron temperature turbulence during suppression of edge localized mode by resonant magnetic perturbations in the DIII-D tokamak,” *Phys. Plasmas* **24**, 112305 (2017).
- ¹³⁹D. Whyte, A. Hubbard, J. Hughes, B. Lipschultz, J. Rice, E. Marmor, M. Greenwald, I. Cziegler, A. Dominguez, T. Golfopoulos, N. Howard, L. Lin, R. McDermott, M. Porkolab, M. Reinke, J. Terry, N. Tsujii, S. Wolfe, S. Wukitch, Y. Lin, and the Alcator C-Mod Team, “I-mode: An H-mode energy confinement regime with L-mode particle transport in Alcator C-Mod,” *Nucl. Fusion* **50**, 105005 (2010).
- ¹⁴⁰Z. X. Liu, X. Q. Xu, X. Gao, A. E. Hubbard, J. W. Hughes, J. R. Walk, C. Theiler, T. Y. Xia, S. G. Baek, T. Golfopoulos, D. Whyte, T. Zhang, and J. G. Li, “The physics mechanisms of the weakly coherent mode in the Alcator C-Mod Tokamak,” *Phys. Plasmas* **23**, 120703 (2016).
- ¹⁴¹T. Happel, M. Griener, D. Silvagni, S. Freethy, P. Hennequin, F. Janky, P. Manz, D. Prisiazhniuk, F. Ryter, M. Bernert, D. Brida, T. Eich, M. Faitsch, L. Gil, L. Guimarães, A. Merle, D. Nille, J. Pinzón, B. Sieglin, U. Stroth, and E. Viezzer, “Stationarity of I-mode operation and I-mode divertor heat fluxes on the ASDEX Upgrade tokamak,” *Nucl. Mater. Energy* **18**, 159–165 (2019).
- ¹⁴²L. Gil, C. Silva, T. Happel, G. Birkenmeier, G. Conway, L. Guimarães, A. Kallenbach, T. Pütterich, J. Santos, P. Schneider, M. Schubert, E. Seliunin, A. Silva, J. Stober, U. Stroth, E. Trier, E. Wolfrum, ASDEX, and EUROfusion, “Stationary ELM-free H-mode in ASDEX Upgrade,” *Nucl. Fusion* **60**, 054003 (2020).
- ¹⁴³A. Kirk, D. Dunai, M. Dunne, G. Huijsmans, S. Pamela, M. Becoulet, J. Harrison, J. Hillesheim, C. Roach, and S. Saarelma, “Recent progress in understanding the processes underlying the triggering of and energy loss associated with type I ELMs,” *Nucl. Fusion* **54**, 114012 (2014).
- ¹⁴⁴B. Vanovac, J. Stober, E. Wolfrum, M. Willensdorfer, L. Gil, M. Faitsch, R. Bielajew, C. Yoo, G. Conway, S. Denk, R. McDermott, A. White, and Upgrade Team ASDEX, “Electron temperature fluctuation levels of the quasi-coherent mode across the plasma radius,” *EPJ Web Conf.* **277**, 03003 (2023).
- ¹⁴⁵B. Vanovac, S. Denk, E. Wolfrum, M. Willensdorfer, W. Suttrop, R. Fischer, N. Luhmann, and ASDEX Upgrade Team, “Mode analysis limitations of ECE-I & ECE measurements at the plasma edge,” *EPJ Web Conf.* **203**, 02011 (2019).
- ¹⁴⁶M. W. Brookman, M. E. Austin, C. C. Petty, R. J. La Haye, K. Barada, T. L. Rhodes, Z. Yan, A. Köhn, M. B. Thomas, J. B. Leddy, and R. G. L. Vann, “Resolving ECRH deposition broadening due to edge turbulence in DIII-D,” *Phys. Plasmas* **28**, 042507 (2021).
- ¹⁴⁷M. Brookman, L. Holland, M. Thomas, M. Austin, K. Barada, K. Gentle, R. La Haye, J. Leddy, C. Petty, T. Rhodes, Z. Yan, R. Vann, and A. Köhn-Seemann, “Broadening of microwave heating beams in the DIII-D tokamak by edge turbulence,” *Nucl. Fusion* **63**, 044001 (2023).
- ¹⁴⁸B. Zhao and M. E. Austin, “Refined interpretation of electron temperature response to neutral beam injection at DIII-D,” *Phys. Plasmas* **30**, 112504 (2023).
- ¹⁴⁹A. Marinoni, O. Sauter, and S. Coda, “A brief history of negative triangularity tokamak plasmas,” *Rev. Mod. Plasma Phys.* **5**, 6 (2021).
- ¹⁵⁰M. E. Austin, A. Marinoni, M. L. Walker, M. W. Brookman, J. S. deGrassie, A. W. Hyatt, G. R. McKee, C. C. Petty, T. L. Rhodes, S. P. Smith, C. Sung, K. E. Thome, and A. D. Turnbull, “Achievement of reactor-relevant performance in negative triangularity shape in the DIII-D tokamak,” *Phys. Rev. Lett.* **122**, 115001 (2019).
- ¹⁵¹M. Fontana, L. Porte, S. Coda, O. Sauter, S. Brunner, A. C. Jayalekshmi, A. Fasoli, G. Merlo, and The TCV Team, “Effects of collisionality and T_e/T_i on fluctuations in positive and negative δ tokamak plasmas,” *Nucl. Fusion* **60**, 016006 (2020).
- ¹⁵²F. Long, T. Zhang, T. Ming, X. Liu, L. Meng, M. Wu, B. Li, R. Liang, M. Wu, B. Hao, T. Tang, M. Chen, S. Liu, Y. Wang, X. Han, H. Liu, H. Zhao, Q. Zang, L. Wang, L. Zeng, G. Li, X. Gao, and The East Team, “Impact of coherent mode on divertor particle and heat flux in a type I ELMy H mode plasma on EAST tokamak,” *Nucl. Fusion* **62**, 096018 (2022).
- ¹⁵³P. A. Molina Cabrera, P. Rodriguez-Fernandez, T. Görler, M. Bergmann, K. Höfler, S. S. Denk, R. Bielajew, G. D. Conway, C. Yoo, A. E. White, and ASDEX Upgrade Team, “Isotope effects on energy transport in the core of ASDEX-Upgrade tokamak plasmas: Turbulence measurements and model validation,” *Phys. Plasmas* **30**, 082304 (2023).
- ¹⁵⁴M. Häse, M. Hirsch, and H. J. Hartfuss, “Temperature fluctuations and their correlation with density fluctuations in W7-AS,” *Rev. Sci. Instrum.* **70**, 1014–1017 (1999).
- ¹⁵⁵A. E. White, W. A. Peebles, T. L. Rhodes, C. H. Holland, G. Wang, L. Schmitz, T. A. Carter, J. C. Hillesheim, E. J. Doyle, L. Zeng, G. R. McKee, G. M. Staebler, R. E. Waltz, J. C. DeBoo, C. C. Petty, and K. H. Burrell, “Measurements of the cross-phase angle between density and electron temperature fluctuations and comparison with gyrokinetic simulations,” *Phys. Plasmas* **17**, 056103 (2010).
- ¹⁵⁶S. J. Freethy, T. Görler, A. J. Creely, G. D. Conway, S. S. Denk, T. Happel, P. Henniquin, C. Koenen, A. E. White, and ASDEX Upgrade Team, “Advances in turbulence measurements using new Correlation ECE and nT-phase diagnostics at ASDEX Upgrade,” *EPJ Web Conf.* **203**, 03001 (2019).
- ¹⁵⁷R. L. Wang, Y. Liu, X. L. Zou, H. L. Zhao, T. F. Zhou, C. Zhou, A. D. Liu, Y. D. Li, P. J. Sun, T. Zhang, and H. Q. Liu, “Electron temperature fluctuations correlated with energy confinement degradation in the EAST Ohmic plasmas,” *Phys. Plasmas* **28**, 072508 (2021).
- ¹⁵⁸L. Chen and F. Zonca, “Physics of Alfvén waves and energetic particles in burning plasmas,” *Rev. Mod. Phys.* **88**, 015008 (2016).
- ¹⁵⁹J. Kim, J. Kang, T. Rhee, J. Jo, H. Han, M. Podestà, J. Lee, S. Lee, J. Bak, M. Choi, R. Nazikian, H. Jhang, J. Ko, M. Joong, Y.-M. Jeon, Y.-S. Na, K. Shinohara, and C. Cheng, “Suppression of toroidal Alfvén eigenmodes by the electron cyclotron current drive in KSTAR plasmas,” *Nucl. Fusion* **62**, 026029 (2022).
- ¹⁶⁰M. Vallar, M. Dreval, M. Garcia-Munoz, S. Sharapov, J. Poley, A. N. Karpushov, P. Lauber, S. Mazzi, and L. Porte, “Excitation of toroidal Alfvén eigenmodes with counter-current NBI in the TCV tokamak,” *Nucl. Fusion* **63**, 046003 (2023).
- ¹⁶¹Y. Nagayama, K. Kawahata, S. Inagaki, T. Morisaki, and K. Narihara, “Electron cyclotron emission diagnostics for helical plasma in the large helical device,” *IEEE Trans. Plasma Sci.* **32**, 1716–1720 (2004).
- ¹⁶²T. Tokuzawa, Y. Takemura, K. Watanabe, S. Sakakibara, Y. Narushima, H. Tsuchiya, Y. Nagayama, S. Inagaki, K. Ida, M. Yoshinuma, K. Tanaka, Y. Suzuki, I. Yamada, and The LHD Experiment Group, “Distorted magnetic island formation during slowing down to mode locking in helical plasmas,” *Nucl. Fusion* **57**, 076003 (2017).
- ¹⁶³K. Ida, T. Kobayashi, M. Yoshinuma, T. Akiyama, T. Tokuzawa, H. Tsuchiya, K. Itoh, and S.-I. Itoh, “Trigger mechanism for the abrupt loss of energetic ions in magnetically confined plasmas,” *Sci. Rep.* **8**, 2804 (2018).
- ¹⁶⁴U. Hoefel, M. Hirsch, S. Kwak, A. Pavone, J. Svensson, T. Stange, H.-J. Hartfuß, J. Schilling, G. Weir, J. W. Oosterbeek, S. Bozhenkov, H. Braune, K.-J. Brunner, N. Chaudhary, H. Damm, G. Fuchert, J. Knauer, H. Laqua, S. Marsen, D. Moseev, E. Pasch, E. R. Scott, F. Wilde, R. Wolf, and W7-X Team, “Bayesian modeling of microwave radiometer calibration on the example of the Wendelstein 7-X electron cyclotron emission diagnostic,” *Rev. Sci. Instrum.* **90**, 043502 (2019).
- ¹⁶⁵M. J. Hole, G. Von Nessi, D. Pretty, J. Howard, B. Blackwell, J. Svensson, and L. C. Appel, “The use of Bayesian inversion to resolve plasma equilibrium,” *Rev. Sci. Instrum.* **81**, 10E127 (2010).

- ¹⁶⁶J. Svensson, O. Ford, D. McDonald, A. Meakins, A. Werner, M. Brix, A. Boboc, M. Beurskens, and Jet Efdá Contributors, "Modelling of JET diagnostics using Bayesian graphical models," *Contrib. Plasma Phys.* **51**, 152–157 (2011).
- ¹⁶⁷J. W. Oosterbeek, M. Stern, N. Chaudhary, J. G. Arnaiz, M. Hirsch, W. Kasperek, C. Lechte, B. Plaum, S. Schmuck, T. Stange, M. Steffen, R. Wolf, and the W7-X Team, "Towards absolutely calibrated ECE Michelson measurements in EC heated plasmas at W7-X," *EPJ Web Conf.* **313**, 03004 (2024).
- ¹⁶⁸G. Weir, P. Xanthopoulos, M. Hirsch, U. Höfel, T. Stange, N. Pablant, O. Grulke, S. Åkäsloppolo, J. Alcúson, S. Bozhenkov, M. Beurskens, A. Dinklage, G. Fuchert, J. Geiger, M. Landreman, A. Langenberg, S. Lazerson, N. Marushchenko, E. Pasch, J. Schilling, E. Scott, Y. Turkin, and T. Klinger, "Heat pulse propagation and anomalous electron heat transport measurements on the optimized stellarator W7-X," *Nucl. Fusion* **61**, 056001 (2021).
- ¹⁶⁹M. Zanini, H. Laqua, H. Thomsen, T. Stange, C. Brandt, H. Braune, K. Brunner, G. Fuchert, M. Hirsch, J. Knauer, U. Höfel, S. Marsen, E. Pasch, K. Rahbarnia, J. Schilling, Y. Turkin, R. Wolf, and A. Zocco, "ECCD-induced sawtooth crashes at W7-X," *Nucl. Fusion* **60**, 106021 (2020).
- ¹⁷⁰N. Chaudhary, M. Hirsch, T. Andreeva, J. Geiger, U. Hoefel, K. Rahbarnia, G. A. Wurden, R. C. Wolf, and the W7-X Team, "Radial localization of electron temperature pedestal and ELM-like events using ECE measurements at Wendelstein 7-X," *EPJ Web Conf.* **277**, 03004 (2023).
- ¹⁷¹M. W. Hirsch, S. Bannmann, M. N. A. Beurskens, C. Biedermann, S. Bozhenkov, K.-J. Brunner, N. Chaudhary, H. Damm, O. Ford, J. Guerrero-Arnaiz, G. Fuchert, X. Han, U. Höfel, J. Huang, J. Knauer, J.-P. Koschinsky, A. Krämer-Flecken, B. Kursinski, A. Langenberg, S. Lazerson, J. Meineke, D. Moseev, J. Oosterbeek, N. Pablant, E. Pasch, A. Pavone, P. Pölöskei, T. Richert, T. Stange, M. Steffen, M. Stern, L. Vanó, R. C. Wolf, H. M. Xiang, M. Zanini, and the W7-X Team, "Core diagnostics for WENDELSTEIN 7-X steady-state exploration until 18 GJ," *Plasma Fusion Res.* **17**, 2406097 (2022).
- ¹⁷²S. Houshmandyar, T. A. Watts, W. L. Rowan, J. Zajac, V. Veselovsky, V. Ivanov, O. Bogar, and V. Weinzettl, "Design of an electron cyclotron emission diagnostics suite for COMPASS Upgrade tokamak," *Rev. Sci. Instrum.* **93**, 113514 (2022).
- ¹⁷³R. Albanese, R. Ambrosino, M. Ariola, G. De Tommasi, A. Pironti, M. Cavinato, A. Neto, F. Piccolo, F. Sartori, R. Ranz, L. Carraro, A. Canton, R. Cavazzana, A. Fassina, P. Franz, P. Innocente, A. Luchetta, G. Manduchi, L. Marrelli, E. Martines, S. Peruzzo, M. Puiatti, P. Scarin, G. Spizzo, M. Spolaore, M. Valisa, G. Gorini, M. Nocente, C. Sozzi, M. Apicella, L. Gabellieri, G. Maddaluno, and G. Ramogida, "Diagnostics, data acquisition and control of the divertor test tokamak experiment," *Fusion Eng. Des.* **122**, 365–374 (2017).
- ¹⁷⁴M. Bassan, P. Andrew, G. Kurskiv, E. Mukhin, T. Hatae, G. Vayakis, E. Yatsuka, and M. Walsh, "Thomson scattering diagnostic systems in ITER," *J. Instrum.* **11**, C01052 (2016).
- ¹⁷⁵H. Van Den Brand, M. De Baar, N. Lopes Cardozo, and E. Westerhof, "ECE for NTM control on ITER," *EPJ Web Conf.* **32**, 03004 (2012).
- ¹⁷⁶J. P. Ziegel, W. L. Rowan, and F. L. Waelbroeck, "Electron cyclotron emission detection of neoclassical tearing modes for control for ITER," *Rev. Sci. Instrum.* **95**, 073510 (2024).
- ¹⁷⁷R. L. Haye, R. Prater, R. Buttery, N. Hayashi, A. Isayama, M. Maraschek, L. Urso, and H. Zohm, "Cross-machine benchmarking for ITER of neoclassical tearing mode stabilization by electron cyclotron current drive," *Nucl. Fusion* **46**, 451–461 (2006).
- ¹⁷⁸H. Van Den Brand, M. R. De Baar, N. J. L. Cardozo, and E. Westerhof, "Integrated modelling of island growth, stabilization and mode locking: Consequences for NTM control on ITER," *Plasma Phys. Controlled Fusion* **54**, 094003 (2012).
- ¹⁷⁹E. Poli, C. Angioni, F. Casson, D. Farina, L. Figini, T. Goodman, O. Maj, O. Sauter, H. Weber, H. Zohm, G. Saibene, and M. Henderson, "On recent results in the modelling of neoclassical-tearing-mode stabilization via electron cyclotron current drive and their impact on the design of the upper EC launcher for ITER," *Nucl. Fusion* **55**, 013023 (2015).
- ¹⁸⁰G. Taylor and R. W. Harvey, "Assessment of an oblique ECE diagnostic for ITER," *Fusion Sci. Technol.* **55**, 64–75 (2009).
- ¹⁸¹G. Taylor, M. E. Austin, J. H. Beno, S. Danani, R. F. Ellis, R. Feder, J. L. Hesler, A. E. Hubbard, D. W. Johnson, R. Kumar, S. Kumar, V. Kumar, A. Ouroua, H. K. B. Pandya, P. E. Phillips, C. Roman, W. L. Rowan, V. Udintsev, G. Vayakis, and M. Walsh, "Status of the design of the ITER ECE diagnostic," *EPJ Web Conf.* **87**, 03002 (2015).
- ¹⁸²G. Taylor, M. E. Austin, A. Basile, J. H. Beno, S. Danani, R. Feder, S. Houshmandyar, A. E. Hubbard, D. W. Johnson, A. Khodak, R. Kumar, S. Kumar, A. Ouroua, S. B. Padasalagi, H. K. B. Pandya, P. E. Phillips, W. L. Rowan, J. Stillerman, S. Thomas, V. S. Udintsev, G. Vayakis, M. Walsh, and D. Weeks, "Update on the status of the ITER ECE diagnostic design," *EPJ Web Conf.* **147**, 02003 (2017).
- ¹⁸³V. Udintsev, S. Danani, G. Taylor, T. Giacomini, J. Guirao, S. Pak, S. Hughes, L. Worth, G. Vayakis, M. Walsh, M. Schneider, H. Pandya, R. Kumar, V. Kumar, S. Jha, S. Thomas, S. B. Padasalagi, S. Kumar, P. E. Phillips, W. L. Rowan, M. Austin, A. Khodak, R. Feder, H. Neilson, A. Basile, A. E. Hubbard, A. Saxena, C. Nazare, P. Maquet, and N. Gimbert, "Progress in ITER ECE diagnostic design and integration," *EPJ Web Conf.* **203**, 03003 (2019).
- ¹⁸⁴R. Kumar, S. Danani, H. Pandya, P. Vaghshahiya, V. Udintsev, G. Taylor, M. Austin, and V. Kumar, "Comparative studies of various types of transmission lines in the frequency range 70 GHz–1 THz for ITER ECE diagnostic," *EPJ Web Conf.* **203**, 04009 (2019).
- ¹⁸⁵D. M. Slocum, E. J. Slingerland, R. H. Giles, and T. M. Goyette, "Atmospheric absorption of terahertz radiation and water vapor continuum effects," *J. Quant. Spectrosc. Radiat. Transfer* **127**, 49–63 (2013).
- ¹⁸⁶H. K. B. Pandya, M. E. Austin, and R. F. Ellis, "Study of transmission line attenuation in broad band millimeter wave frequency range," *Rev. Sci. Instrum.* **84**, 103505 (2013).
- ¹⁸⁷S. Schmuck, J. Fessey, T. Gerbaud, B. Alper, M. N. A. Beurskens, E. De La Luna, A. Sirinelli, M. Zerbini, and JET-EFDA Contributors, "Electron cyclotron emission measurements on JET: Michelson interferometer, new absolute calibration, and determination of electron temperature," *Rev. Sci. Instrum.* **83**, 125101 (2012).
- ¹⁸⁸A. Ouroua, J. Beno, A. Bryant, D. Weeks, P. Phillips, and W. Rowan, "Design, analysis, and testing of a hot calibration source for the ITER-ECE diagnostic system," *Fusion Sci. Technol.* **72**, 331–336 (2017).
- ¹⁸⁹A. Ouroua, J. Beno, A. Bryant, A. Khodak, P. Phillips, W. Rowan, G. Taylor, and D. Weeks, "Prototype design of a 700 °C in-vacuum blackbody source for in situ calibration of the ITER ECE diagnostic," *IEEE Trans. Plasma Sci.* **46**, 1239–1246 (2018).
- ¹⁹⁰T. Wakatsuki, H. Urano, M. Yoshida, N. Tsujii, S. Inoue, S. Kojima, T. Nakano, M. Fukumoto, Y. Ohtani, R. Sano, and S. Ide, "Achievement of the first tokamak plasma with low inductive electric field in JT-60SA," *Nucl. Fusion* **64**, 104003 (2024).
- ¹⁹¹T. Tokuzawa, M. Yoshida, R. Imazawa, S. Nakagawa, S. Inagaki, F. Kin, S. Chiba, N. Suzuki, T. Nasu, A. Fujisawa, and K. Ida, "Preparatory study of feasibility for a vertical viewing electron cyclotron emission diagnostic for the JT-60SA tokamak," *Rev. Sci. Instrum.* **95**, 083531 (2024).
- ¹⁹²R. James, S. Janz, R. Ellis, D. Boyd, and J. Lohr, "Vertical-viewing electron cyclotron emission diagnostic for the DIII-D tokamak," *Rev. Sci. Instrum.* **59**, 1611–1613 (1988).
- ¹⁹³D. R. Roberts, R. F. Steimle, G. Giruzzi, G. Cima, and C. Watts, "Vertical viewing of electron-cyclotron emissions for diagnosing fast-electron dynamics in TEXT-U," *Rev. Sci. Instrum.* **66**, 427–429 (1995).
- ¹⁹⁴I. G. J. Classen, J. E. Boom, W. Suttrop, E. Schmid, B. Tobias, C. W. Domier, N. C. Luhmann, A. J. H. Donné, R. J. E. Jaspers, P. C. De Vries, H. K. Park, T. Munsat, M. García-Muñoz, and P. A. Schneider, "2D electron cyclotron emission imaging at ASDEX Upgrade (invited)," *Rev. Sci. Instrum.* **81**, 10D929 (2010).
- ¹⁹⁵T. Munsat, C. W. Domier, X. Kong, T. Liang, N. C. Luhmann, Jr., B. J. Tobias, W. Lee, H. K. Park, G. Yun, I. G. J. Classen, and A. J. H. Donné, "Electron cyclotron emission imaging in tokamak plasmas," *Appl. Opt.* **49**, E20 (2010).
- ¹⁹⁶I. G. J. Classen, E. Westerhof, C. W. Domier, A. J. H. Donné, R. J. E. Jaspers, N. C. Luhmann, H. K. Park, M. J. Van De Pol, G. W. Spakman, and M. W. Jakubowski, "Effect of heating on the suppression of tearing modes in tokamaks," *Phys. Rev. Lett.* **98**, 035001 (2007).
- ¹⁹⁷H. K. Park, N. C. Luhmann, A. J. H. Donné, I. G. J. Classen, C. W. Domier, E. Mazzucato, T. Munsat, M. J. Van De Pol, and Z. Xia, "Observation of high-field-side crash and heat transfer during sawtooth oscillation in magnetically confined plasmas," *Phys. Rev. Lett.* **96**, 195003 (2006).

- ¹⁹⁸G. S. Yun, W. Lee, M. J. Choi, J. Lee, H. K. Park, B. Tobias, C. W. Domier, N. C. Luhmann, A. J. H. Donné, J. H. Lee, and KSTAR Team, "Two-dimensional visualization of growth and burst of the edge-localized filaments in KSTAR H-mode plasmas," *Phys. Rev. Lett.* **107**, 045004 (2011).
- ¹⁹⁹I. G. J. Classen, P. Lauber, D. Curran, J. E. Boom, B. J. Tobias, C. W. Domier, N. C. Luhmann, H. K. Park, M. Garcia Munoz, B. Geiger, M. Maraschek, M. A. Van Zeeland, S. Da Graça, and the ASDEX Upgrade Team, "Investigation of fast particle driven instabilities by 2D electron cyclotron emission imaging on ASDEX Upgrade," *Plasma Phys. Controlled Fusion* **53**, 124018 (2011).
- ²⁰⁰B. J. Tobias, I. G. J. Classen, C. W. Domier, W. W. Heidbrink, N. C. Luhmann, R. Nazikian, H. K. Park, D. A. Spong, and M. A. Van Zeeland, "Fast ion induced shearing of 2D Alfvén eigenmodes measured by electron cyclotron emission imaging," *Phys. Rev. Lett.* **106**, 075003 (2011).
- ²⁰¹D. A. Spong, E. M. Bass, W. Deng, W. W. Heidbrink, Z. Lin, B. Tobias, M. A. Van Zeeland, M. E. Austin, C. W. Domier, and N. C. Luhmann, "Verification and validation of linear gyrokinetic simulation of Alfvén eigenmodes in the DIII-D tokamak," *Phys. Plasmas* **19**, 082511 (2012).
- ²⁰²J. Lee, G. S. Yun, M. J. Choi, J.-M. Kwon, Y.-M. Jeon, W. Lee, N. C. Luhmann, and H. K. Park, "Nonlinear interaction of edge-localized modes and turbulent eddies in toroidal plasma under $n = 1$ magnetic perturbation," *Phys. Rev. Lett.* **117**, 075001 (2016).
- ²⁰³M. Jiang, X. T. Ding, Z. B. Shi, W. Chen, L. M. Yu, J. Q. Dong, Y. Xu, Y. Liu, B. S. Yuan, W. L. Zhong, Y. Zhou, Y. G. Li, Z. C. Yang, P. W. Shi, Y. B. Dong, Q. W. Yang, X. R. Duan, and HL-2A Team, "Observation of the double e-fishbone instability in HL-2A ECRH/ECCD plasmas," *Phys. Plasmas* **24**, 022110 (2017).
- ²⁰⁴H. K. Park, "Newly uncovered physics of MHD instabilities using 2-D electron cyclotron emission imaging system in toroidal plasmas," *Adv. Phys. X* **4**, 1633956 (2019).
- ²⁰⁵R. P. Hsia, B. H. Deng, W. R. Geck, C. Liang, C. W. Domier, N. C. Luhmann, Jr., D. L. Brower, and G. Cima, "Hybrid electron cyclotron emission imaging array system for Texas experimental tokamak upgrade," *Rev. Sci. Instrum.* **68**, 488–491 (1997).
- ²⁰⁶B. H. Deng, D. L. Brower, G. Cima, C. W. Domier, N. C. Luhmann, and C. Watts, "Mode structure of turbulent electron temperature fluctuations in the Texas Experimental Tokamak Upgrade," *Phys. Plasmas* **5**, 4117–4120 (1998).
- ²⁰⁷B. H. Deng, R. P. Hsia, C. W. Domier, S. R. Burns, T. R. Hillyer, N. C. Luhmann, T. Oyevaar, A. J. H. Donné, and RTP Team, "Electron cyclotron emission imaging diagnostic system for Rijnhuizen Tokamak Project," *Rev. Sci. Instrum.* **70**, 998–1001 (1999).
- ²⁰⁸B. H. Deng, C. W. Domier, N. C. Luhmann, D. L. Brower, G. Cima, A. J. H. Donné, T. Oyevaar, and M. J. Van De Pol, "ECE imaging of electron temperature and electron temperature fluctuations (invited)," *Rev. Sci. Instrum.* **72**, 301–306 (2001).
- ²⁰⁹B. H. Deng, C. W. Domier, N. C. Luhmann, A. J. H. Donné, and M. J. Van De Pol, "Electron cyclotron emission imaging diagnostic on TEXTOR," *Rev. Sci. Instrum.* **72**, 368–370 (2001).
- ²¹⁰B. H. Deng, C. W. Domier, N. C. Luhmann, D. L. Brower, A. J. H. Donné, T. Oyevaar, and M. J. Van De Pol, "Electron cyclotron emission imaging diagnostic of Te profiles and fluctuations," *Phys. Plasmas* **8**, 2163–2169 (2001).
- ²¹¹I. G. J. Classen, C. W. Domier, N. C. Luhmann, A. V. Bogomolov, W. Suttrop, J. E. Boom, B. J. Tobias, A. J. H. Donné, and ASDEX Upgrade Team, "Dual array 3D electron cyclotron emission imaging at ASDEX Upgrade," *Rev. Sci. Instrum.* **85**, 11D833 (2014).
- ²¹²B. Tobias, C. W. Domier, T. Liang, X. Kong, L. Yu, G. S. Yun, H. K. Park, I. G. J. Classen, J. E. Boom, A. J. H. Donné, T. Munsat, R. Nazikian, M. Van Zeeland, R. L. Boivin, and N. C. Luhmann, "Commissioning of electron cyclotron emission imaging instrument on the DIII-D tokamak and first data," *Rev. Sci. Instrum.* **81**, 10D928 (2010).
- ²¹³B. Gao, J. Xie, Z. Mao, C. Luo, Y. Zhu, Z. Zhao, L. Tong, W. D. Liu, N. Luhmann, C. Domier, and B. Tobias, "The electron cyclotron emission imaging system on EAST with continuous large observation area," *J. Instrum.* **13**, P02009 (2018).
- ²¹⁴Z. Yang, M. Jiang, Z. Shi, X. Ding, N. Luhmann, W. Zhong, W. Chen, P. Shi, Y. Xu, J. Wen, A. Liang, Y. Liu, Q. Yang, and HL-2A Team, "Development of ECE/ECEI diagnostics and MHD-related studies on HL-2A tokamak," EPJ Web Conf. **203**, 03014 (2019).
- ²¹⁵X. Xie, J. Zhou, Y. Zhu, X. Pan, H. Zhou, G. Yu, N. Luhmann, G. Zhuang, and Z. Yang, "Quasi-optical electron cyclotron emission imaging diagnostic advancements on the J-TEXT tokamak," *Fusion Eng. Des.* **155**, 111636 (2020).
- ²¹⁶H. Tsuchiya, D. Kuwahara, T. Tokuzawa, Y. Nagayama, Y. Takemura, and LHD Experiment Group, "Installation of new electron cyclotron emission imaging in LHD," *Plasma Fusion Res.* **13**, 3402063 (2018).
- ²¹⁷Y. Goto, T. Tokuzawa, D. Kuwahara, K. Ichinose, H. Tsuchiya, M. Nishiura, T. Shimizu, S. Kubo, and I. Yamada, "Development of the Q-band ECE imaging system in the large helical device," *J. Instrum.* **17**, C01016 (2022).
- ²¹⁸G. S. Yun, W. Lee, M. J. Choi, J. Lee, M. Kim, J. Leem, Y. Nam, G. H. Choe, H. K. Park, H. Park, D. S. Woo, K. W. Kim, C. W. Domier, N. C. Luhmann, N. Ito, A. Mase, and S. G. Lee, "Quasi 3D ECE imaging system for study of MHD instabilities in KSTAR," *Rev. Sci. Instrum.* **85**, 11D820 (2014).
- ²¹⁹F. M. Laggner, E. Wolfrum, M. Cavedon, F. Mink, E. Viezzer, M. G. Dunne, P. Manz, H. Doerk, G. Birkenmeier, R. Fischer, S. Fietz, M. Maraschek, M. Willensdorfer, F. Aumayr, the EUROfusion MST1 Team, and the ASDEX Upgrade Team, "High frequency magnetic fluctuations correlated with the inter-ELM pedestal evolution in ASDEX Upgrade," *Plasma Phys. Controlled Fusion* **58**, 065005 (2016).
- ²²⁰B. Vanovac, E. Wolfrum, M. Hoelzl, M. Willensdorfer, M. Cavedon, G. Harrer, F. Mink, S. Denk, S. Freethy, M. Dunne, P. Manz, N. Luhmann, and The ASDEX Upgrade Team, "Characterization of low-frequency inter-ELM modes of H-mode discharges at ASDEX Upgrade," *Nucl. Fusion* **58**, 112011 (2018).
- ²²¹B. Vanovac, J. Puchmayr, R. Bielajew, M. Willensdorfer, E. Wolfrum, M. Cavedon, E. Strumberger, M. G. Dunne, and W. Suttrop, "Impact of toroidal rotation on the resistive ballooning modes in ASDEX Upgrade tokamak," *Plasma Phys. Controlled Fusion* **65**, 095011 (2023).
- ²²²E. J. Doyle, L. R. Baylor, K. H. Burrell, T. A. Casper, J. C. DeBoo, D. R. Ernst, A. M. Garofalo, P. Gohil, C. M. Greenfield, R. J. Groebner, A. W. Hyatt, G. L. Jackson, T. C. Jernigan, J. E. Kinsey, L. L. Lao, C. J. Lasnier, J.-N. Leboeuf, M. Makowski, G. R. McKee, R. A. Moyer, M. Murakami, T. H. Osborne, W. A. Peebles, M. Porkolab, G. D. Porter, T. L. Rhodes, J. C. Rost, D. Rudakov, G. M. Staebler, B. W. Stallard, E. J. Strait, R. D. Sydora, E. J. Synakowski, M. R. Wade, G. Wang, J. G. Watkins, W. P. West, and L. Zeng, "The quiescent double barrier regime in the DIII-D tokamak," *Plasma Phys. Controlled Fusion* **43**, A95–A112 (2001).
- ²²³C. Sung, T. L. Rhodes, G. M. Staebler, Z. Yan, G. R. McKee, S. P. Smith, T. H. Osborne, and W. A. Peebles, "Physics of increased edge electron temperature and density turbulence during ELM-free QH-mode operation on DIII-D," *Phys. Plasmas* **25**, 055904 (2018).
- ²²⁴W. Suttrop, V. Hynönen, T. Kurki-Suonio, P. Lang, M. Maraschek, R. Neu, A. Stäbler, G. Conway, S. Hacquin, M. Kempenaars, P. Lomas, M. Nave, R. Pitts, K.-D. Zastrow, and T. A. U. Team, and C. T. T. J.-E. Workprogramme, "Studies of the 'Quiescent H-mode' regime in ASDEX Upgrade and JET," *Nucl. Fusion* **45**, 721–730 (2005).
- ²²⁵Z. Yan, G. R. McKee, R. J. Groebner, P. B. Snyder, T. H. Osborne, and K. H. Burrell, "High-frequency coherent edge fluctuations in a high-pedestal-pressure quiescent H-mode plasma," *Phys. Rev. Lett.* **107**, 055004 (2011).
- ²²⁶G. Yu, R. Nazikian, Y. Zhu, Y. Zheng, G. Kramer, A. Diallo, Z. Li, X. Chen, D. Ernst, Y. Zheng, M. Austin, and N. C. Luhmann, Jr., "ECEI characterization of pedestal fluctuations in quiescent H-mode plasmas in DIII-D," *Plasma Phys. Controlled Fusion* **64**, 095014 (2022).
- ²²⁷A. H. Boozer, "Theory of tokamak disruptions," *Phys. Plasmas* **19**, 058101 (2012).
- ²²⁸R. M. Churchill, B. Tobias, Y. Zhu, and DIII-D Team, "Deep convolutional neural networks for multi-scale time-series classification and application to tokamak disruption prediction using raw, high temporal resolution diagnostic data," *Phys. Plasmas* **27**, 062510 (2020).
- ²²⁹G. Yu, G. J. Kramer, Y. Zhu, X. Li, Y. Wang, A. Diallo, Y. Ren, J. H. Yu, Y. Chen, X. Liu, J. Cao, B. Zhao, M. Austin, and N. C. Luhmann, "Noise suppression for MHD characterization with electron cyclotron emission imaging 1D technique," *Plasma Phys. Controlled Fusion* **63**, 055001 (2021).
- ²³⁰G. Yu, Z. Li, G. Kramer, F. Scotti, A. O. Nelson, A. Diallo, C. Lasnier, M. E. Austin, X. Qin, Y. Chen, Y. Zheng, Y. Zhu, and N. C. Luhmann, "Understanding the negative triangularity ELM trigger and ELM free state on DIII-D with ECE-imaging," *Phys. Plasmas* **30**, 062505 (2023).

- ²³¹A. C. C. Sips, F. T. S. S. Operation, and T. T. P. T. G. Activity, "Advanced scenarios for ITER operation," *Plasma Phys. Controlled Fusion* **47**, A19–A40 (2005).
- ²³²Y. Lee, S. Kim, J. Kim, B. Kim, M. Park, J. Kwon, M. Choi, S. Hahn, M. Lee, S. Yang, S. Hong, C. Lee, S. Park, C. Byun, H.-S. Kim, J. Chung, and Y.-S. Na, "Effect of coherent edge-localized mode on transition to high-performance hybrid scenarios in KSTAR," *Nucl. Fusion* **63**, 126032 (2023).
- ²³³M. Cao and P. Diamond, "Quasi-mode evolution in a stochastic magnetic field," *Nucl. Fusion* **64**, 036003 (2024).
- ²³⁴M. J. Choi, J.-M. Kwon, J. Kim, T. Rhee, J.-G. Bak, G. Shin, H.-S. Kim, H. Jhang, K. Kim, G. S. Yun, M. Kim, S. Kim, H. H. Kaang, J.-K. Park, H. H. Lee, Y. In, J. Lee, M. Kim, B.-H. Park, and H. K. Park, "Stochastic fluctuation and transport of tokamak edge plasmas with the resonant magnetic perturbation field," *Phys. Plasmas* **29**, 122504 (2022).
- ²³⁵D.-K. Kim, J. Lee, D. J. Lee, and G. S. Yun, "Development of a toroidally resolved broadband ECE imaging system for measurement of turbulent fluctuations on the KSTAR," *Rev. Sci. Instrum.* **95**, 083507 (2024).
- ²³⁶Y. Zhu, J.-H. Yu, G. Yu, Y. Ye, B. Tobias, A. Diallo, G. Kramer, Y. Ren, C. W. Domier, X. Li, C. Luo, M. Chen, Y. Chen, and N. C. Luhmann, "W-band system-on-chip electron cyclotron emission imaging system on DIII-D," *Rev. Sci. Instrum.* **91**, 093504 (2020).
- ²³⁷Y. Zheng, G. Yu, J. Chen, Y. Chen, Y. Zhu, C. Domier, D. Brower, and N. Luhmann, "System-on-chip integrated circuit technology applications on the DIII-D tokamak for multi-field measurements," *J. Instrum.* **17**, C01013 (2022).
- ²³⁸Y. Zhu, Y. Ying, J.-H. Yu, Y. Ye, J. Dannenberg, X. Liu, and N. Luhmann, "System-on-Chip approach millimeter-wave imaging development for fusion plasma diagnostics," in *2022 47th International Conference on Infrared, Millimeter and Terahertz Waves (IRMMW-THz)* (IEEE, Delft, Netherlands, 2022), pp. 1–2.
- ²³⁹X. Li, P.-J. Chen, Y. Chen, R. Hu, C.-C. Lin, C.-H. Yang, H. Yu, S. Qiu, C. Domier, G. Yu, and Y. Zhu, "GaN-based W-band receiver chip development for fusion plasma diagnostics," *J. Instrum.* **19**, P06046 (2024).
- ²⁴⁰D. Ji, B. Ercan, and S. Chowdhury, "Experimental determination of impact ionization coefficients of electrons and holes in gallium nitride using homo-junction structures," *Appl. Phys. Lett.* **115**, 073503 (2019).
- ²⁴¹G. H. Lee, J. S. Lee, D. H. Kim, S. H. Nashuha, M. J. Kim, B. C. Min, J. H. Lee, W. C. Lee, G. S. Yun, T. G. Kim, B. T. Kim, H. C. Choi, H. K. Park, Y. K. In, and K. W. Kim, "W-band modular antenna/detector array for the electron cyclotron emission imaging system in KSTAR," *Appl. Sci.* **12**, 2431 (2022).
- ²⁴²D. Wagner, W. Kasperek, F. Leuterer, F. Monaco, T. Ruess, H. Schutz, J. Stober, and M. Thumm, "Compact multi-frequency sub-THz notch filters with rejection within and above the pass band," in *2022 47th International Conference on Infrared, Millimeter and Terahertz Waves (IRMMW-THz)* (IEEE, Delft, Netherlands, 2022), pp. 1–2.
- ²⁴³S. Qiu, L. Himes, C. Domier, X. Tang, X. Liu, F. Hu, G. Yu, X. Li, Y. Zhu, N. Luhmann, J. Xie, and Z. Wu, "Design of a 140 GHz waveguide notch filter for millimeter-wave receiver module protection in fusion plasma diagnostics," *Rev. Sci. Instrum.* **95**, 023503 (2024).
- ²⁴⁴X. Li, Y. Zhu, G. Yu, J. Cao, G. Xu, and N. Luhmann, "High level of integration of front-end imaging optics system for electron cyclotron emission imaging diagnostics on the DIII-D tokamak," *Fusion Eng. Des.* **172**, 112915 (2021).
- ²⁴⁵M. Jiang, Y. Zhu, X. Yu, Z. Shi, N. Luhmann, Z. Yang, W. Deng, Z. Yang, Y. Zhou, and R. Tong, "Optical design and synthetic analysis of the electron cyclotron emission imaging diagnostic of HL-2M tokamak," *Fusion Eng. Des.* **191**, 113570 (2023).
- ²⁴⁶H. Zhao, T. Zhou, Y. Liu, A. Ti, B. Ling, X. Feng, A. Liu, C. Zhou, and L. Hu, "A multi-channel correlation ECE system for electron temperature fluctuation measurement on EAST tokamak," *Fusion Eng. Des.* **149**, 111336 (2019).
- ²⁴⁷R. Xie, S. Houshmandyar, and M. E. Austin, "Active control of electron cyclotron emission radiometer channel frequencies for improved electron temperature measurements," *Rev. Sci. Instrum.* **92**, 033530 (2021).
- ²⁴⁸J. B. Kim, W. Lee, G. S. Yun, H. K. Park, C. W. Domier, and N. C. Luhmann, "Data acquisition and processing system of the electron cyclotron emission imaging system of the KSTAR tokamak," *Rev. Sci. Instrum.* **81**, 10D931 (2010).
- ²⁴⁹C. Li, T. Lan, Y. Wang, J. Liu, J. Xie, T. Lan, H. Li, and H. Qin, "An automatic data cleaning procedure for electron cyclotron emission imaging on EAST tokamak using machine learning algorithm," *J. Instrum.* **13**, P10029 (2018).
- ²⁵⁰Z. Zhang, Z. Yang, Y. Gao, X. Zha, Z. Jin, Q. Luo, W. Zheng, Q. Zhao, N. Wang, L. Gao, and Y. Pan, "Realization of automatic data cleaning and feedback conditioning for J-TEXT ECEI signals based on machine learning," *Fusion Eng. Des.* **177**, 113065 (2022).
- ²⁵¹Y. Zhu, J. Xiao, T. Lan, and J. Xie, "A spectral clustering based method for automatic plasma pattern identification in electron cyclotron emission imaging on EAST Tokamak," *J. Instrum.* **15**, P07006 (2020).
- ²⁵²J. Decker, "Electron Bernstein wave current drive modeling in toroidal plasma confinement," Ph.D. thesis (Massachusetts Institute of Technology, 2005).
- ²⁵³A. K. Ram, J. Decker, and Y. Peysson, "On electron Bernstein waves in spherical tori," *J. Plasma Phys.* **71**, 675–693 (2005).
- ²⁵⁴J. Urban, J. Decker, Y. Peysson, J. Preinhaelter, V. Shevchenko, G. Taylor, L. Vahala, and G. Vahala, "A survey of electron Bernstein wave heating and current drive potential for spherical tokamaks," *Nucl. Fusion* **51**, 083050 (2011).
- ²⁵⁵V. F. Shevchenko, M. De Bock, S. J. Freethy, A. N. Saveliev, and R. G. L. Vann, "Two-dimensional studies of electron Bernstein wave emission in MAST," *Fusion Sci. Technol.* **59**, 663–669 (2011).
- ²⁵⁶S. Alberti, G. Arnoux, L. Porte, J.-P. Hogge, B. Marletaz, P. Marmillod, Y. Martin, S. Nowak, and T. Team, "Third-harmonic, top-launch, ECRH experiments on TCV tokamak," *Nucl. Fusion* **45**, 1224–1231 (2005).
- ²⁵⁷T. Shimozuma, H. Igami, S. Kubo, Y. Yoshimura, H. Takahashi, M. Osakabe, T. Mutoh, M. Nishiura, H. Idei, K. Nagasaki, N. Marushchenko, Y. Turkin, and The LHD Experiment Group, "Optimization of the high harmonic ECRH scenario to extend a heating plasma parameter range in LHD," *Nucl. Fusion* **55**, 063035 (2015).
- ²⁵⁸N. B. Marushchenko, P. Aleynikov, C. D. Beidler, A. Dinklage, J. Geiger, P. Helander, H. P. Laqua, H. Maassberg, Y. Turkin, and W7-X Team, "Reduced field Scenario with X3 heating in W7-X," *EPJ Web Conf.* **203**, 01006 (2019).
- ²⁵⁹J. Stober, M. Reisner, C. Angioni, A. B. Navarro, V. Bobkov, A. Bock, G. Denisov, E. Fable, R. Fischer, G. Gantenbein, L. Gil, T. Görler, V. Igochine, W. Kasperek, F. Leuterer, A. Litvak, R. McDermott, A. Meier, F. Monaco, M. Münich, V. Nichiporenko, B. Plaum, U. Plank, E. Poli, L. Popov, T. Pütterich, T. Scherer, M. Schubert, W. Suttrop, E. Tai, M. Thumm, D. Wagner, and H. Zohm, "Exploring fusion-reactor physics with high-power electron cyclotron resonance heating on ASDEX Upgrade," *Plasma Phys. Controlled Fusion* **62**, 024012 (2020).
- ²⁶⁰H. P. Laqua, "Electron Bernstein wave heating and diagnostic," *Plasma Phys. Controlled Fusion* **49**, R1–R42 (2007).
- ²⁶¹J. Preinhaelter and V. Kopecký, "Penetration of high-frequency waves into a weakly inhomogeneous magnetized plasma at oblique incidence and their transformation to Bernstein modes," *J. Plasma Phys.* **10**(1), 1 (1973).
- ²⁶²D. B. Batchelor and T. S. Bigelow, "Electron cyclotron heating and current drive approach for low-temperature startup plasmas using O-X-EBW mode conversion," in *AIP Conference Proceedings* (AIP, Savannah, GA, 1997), pp. 215–218.
- ²⁶³F. R. Hansen, J. P. Lynov, C. Maroli, and V. Petrillo, "Full-wave calculations of the O-X mode conversion process," *J. Plasma Phys.* **39**, 319 (1988).
- ²⁶⁴E. Mjølhus, "Linear conversion in a magnetized plasma with density gradient parallel to the magnetic field," *J. Plasma Phys.* **30**, 179 (1983).
- ²⁶⁵S. J. Diem, G. Taylor, J. B. Caughman, P. C. Efthimion, H. Kugel, B. P. LeBlanc, C. K. Phillips, J. Preinhaelter, S. A. Sabbagh, and J. Urban, "Collisional damping of electron Bernstein waves and its mitigation by evaporated lithium conditioning in spherical-tokamak plasmas," *Phys. Rev. Lett.* **103**, 015002 (2009).
- ²⁶⁶M. G. Senstius, S. K. Nielsen, R. G. Vann, and S. K. Hansen, "Particle-in-cell simulations of parametric decay instabilities at the upper hybrid layer of fusion plasmas to determine their primary threshold," *Plasma Phys. Controlled Fusion* **62**, 025010 (2020).
- ²⁶⁷A. K. Ram and S. D. Schultz, "Excitation, propagation, and damping of electron Bernstein waves in tokamaks," *Phys. Plasmas* **7**, 4084 (2000).
- ²⁶⁸F. Volpe, H. P. Laqua, and W7-AS Team, "BXO mode-converted electron Bernstein emission diagnostic (invited)," *Rev. Sci. Instrum.* **74**, 1409–1413 (2003).

- ²⁶⁹J. B. O. Caughman, Á. Fernández, Á. Cappa, F. Castejón, J. M. Garcia-Regaña, D. A. Rasmussen, and J. B. Wilgen, "Initial electron Bernstein wave emission measurements on the TJ-II stellarator," *Fusion Sci. Technol.* **57**, 41–47 (2010).
- ²⁷⁰M. Otte, H. P. Laqua, E. Chlechowicz, M. Glaubitz, S. Marsen, Y. Y. Podoba, T. Stange, F. Wagner, R. Wolf, and D. Zhang, "Electron Bernstein waves at the WEGA stellarator—Heating and emission," *Plasma Fusion Res.* **5**, S2011 (2010).
- ²⁷¹K. Nagasaki, Y. Kato, Y. Oka, H. Igami, T. Minami, S. Kado, S. Kobayashi, S. Ohshima, Y. Nakamura, A. Ishizawa, T. Mizuuchi, H. Okada, S. Konoshima, R. Matoike, A. Iwata, M. Luo, P. Zhang, C. Wang, Y. Kondo, and N. Marushchenko, "Electron temperature measurement using electron Bernstein emission in Heliotron J," in *Proceedings of the 47th EPS Conference on Plasma Physics (ECA, Sitges, Spain, 2021)*, Vol. 45A, p. P5.1004.
- ²⁷²G. Taylor, P. Efthimion, B. Jones, T. Munsat, J. Spaleta, J. Hosea, R. Kaita, R. Majeski, and J. Menard, "Electron Bernstein wave electron temperature profile diagnostic (invited)," *Rev. Sci. Instrum.* **72**, 285–292 (2001).
- ²⁷³S. Shiraiwa, Y. Nagashima, M. Ushigome, T. Yamada, T. Taniguchi, S. Ohara, K. Yamagishi, H. Kasahara, D. Iijima, Y. Kobori, T. Nishi, M. Aramasu, A. Ejiri, and Y. Takase, "Electron Bernstein wave emission diagnostic assisted by reflectometry on TST-2 spherical tokamak," *Rev. Sci. Instrum.* **74**, 1453–1456 (2003).
- ²⁷⁴J. Zajac, J. Preinhaelter, J. Urban, M. Aftanas, P. Bílková, P. Böhm, V. Fuchs, S. Nanobashvili, V. Weinzettl, and F. Žáček, "First results from EBW emission diagnostics on COMPASS," *Rev. Sci. Instrum.* **83**, 10E327 (2012).
- ²⁷⁵A. Mueck, Y. Camenen, S. Coda, L. Curchod, T. P. Goodman, H. P. Laqua, A. Pochelon, L. Porte, V. S. Udintsev, F. Volpe, and TCV Team, "Electron Bernstein wave heating and emission in the TCV tokamak," *Fusion Sci. Technol.* **52**, 221–229 (2007).
- ²⁷⁶P. K. Chattopadhyay, J. K. Anderson, T. M. Biewer, D. Craig, C. B. Forest, R. W. Harvey, and A. P. Smirnov, "Electron Bernstein wave emission from an overdense reversed field pinch plasma," *Phys. Plasmas* **9**, 752–755 (2002).
- ²⁷⁷W. Bin, A. Bruschi, O. D'Arcangelo, C. Galperti, G. Granucci, A. Moro, S. Nowak, and G. Pucella, "Feasibility study of O–X coupling for overdense plasma heating through O–X–B mode conversion in FTU," *Nucl. Fusion* **53**, 083020 (2013).
- ²⁷⁸S. Freethy, L. Figini, M. Henderson, H. El-Haroun, B. Eliason, S. Gibson, K. Kirov, A. Köhn-Seemann, I. Konoplev, S. Saarelma, R. Sharma, D. Speirs, R. Vann, H. Webster, T. Wilson, and the STEP Team, "Microwave current drive for STEP and MAST Upgrade," in *EPT Web of Conferences*, edited by E. Poli, Y. Liu, and V. Udintsev (EDP Sciences, 2023), Vol. 277, p. 04001.
- ²⁷⁹S. J. Freethy, V. F. Shevchenko, and R. G. L. Vann, "Optimization of wide field interferometric arrays via simulated annealing of a beam efficiency function," *IEEE Trans. Antennas Propag.* **60**, 5442–5446 (2012).
- ²⁸⁰V. F. Shevchenko, R. G. L. Vann, S. J. Freethy, and B. K. Huang, "Synthetic aperture microwave imaging with active probing for fusion plasma diagnostics," *J. Instrum.* **7**, P10016 (2012).
- ²⁸¹A. R. Thompson, J. M. Moran, and G. W. Swenson, *Interferometry and Synthesis in Radio Astronomy*, Astronomy and Astrophysics Library (Springer International Publishing, Cham, 2017).
- ²⁸²S. Freethy, "Synthetic aperture imaging of B–X–O mode conversion," Ph.D. thesis (University of York, 2012).
- ²⁸³B. HUANG, "Development of FPGAs controlled diagnostics on the MAST fusion reactor," Doctoral dissertation (Durham University, 2013).
- ²⁸⁴H. Idei, M. Fukuyama, S. Sakai, K. Mishra, K. Nishimura, R. Ikezoe, T. Onchi, T. Ido, and K. Hanada, "Adaptive Capon beamforming for lensless electron cyclotron emission imaging with high spatial resolution," *Rev. Sci. Instrum.* **93**, 103531 (2022).
- ²⁸⁵S. J. Freethy, B. K. Huang, V. F. Shevchenko, and R. G. L. Vann, "Lensless passive and active microwave imaging on MAST," *Plasma Phys. Controlled Fusion* **55**, 124010 (2013).
- ²⁸⁶M. I. Skolnik, *Introduction to Radar Systems*, 3rd ed., McGraw-Hill Electrical Engineering Series (McGraw Hill, Boston, MA; Burr Ridge, IL; Dubuque, IA, 2001).
- ²⁸⁷G. Breit and M. A. Tuve, "A test of the existence of the conducting layer," *Phys. Rev.* **28**, 554–575 (1926).
- ²⁸⁸A. I. Anisimov, N. I. Vinogradov, V. E. Golant, and B. P. Konstantinov, "Method of investigating electron spatial distribution in a plasma," *Sov. Phys.* **5**, 939 (1961).
- ²⁸⁹F. Simonet, "Measurement of electron density profile by microwave reflectometry on tokamaks," *Rev. Sci. Instrum.* **56**, 664–669 (1985).
- ²⁹⁰C. Laviron, A. J. H. Donné, M. E. Manso, and J. Sanchez, "Reflectometry techniques for density profile measurements on fusion plasmas," *Plasma Phys. Controlled Fusion* **38**, 905–936 (1996).
- ²⁹¹E. Mazzucato, "Microwave reflectometry for magnetically confined plasmas," *Rev. Sci. Instrum.* **69**, 2201–2217 (1998).
- ²⁹²G.-C. Hsieh and J. Hung, "Phase-locked loop techniques. A survey," *IEEE Trans. Ind. Electron.* **43**, 609–615 (1996).
- ²⁹³P. Varela, M. Manso, A. Silva, and T. C. Team, and T. A. U. Team, "Review of data processing techniques for density profile evaluation from broadband FM-CW reflectometry on ASDEX Upgrade," *Nucl. Fusion* **46**, S693–S707 (2006).
- ²⁹⁴R. B. Morales, S. Hacquin, S. Heuraux, and R. Sabot, "New density profile reconstruction methods in X-mode reflectometry," *Rev. Sci. Instrum.* **88**, 043503 (2017).
- ²⁹⁵H. Bottollier-Curtet and G. Ichtchenko, "Microwave reflectometry with the extraordinary mode on tokamaks: Determination of the electron density profile of Petula-B," *Rev. Sci. Instrum.* **58**, 539–546 (1987).
- ²⁹⁶L. Zeng, W. A. Peebles, E. J. Doyle, T. L. Rhodes, and G. Wang, "Relativistic effects on reconstruction of density profiles via reflectometry in ITER and potential for electron temperature measurements," *Plasma Phys. Controlled Fusion* **49**, 1277–1287 (2007).
- ²⁹⁷G. Kramer, R. Nazikian, E. Valeo, R. Budny, C. Kessel, and D. Johnson, "2D reflectometer modelling for optimizing the ITER low-field side X-mode reflectometer system," *Nucl. Fusion* **46**, S846–S852 (2006).
- ²⁹⁸C. A. J. Hugenholtz and S. H. Heijnen, "Pulse radar technique for reflectometry on thermonuclear plasmas," *Rev. Sci. Instrum.* **62**, 1100–1101 (1991).
- ²⁹⁹T. Tokuzawa, K. Kawahata, R. O. Pavlichenko, K. Tanaka, and A. Ejiri, "Pulsed radar reflectometry on the LHD," *Rev. Sci. Instrum.* **72**, 328–331 (2001).
- ³⁰⁰V. F. Shevchenko, A. A. Petrov, and V. G. Petrov, "Pulse radar reflectometry for fusion plasma diagnostics," *Int. J. Infrared Millimeter Waves* **14**, 1755–1768 (1993).
- ³⁰¹C. W. Domier, N. C. Luhmann, A. E. Chou, W.-M. Zhang, and A. J. Romanowsky, "Ultrashort-pulse reflectometry (invited)," *Rev. Sci. Instrum.* **66**, 399–401 (1995).
- ³⁰²P. Molina Cabrera, S. Coda, L. Porte, A. Smolders, and TCV Team, "V-band nanosecond-scale pulse reflectometer diagnostic in the TCV tokamak," *Rev. Sci. Instrum.* **90**, 123501 (2019).
- ³⁰³X. Li, R. Chen, G. Xu, C. Domier, X. Liu, Y. Zhang, T. Zhou, Y. Zhu, G. Yu, S. Qiu, H. Yu, and N. C. Luhmann, "Development of ultra-short pulse reflectometry on the Experimental Advanced Superconducting Tokamak (EAST)," *Rev. Sci. Instrum.* **95**, 073519 (2024).
- ³⁰⁴S. Hacquin, S. Heuraux, M. Colin, and G. Leclert, "Use of dispersive effects for density profile reconstruction from pulse radar reflectometry measurements alone," *Plasma Phys. Controlled Fusion* **42**, 347–358 (2000).
- ³⁰⁵V. Zhuravlev, J. Sanchez, E. De La Luna, M. Hirsch, T. Estrada, B. Brañas, M. Frances, T. Geist, H. Hartfuss, G. Hanson, J. Wilgen, and R. Kaita, "Amplitude modulation reflectometry for density profile measurements," *Fusion Eng. Des.* **34**–**35**, 421–424 (1997).
- ³⁰⁶Y. Lin, J. Irby, P. Stek, I. Hutchinson, J. Snipes, R. Nazikian, and M. McCarthy, "Upgrade of reflectometry profile and fluctuation measurements in Alcator C-Mod," *Rev. Sci. Instrum.* **70**, 1078–1081 (1999).
- ³⁰⁷T. Estrada, J. Sánchez, B. V. Milligen, L. Cupido, A. Silva, M. E. Manso, and V. Zhuravlev, "Density profile measurements by AM reflectometry in TJ-II," *Plasma Phys. Controlled Fusion* **43**, 1535–1545 (2001).
- ³⁰⁸Z. Shi, W. Zhong, and M. Jiang, "Progress of microwave diagnostics development on the HL-2A tokamak," *Plasma Sci. Technol.* **20**, 094007 (2018).
- ³⁰⁹G. Conway, "Microwave reflectometry for fusion plasma diagnosis," *Nucl. Fusion* **46**, S665–S669 (2006).
- ³¹⁰R. Sabot, "Reflectometry: A reliable and sensitive plasma diagnostic for density profile and turbulence measurements on Tore-Supra," in *AIP Conference Proceedings (AIP, Opole-Turawa, Poland, 2006)*, Vol. 812, pp. 112–119.
- ³¹¹F. Clairet, C. Bottereau, A. Medvedeva, D. Molina, G. D. Conway, A. Silva, and U. Stroth, ASDEX Upgrade Team, Tore Supra Team, and EUROfusion MST1 Team, "1 μ s broadband frequency sweeping reflectometry for plasma density and fluctuation profile measurements," *Rev. Sci. Instrum.* **88**, 113506 (2017).

- ³¹²A. Sirinelli, B. Alper, C. Bottereau, F. Clairet, L. Cupido, J. Fessey, C. Hogben, L. Meneses, G. Sandford, M. J. Walsh, and J.-E. Contributors, "Multiband reflectometry system for density profile measurement with high temporal resolution on JET tokamak," *Rev. Sci. Instrum.* **81**, 10D939 (2010).
- ³¹³O. Bogar, J. Zajac, F. Zacek, M. Varavin, M. Hron, R. Panek, and A. Silva, "Microwave reflectometer for density profile and turbulence measurements on the COMPASS tokamak," *Rev. Sci. Instrum.* **91**, 013515 (2020).
- ³¹⁴R. Sabot, F. Clairet, C. Honoré, C. Bottereau, J.-M. Chareau, F. Gabillet, P. Hennequin, S. Heurax, G. Leclert, A. Sirinelli, A. Truc, and L. Vermare, "Advances of reflectometry on Tore-Supra: From edge density profile to core density fluctuations," *Int. J. Infrared Millimeter Waves* **25**, 229–246 (2004).
- ³¹⁵Y. Wang, X. Gao, B. Ling, S. Zhang, T. Zhang, X. Han, S. Liu, Z. Liu, Y. Liu, and A. Ti, "Development of the W-band density profile and fluctuation reflectometer on EAST," *Fusion Eng. Des.* **88**, 2950–2955 (2013).
- ³¹⁶S. Zhang, X. Gao, B. Ling, Y. Wang, T. Zhang, X. Han, Z. Liu, J. Bu, and J. Li, "Density profile and fluctuation measurements by microwave reflectometry on EAST," *Plasma Sci. Technol.* **16**, 311–315 (2014).
- ³¹⁷Z. Yang, M. Jiang, Z. Shi, W. Zhong, P. Shi, Y. Liu, J. Wen, and K. Fang, "Application of dynamic calibration and control waveform optimization techniques in the fast sweeping reflectometer upgrade on the HL-2A tokamak," *J. Instrum.* **16**, P05020 (2021).
- ³¹⁸Z. Jin and Z. Yang, "Measurement of plasma density profile for edge plasma on J-TEXT Tokamak," in *2023 IEEE 4th China International Youth Conference on Electrical Engineering (CIYCEE)* (IEEE, Chengdu, China, 2023), pp. 1–6.
- ³¹⁹A. Silva, M. Manso, P. Varela, L. Cupido, L. Meneses, and ASDEX Upgrade Team, "Recent improvements of the broadband FMCW reflectometry system for density profile measurements on ASDEX Upgrade," *Rev. Sci. Instrum.* **77**, 10E932 (2006).
- ³²⁰S.-H. Seo and K. D. Lee, "Development of frequency modulation reflectometer for KSTAR tokamak: Data analysis based on Gaussian derivative wavelet," *Rev. Sci. Instrum.* **83**, 10E342 (2012).
- ³²¹G. Wang, E. J. Doyle, W. A. Peebles, L. Zeng, T. L. Rhodes, S. Kubota, X. Nguyen, and N. A. Crocker, "High-resolution dual-polarization frequency modulated reflectometer density profile measurements on DIII-D," *Rev. Sci. Instrum.* **75**, 3800–3803 (2004).
- ³²²G. Vayakis, T. Ando, N. Bretz, L. De Kock, A. J. H. Donné, E. J. Doyle, J. Irby, E. Martin, M. Manso, A. Mase, J. Sanchez, V. A. Vershkov, D. Wagner, C. I. Walker, ITER Joint Central Team, and Home Teams, "Overview of the ITER reflectometry diagnostic systems," in *Diagnostics for Experimental Thermonuclear Fusion Reactors 2*, edited by P. E. Stott, G. Gorini, P. Prandoni, and E. Sindoni (Springer US, Boston, MA, 1998), pp. 97–106.
- ³²³T. L. Rhodes, W. A. Peebles, L. Zeng, V. Hall-Chen, K. Ronald, S. Kubota, Y. Meng, R. Lantsov, C. M. Michael, N. A. Crocker, and R. Scannell, "Design of a low frequency, density profile reflectometer system for the MAST-U spherical tokamak," *Rev. Sci. Instrum.* **95**, 083528 (2024).
- ³²⁴V. Weinzettl, P. Bilkova, I. Duran, M. Hron, R. Panek, T. Markovic, M. Varavin, J. Cavalier, K. Kovarik, A. Torres, E. Matveeva, P. Böhm, O. Ficker, J. Horacek, J. Cerovsky, J. Zajac, J. Adamek, M. Dimitrova, M. Imrisek, M. Sos, E. Tomesova, P. Vondracek, K. Mikszuta-Michalik, J. Svoboda, D. Naydenkova, K. Bogar, J. Caloud, V. Ivanov, S. Lukes, A. Podolnik, O. Bogar, S. Entler, A. Havranek, J. Preinhaelter, F. Jaulmes, R. Dejarnac, V. Balner, V. Veselovsky, P. Belina, M. Kral, J. Gerardin, J. Vlcek, M. Tadros, P. Turjanica, V. Kindl, J. Reboun, W. Rowan, S. Houshmandyar, M. Scholz, J. Bielecki, D. Makowski, M. Chernyshova, and D. Cipciar, "Development of the diagnostic tools for the COMPASS-U tokamak and plans for the first plasma," *Fusion Eng. Des.* **191**, 113545 (2023).
- ³²⁵Y. Lin, V. Nikolaeva, D. Hachmeister, E. Kowalski, and M. L. Reinke, "Edge scanning reflectometry for density profile measurement on the SPARC tokamak," *Rev. Sci. Instrum.* **95**, 083540 (2024).
- ³²⁶C. Laviron, "Comparison of different reflectometry techniques," in *Diagnostics for Experimental Thermonuclear Fusion Reactors*, edited by P. E. Stott, G. Gorini, and E. Sindoni (Springer US, Boston, MA, 1996), pp. 107–116.
- ³²⁷J. Santos, L. Guimarães, M. Zilker, W. Treutterer, and M. Manso, "Reflectometry-based plasma position feedback control demonstration at ASDEX Upgrade," *Nucl. Fusion* **52**, 032003 (2012).
- ³²⁸P. Lourenço, J. Santos, A. Havránek, O. Bogar, J. Havlíček, J. Zajac, A. Silva, A. Batista, M. Hron, R. Pánek, and H. Fernandes, "Real-time plasma position reflectometry system development and integration on COMPASS tokamak," *Fusion Eng. Des.* **160**, 112017 (2020).
- ³²⁹G. De Masi, R. Cavazzana, F. Ruffini, G. Marchiori, M. Moresco, R. Agnello, L. Cordaro, M. Bernardi, E. Giroto, A. Tiso, and S. Peruzzo, "Technology challenges and integration of the plasma position reflectometer in RFX-mod2," *Fusion Eng. Des.* **201**, 114257 (2024).
- ³³⁰J. Santos, A. Silva, F. Da Silva, Y. Nietiadi, R. Luís, J. Ferreira, G. De Masi, O. Tudisco, R. Cavazzana, P. Resende, J. Abrantes, S. Heurax, E. Ricardo, and T. Ribeiro, "Design and performance analysis of a High Field Side antenna for Plasma Position Reflectometry control on DTT," *Fusion Eng. Des.* **201**, 114275 (2024).
- ³³¹E. Ricardo, F. D. Silva, S. Heurax, and A. Silva, "Assessment of a multi-reflectometers positioning system for DEMO plasmas," *J. Instrum.* **14**, C08010 (2019).
- ³³²G. S. Li, Y. Yang, Y. M. Wang, T. F. Ming, X. Han, S. C. Liu, E. H. Wang, Y. K. Liu, W. J. Yang, G. Q. Li, Q. S. Hu, and X. Gao, "Preliminary consideration of CFETR ITER-like case diagnostic system," *Rev. Sci. Instrum.* **87**, 11D401 (2016).
- ³³³Y. Q. Shen, Z. C. Yang, W. L. Zhong, M. Jiang, Z. B. Shi, J. Santos, P. W. Shi, R. H. Tong, G. Q. Xue, Y. Zhou, J. Wen, X. Yu, W. C. Deng, S. Wang, Z. J. Yang, Z. Y. Chen, D. Li, X. Q. Zha, Z. Y. Jin, X. Xu, and M. Xu, "Plasma position measurements by O-mode and X-mode reflectometry systems in tokamak plasmas," *Rev. Sci. Instrum.* **94**, 063505 (2023).
- ³³⁴R. Nazikian, G. J. Kramer, and E. Valeo, "A tutorial on the basic principles of microwave reflectometry applied to fluctuation measurements in fusion plasmas," *Phys. Plasmas* **8**, 1840–1855 (2001).
- ³³⁵S. J. Zweben, J. A. Boedo, O. Grulke, C. Hidalgo, B. LaBombard, R. J. Maqueda, P. Scarin, and J. L. Terry, "Edge turbulence measurements in toroidal fusion devices," *Plasma Phys. Controlled Fusion* **49**, S1–S23 (2007).
- ³³⁶A. E. Costley, P. Cripwell, R. Prentice, and A. C. C. Sips, "Recent developments in microwave reflectometry at JET (invited)," *Rev. Sci. Instrum.* **61**, 2823–2828 (1990).
- ³³⁷A. Krämer-Flecken, S. Soldatov, C. Busch, Y. Liang, M. V. Hellermann, R. Wolf, O. Zimmermann, and T. TEXTOR-Team, "Reflectometry measurements during operation of the dynamic ergodic divertor at TEXTOR," *Nucl. Fusion* **46**, S730–S742 (2006).
- ³³⁸A. Krämer-Flecken, S. Soldatov, Y. Xu, and T. Zhang, "Correlation reflectometry in fusion plasmas—An application at TEXTOR," *Plasma Phys. Controlled Fusion* **53**, 074020 (2011).
- ³³⁹G. D. Conway, "2D modelling of radial correlation reflectometry," *Plasma Phys. Controlled Fusion* **39**, 407–421 (1997).
- ³⁴⁰E. J. Valeo, G. J. Kramer, and R. Nazikian, "Two-dimensional simulations of correlation reflectometry in fusion plasmas," *Plasma Phys. Controlled Fusion* **44**, L1–L10 (2002).
- ³⁴¹G. Hanson, J. Harris, J. Wilgen, C. Thomas, S. Aceto, L. Baylor, J. Bell, B. Branas, J. Dunlap, A. England, C. Hidalgo, M. Murakami, D. Rasmussen, J. S. Sanz, J. Schwelberger, T. Uckan, and J. Zielinski, "Density fluctuation measurements in ATF using correlation reflectometry," *Nucl. Fusion* **32**, 1593–1608 (1992).
- ³⁴²A. Krämer-Flecken, S. Soldatov, H. R. Koslowski, and O. Zimmermann, "Properties of geodesic acoustic modes and the relation to density fluctuations," *Phys. Rev. Lett.* **97**, 045006 (2006).
- ³⁴³A. Krämer-Flecken, S. Soldatov, B. Vowinkel, and P. Müller, "Correlation reflectometry at TEXTOR," *Rev. Sci. Instrum.* **81**, 113502 (2010).
- ³⁴⁴A. V. Melnikov, V. A. Vershkov, L. G. Eliseev, S. A. Grashin, A. V. Gudozhnik, L. I. Krupnik, S. E. Lysenko, V. A. Mavrin, S. V. Perfilov, D. A. Shelukhin, S. V. Soldatov, M. V. Ufimtsev, A. O. Urazbaev, G. V. Oost, and L. G. Zimeleva, "Investigation of geodesic acoustic mode oscillations in the T-10 tokamak," *Plasma Phys. Controlled Fusion* **48**, S87–S110 (2006).
- ³⁴⁵N. Oyama, H. Takenaga, T. Suzuki, Y. Sakamoto, A. Isayama, and The Jt-60 Team, "Density fluctuation measurements using a frequency hopping reflectometer in JT-60U," *Plasma Fusion Res.* **6**, 1402014 (2011).
- ³⁴⁶G. D. Conway, G. Vayakis, J. A. Fessey, and D. V. Bartlett, "A reflectometer for fluctuation and correlation studies on the Joint European Torus tokamak," *Rev. Sci. Instrum.* **70**, 3921–3929 (1999).

- ³⁴⁷S. Hacquin, L. Meneses, L. Cupido, S. Sharapov, B. Alper, J. Fessey, A. Klein, D. Testa, and JET-EFDA Contributors, “X-mode reflectometry measurements in the JET plasma core region,” *Rev. Sci. Instrum.* **77**, 10E925 (2006).
- ³⁴⁸D. Prisiazhniuk, G. D. Conway, A. Krämer-Flecken, U. Stroth, and the ASDEX Upgrade Team, “Density fluctuation correlation measurements in ASDEX Upgrade using poloidal and radial correlation reflectometry,” *Plasma Phys. Controlled Fusion* **60**, 075003 (2018).
- ³⁴⁹H. M. Xiang, T. Zhang, F. Wen, H. Qu, M. F. Wu, K. N. Geng, G. S. Li, Y. M. Wang, X. Han, Z. X. Liu, F. B. Zhong, K. X. Ye, S. B. Zhang, and X. Gao, “Development of an ordinary mode multi-channel correlation reflectometer on EAST tokamak,” *Rev. Sci. Instrum.* **89**, 10H103 (2018).
- ³⁵⁰Z. Zhou, T. Zhang, M. Wu, K. Ye, F. Zhong, J. Huang, K. Geng, Y. Liu, G. Li, H. Xiang, Y. Wang, F. Wen, and S. Liu, “Experimental study of core and edge fluctuations by reflectometry on EAST tokamak,” *Plasma Sci. Technol.* **23**, 075101 (2021).
- ³⁵¹G. Li, T. Zhang, K. Geng, F. Wen, Z. Zhou, Z. Zhou, L. Yu, F. Zhong, K. Ye, S. Yang, J. Ma, S. Zhang, G. Li, and X. Gao, “Development of O-mode polarized V-band multichannel poloidal correlation reflectometry on EAST tokamak,” *IEEE Trans. Plasma Sci.* **52**, 423–430 (2024).
- ³⁵²M. Wu, F. Wen, H. Xiang, T. Zhang, G. Mao, Z. Liu, Y. Wang, G. Li, Y. Liu, K. Geng, F. Zhong, K. Ye, J. Huang, Z. Zhou, X. Han, S. Zhang, G. Zhuang, and X. Gao, “W-band multi-channel correlation reflectometry for core turbulence measurement on EAST,” *J. Instrum.* **15**, P12009 (2020).
- ³⁵³T. Windisch, A. Krämer-Flecken, J. Velasco, A. Könies, C. Nührenberg, O. Grulke, T. Klinger, and the W7-X Team, “Poloidal correlation reflectometry at W7-X: Radial electric field and coherent fluctuations,” *Plasma Phys. Controlled Fusion* **59**, 105002 (2017).
- ³⁵⁴A. Krämer-Flecken, S. Soldatov, Y. Xu, H. Arnichand, S. Hacquin, R. Sabot, and T. T. Team, “Long-range correlation properties of quasi-coherent modes at TEXTOR,” *New J. Phys.* **17**, 073007 (2015).
- ³⁵⁵C. P. Ritz, E. J. Powers, T. L. Rhodes, R. D. Bengtson, K. W. Gentle, H. Lin, P. E. Phillips, A. J. Wootton, D. L. Brower, N. C. Luhmann, W. A. Peebles, P. M. Schoch, and R. L. Hickok, “Advanced plasma fluctuation analysis techniques and their impact on fusion research (invited),” *Rev. Sci. Instrum.* **59**, 1739–1744 (1988).
- ³⁵⁶H. Thomsen, M. Endler, J. Bleuel, A. V. Chankin, S. K. Erents, G. F. Matthews, and Contributors to the EFDA-JET workprogramme, “Parallel correlation measurements in the scrape-off layer of the Joint European Torus,” *Phys. Plasmas* **9**, 1233–1240 (2002).
- ³⁵⁷T. L. Rhodes, J.-N. Leboeuf, R. D. Sydora, R. J. Groebner, E. J. Doyle, G. R. McKee, W. A. Peebles, C. L. Rettig, L. Zeng, and G. Wang, “Comparison of turbulence measurements from DIII-D low-mode and high-performance plasmas to turbulence simulations and models,” *Phys. Plasmas* **9**, 2141–2148 (2002).
- ³⁵⁸A. Krämer-Flecken, X. Han, M. Otte, G. Anda, S. A. Bozhenkov, D. Dunai, G. Fuchert, J. Geiger, O. Grulke, E. Pasch, E. R. Scott, E. Trier, M. Vécsei, T. Windisch, S. Zoletnik, and the W7-X Team, “Investigation of turbulence rotation in the SOL and plasma edge of W7-X for different magnetic configurations,” *Plasma Sci. Technol.* **22**, 064004 (2020).
- ³⁵⁹A. Krämer-Flecken, J. H. E. Proll, G. Weir, P. Costello, G. Fuchert, J. Geiger, S. Heurax, A. Knieps, A. Langenberg, S. Vaz Mendes, N. Pablant, E. Pasch, K. Rahbarnia, R. Sabot, L. Salazar, H. M. Smith, H. Thomsen, T. Windisch, H. M. Xiang, and the W7-X-Team, “Observation and characterisation of trapped electron modes in Wendelstein 7-X,” *Plasma Phys. Controlled Fusion* **67**, 025014 (2025).
- ³⁶⁰J. Connor, T. Fukuda, X. Garbet, C. Gormezano, V. Mukhovatov, M. Wakatani, T. I. D. Group, T. I. T. G. O. Transport, and I. B. Physics, “A review of internal transport barrier physics for steady-state operation of tokamaks,” *Nucl. Fusion* **44**, R1–R49 (2004).
- ³⁶¹M. Wu, Z. Liu, G. Li, X. Han, T. Zhang, Y. Li, T. Zhou, Y. Chao, S. Wang, X. Wu, K. Geng, H. Xiang, F. Zhong, K. Ye, J. Huang, Z. Zhou, S. Yang, F. Wen, Y. Wang, S. Zhang, G. Zhuang, X. Gao, and T. East Team, “Experimental study of the core instability before and after internal transport barrier formation in EAST,” *Nucl. Fusion* **63**, 016008 (2023).
- ³⁶²E. Holzhauser, M. Hirsch, T. Grossmann, B. Brañas, and F. Serra, “Theoretical and experimental investigation of the phase-runaway in microwave reflectometry,” *Plasma Phys. Controlled Fusion* **40**, 1869–1886 (1998).
- ³⁶³M. Hirsch, E. Holzhauser, J. Baldzuhn, B. Kurzan, and B. Scott, “Doppler reflectometry for the investigation of propagating density perturbations,” *Plasma Phys. Controlled Fusion* **43**, 1641–1660 (2001).
- ³⁶⁴G. D. Conway, J. Schirmer, S. Klenge, W. Suttrop, and E. Holzhauser, and T. A. U. Team, “Plasma rotation profile measurements using Doppler reflectometry,” *Plasma Phys. Controlled Fusion* **46**, 951–970 (2004).
- ³⁶⁵G. D. Conway, C. Angioni, F. Ryter, P. Sauter, and J. Vicente, “Mean and oscillating plasma flows and turbulence interactions across the L–H confinement transition,” *Phys. Rev. Lett.* **106**, 065001 (2011).
- ³⁶⁶E. Z. Gusakov and A. V. Surkov, “Spatial and wavenumber resolution of Doppler reflectometry,” *Plasma Phys. Controlled Fusion* **46**, 1143–1162 (2004).
- ³⁶⁷E. Blanco and T. Estrada, “Study of Doppler reflectometry capability to determine the perpendicular velocity and the k-spectrum of the density fluctuations using a 2D full-wave code,” *Plasma Phys. Controlled Fusion* **50**, 095011 (2008).
- ³⁶⁸M. Hirsch, J. Baldzuhn, B. Kurzan, and E. Holzhauser, “Doppler reflectometry for the investigation of poloidally propagating density perturbations,” Technical Report No. EUR-CEA-FC-1674 (International Atomic Energy Agency (IAEA), France, 1999).
- ³⁶⁹X. L. Zou, T. F. Seak, M. Paume, J.-M. Chareau, C. Bottereau, and G. Leclert, in *Proceedings of the 4th Reflectometry Workshop* (Cadarache, France, 1999).
- ³⁷⁰P. Hennequin, C. Honoré, A. Truc, A. Quéméneur, N. Lemoine, J.-M. Chareau, and R. Sabot, “Doppler backscattering system for measuring fluctuations and their perpendicular velocity on Tore Supra,” *Rev. Sci. Instrum.* **75**, 3881–3883 (2004).
- ³⁷¹T. Happel, T. Estrada, E. Blanco, V. Tribaldos, A. Cappa, and A. Bustos, “Doppler reflectometer system in the stellarator TJ-II,” *Rev. Sci. Instrum.* **80**, 073502 (2009).
- ³⁷²T. Tokuzawa, A. Ejiri, K. Kawahata, K. Tanaka, I. Yamada, M. Yoshinuma, K. Ida, and C. Suzuki, “Microwave Doppler reflectometer system in LHD,” *Rev. Sci. Instrum.* **83**, 10E322 (2012).
- ³⁷³T. Estrada, E. Sánchez, J. García-Regaña, J. Alonso, E. Ascasibar, I. Calvo, A. Cappa, D. Carralero, C. Hidalgo, M. Liniers, I. Pastor, J. Velasco, and the TJ-II Team, “Turbulence and perpendicular plasma flow asymmetries measured at TJ-II plasmas,” *Nucl. Fusion* **59**, 076021 (2019).
- ³⁷⁴J. Schirmer, G. D. Conway, E. Holzhauser, W. Suttrop, H. Zohm, and T. A. U. Team, “Radial correlation length measurements on ASDEX Upgrade using correlation Doppler reflectometry,” *Plasma Phys. Controlled Fusion* **49**, 1019–1039 (2007).
- ³⁷⁵J. Schirmer, G. Conway, H. Zohm, W. Suttrop, and T. A. U. Team, “The radial electric field and its associated shear in the ASDEX Upgrade tokamak,” *Nucl. Fusion* **46**, S780–S791 (2006).
- ³⁷⁶P. A. Molina Cabrera, W. Kasperek, T. Happel, H. Eixenberger, L. Kammerloher, P. Hennequin, K. Höfler, C. Honoré, and ASDEX Upgrade Team, “W-band tunable, multi-channel, frequency comb Doppler backscattering diagnostic in the ASDEX-Upgrade tokamak,” *Rev. Sci. Instrum.* **94**, 083504 (2023).
- ³⁷⁷J. C. Hillesheim, W. A. Peebles, T. L. Rhodes, L. Schmitz, T. A. Carter, P.-A. Gourdain, and G. Wang, “A multichannel, frequency-modulated, tunable Doppler backscattering and reflectometry system,” *Rev. Sci. Instrum.* **80**, 083507 (2009).
- ³⁷⁸W. A. Peebles, T. L. Rhodes, J. C. Hillesheim, L. Zeng, and C. Wannberg, “A novel, multichannel, comb-frequency Doppler backscatter system,” *Rev. Sci. Instrum.* **81**, 10D902 (2010).
- ³⁷⁹S. Chowdhury, N. A. Crocker, W. A. Peebles, T. L. Rhodes, L. Zeng, R. Lantsov, B. Van Compernelle, M. Brookman, R. I. Pinsker, and C. Lau, “A novel Doppler backscattering (DBS) system to simultaneously measure radio frequency plasma fluctuations and low frequency turbulence,” *Rev. Sci. Instrum.* **94**, 073504 (2023).
- ³⁸⁰S. Liu, C. Zhou, A. D. Liu, G. Zhuang, X. Feng, J. Zhang, X. M. Zhong, J. X. Ji, S. B. Zhang, H. Q. Liu, S. X. Wang, H. R. Fan, S. F. Wang, L. T. Gao, W. X. Shi, X. Y. Chen, and W. D. Liu, “An E-band multi-channel Doppler backscattering system on EAST,” *Rev. Sci. Instrum.* **94**, 123507 (2023).
- ³⁸¹J. Q. Hu, C. Zhou, A. D. Liu, M. Y. Wang, E. J. Doyle, W. A. Peebles, G. Wang, X. H. Zhang, J. Zhang, X. Feng, J. X. Ji, H. Li, T. Lan, J. L. Xie, W. X. Ding, W. D. Liu, and C. X. Yu, “An eight-channel Doppler backscattering system in the

- experimental advanced superconducting tokamak,” *Rev. Sci. Instrum.* **88**, 073504 (2017).
- ³⁸²X. Feng, A. D. Liu, C. Zhou, M. Y. Wang, J. Zhang, Z. Y. Liu, Y. Liu, T. F. Zhou, S. B. Zhang, D. F. Kong, L. Q. Hu, J. X. Ji, H. R. Fan, H. Li, T. Lan, J. L. Xie, W. Z. Mao, Z. X. Liu, W. X. Ding, G. Zhuang, and W. D. Liu, “Five-channel tunable W-band Doppler backscattering system in the experimental advanced superconducting tokamak,” *Rev. Sci. Instrum.* **90**, 024704 (2019).
- ³⁸³A. Ponomarenko, A. Yashin, G. Kurskiy, V. Minaev, A. Petrov, Y. Petrov, N. Sakharov, and N. Zhiltsov, “First results of the implementation of the Doppler backscattering diagnostic for the investigation of the transition to H-mode in the spherical tokamak Globus-M2,” *Sensors* **23**, 830 (2023).
- ³⁸⁴N. Smith, K. Nagasaki, J. H. Prohl, H. Okada, T. Minami, S-i Kado, S. Kobayashi, S. Ohshima, S. Konoshima, T. Mizuuchi, Y. Nakamura, A. Ishizawa, T. Tomita, T. Fukuda, and Y. Kondo, “Measurement of radial correlation lengths of electron density fluctuations in Heliotron J using O-mode reflectometry,” *Plasma Fusion Res.* **15**, 1202054 (2020).
- ³⁸⁵Y. Kondo, S. Ohshima, D. Kuwahara, K. Inoshita, T. Fukuda, T. Minami, S. Kado, S. Kobayashi, S. Konoshima, T. Mizuuchi, H. Okada, T. Tomita, and K. Nagasaki, “Development of dual X-mode Doppler reflectometry system in Heliotron J,” *J. Instrum.* **17**, C05023 (2022).
- ³⁸⁶Y. Kondo, “Doppler reflectometry at Heliotron J” (2024).
- ³⁸⁷Z. Shi, W. Zhong, Z. Yang, A. Liang, J. Wen, M. Jiang, P. Shi, B. Fu, C. Chen, Z. Liu, X. Ding, and Q. Yang, “A multiplexer-based multi-channel microwave Doppler backward scattering reflectometer on the HL-2A tokamak,” *Rev. Sci. Instrum.* **89**, 10H104 (2018).
- ³⁸⁸R. Tong, Y. Zhou, W. Zhong, J. Wen, Z. Shi, X. Zou, A. Liang, Z. Yang, M. Jiang, X. Yu, and Y. Shen, “A new Q-band comb-based multi-channel microwave Doppler backward scattering diagnostic developed on the HL-3 tokamak,” *Plasma Sci. Technol.* **27**, 015102 (2025).
- ³⁸⁹X. H. Ren, Z. J. Yang, Z. B. Shi, Z. C. Yang, X. Q. Zha, Y. Gao, and Z. C. Zhang, “Development of a tunable multi-channel Doppler reflectometer on J-TEXT tokamak,” *Rev. Sci. Instrum.* **92**, 033545 (2021).
- ³⁹⁰T. Tokuzawa, H. Tsuchiya, T. Tsujimura, M. Emoto, H. Nakanishi, S. Inagaki, K. Ida, H. Yamada, A. Ejiri, K. Y. Watanabe, K. Oguri, T. Akiyama, K. Tanaka, I. Yamada, and LHD Experiment Group, “Microwave frequency comb Doppler reflectometer applying fast digital data acquisition system in LHD,” *Rev. Sci. Instrum.* **89**, 10H118 (2018).
- ³⁹¹T. Nasu, T. Tokuzawa, T. I. Tsujimura, K. Ida, M. Yoshinuma, T. Kobayashi, K. Tanaka, M. Emoto, S. Inagaki, A. Ejiri, and J. Kohagura, “Receiver circuit improvement of dual frequency-comb ka-band Doppler backscattering system in the large helical device (LHD),” *Rev. Sci. Instrum.* **93**, 113518 (2022).
- ³⁹²T. L. Rhodes, C. A. Michael, P. Shi, R. Scannell, S. Stormont, Q. Pratt, R. Lantsov, I. Fitzgerald, V. H. Hall-Chen, N. A. Crocker, and W. A. Peebles, “Design elements and first data from a new Doppler backscattering system on the MAST-U spherical tokamak,” *Rev. Sci. Instrum.* **93**, 113549 (2022).
- ³⁹³P. Shi, R. Scannell, J. Wen, Z. Shi, C. Michael, T. Rhodes, V. Hall-Chen, Z. Yang, M. Jiang, and W. Zhong, “First data and preliminary experimental results from a new Doppler backscattering system on the MAST-U spherical tokamak,” *J. Instrum.* **18**, C11022 (2023).
- ³⁹⁴P. Molina Cabrera, S. Coda, L. Porte, N. Offeddu, P. Lavanchy, M. Silva, M. Toussaint, and TCV Team, “V-band Doppler backscattering diagnostic in the TCV tokamak,” *Rev. Sci. Instrum.* **89**, 083503 (2018).
- ³⁹⁵V. V. Bulanin, L. G. Askinazi, A. A. Belokurov, V. A. Kornev, V. Lebedev, A. V. Petrov, A. S. Tukachinsky, M. I. Vildjunas, F. Wagner, and A. Y. Yashin, “GAM observation in the TUMAN-3M tokamak,” *Plasma Phys. Controlled Fusion* **58**, 045006 (2016).
- ³⁹⁶D. Carralero, T. Estrada, T. Windisch, J. Velasco, J. Alonso, M. Beurskens, S. Bozhnenkov, H. Damm, G. Fuchert, Y. Gao, M. Jakubowski, H. Nieman, N. Pablant, E. Pasch, G. Weir, and the Wendelstein 7-X Team, “Characterization of the radial electric field and edge velocity shear in Wendelstein 7-X,” *Nucl. Fusion* **60**, 106019 (2020).
- ³⁹⁷F. D. Silva, S. Heurax, E. Ricardo, A. Silva, and T. Ribeiro, “Benchmarking 2D against 3D FDTD codes in the assessment of reflectometry performance in fusion devices,” *J. Instrum.* **14**, C08004 (2019).
- ³⁹⁸A. Yashin, V. Bulanin, A. Petrov, and A. Ponomarenko, “Review of advanced implementation of Doppler backscattering method in Globus-M,” *Appl. Sci.* **11**, 8975 (2021).
- ³⁹⁹L. Schmitz, E. Ruskov, B. H. Deng, H. Gota, D. Gupta, M. Tuszewski, J. Douglass, W. A. Peebles, M. Binderbauer, and T. Tajima, “Multi-channel Doppler backscattering measurements in the C-2 field reversed configuration,” *Rev. Sci. Instrum.* **85**, 11D840 (2014).
- ⁴⁰⁰T. Tokuzawa, S. Inagaki, M. Inomoto, A. Ejiri, T. Nasu, T. I. Tsujimura, and K. Ida, “Application of dual frequency comb method as an approach to improve the performance of multi-frequency simultaneous radiation Doppler radar for high temperature plasma diagnostics,” *Appl. Sci.* **12**, 4744 (2022).
- ⁴⁰¹N. A. Crocker, W. A. Peebles, S. Kubota, J. Zhang, R. E. Bell, E. D. Fredrickson, N. N. Gorelenkov, B. P. LeBlanc, J. E. Menard, M. Podestà, S. A. Sabbagh, K. Tritz, and H. Yuh, “High spatial sampling global mode structure measurements via multichannel reflectometry in NSTX,” *Plasma Phys. Controlled Fusion* **53**, 105001 (2011).
- ⁴⁰²Z. Shi, W. Zhong, M. Jiang, Z. Yang, B. Zhang, P. Shi, W. Chen, J. Wen, C. Chen, B. Fu, Z. Liu, X. Ding, Q. Yang, and X. Duan, “A novel multi-channel quadrature Doppler backward scattering reflectometer on the HL-2A tokamak,” *Rev. Sci. Instrum.* **87**, 113501 (2016).
- ⁴⁰³R. Soga, T. Tokuzawa, K. Watanabe, K. Tanaka, I. Yamada, S. Inagaki, and N. Kasuya, “Developments of frequency comb microwave reflectometer for the interchange mode observations in LHD plasma,” *J. Instrum.* **11**, C02009 (2016).
- ⁴⁰⁴C. Lechte, G. D. Conway, T. Görler, C. Tröster-Schmid, and the ASDEX Upgrade Team, “X mode Doppler reflectometry k-spectral measurements in ASDEX Upgrade: Experiments and simulations,” *Plasma Phys. Controlled Fusion* **59**, 075006 (2017).
- ⁴⁰⁵D. Carralero, T. Estrada, E. Maragkoudakis, T. Windisch, J. Alonso, M. Beurskens, S. Bozhnenkov, I. Calvo, H. Damm, O. Ford, G. Fuchert, J. García-Regaña, N. Pablant, E. Sánchez, E. Pasch, J. Velasco, and T. Wendelstein 7-X Team, “An experimental characterization of core turbulence regimes in Wendelstein 7-X,” *Nucl. Fusion* **61**, 096015 (2021).
- ⁴⁰⁶D. Carralero, T. Estrada, E. Maragkoudakis, T. Windisch, J. A. Alonso, J. L. Velasco, O. Ford, M. Jakubowski, S. Lazerson, M. Beurskens, S. Bozhnenkov, I. Calvo, H. Damm, G. Fuchert, J. M. García-Regaña, U. Höfel, N. Marushchenko, N. Pablant, E. Sánchez, H. M. Smith, E. Pasch, and T. Stange, “On the role of density fluctuations in the core turbulent transport of Wendelstein 7-X,” *Plasma Phys. Controlled Fusion* **64**, 044006 (2022).
- ⁴⁰⁷Q. Pratt, T. Rhodes, C. Chrystal, and T. Carter, “Comparison of Doppler back-scattering and charge exchange measurements of $E \times B$ plasma rotation in the DIII-D tokamak under varying torque conditions,” *Plasma Phys. Controlled Fusion* **64**, 095017 (2022).
- ⁴⁰⁸K. Barada, T. L. Rhodes, K. H. Burrell, L. Zeng, L. Bardóczy, X. Chen, C. M. Muscatello, and W. A. Peebles, “Quasistationary plasma predator-prey system of coupled turbulence, drive, and sheared $E \times B$ flow during high performance DIII-D tokamak discharges,” *Phys. Rev. Lett.* **120**, 135002 (2018).
- ⁴⁰⁹K. Barada, T. L. Rhodes, K. H. Burrell, L. Zeng, X. Chen, M. E. Austin, L. Bardóczy, C. M. Muscatello, and W. A. Peebles, “Long-lived predator-prey dynamics in the pedestal of near-zero torque high performance DIII-D plasmas,” *Phys. Plasmas* **26**, 092501 (2019).
- ⁴¹⁰Q. Pratt, V. Hall-Chen, T. Neiser, R. Hong, J. Damba, T. Rhodes, K. Thome, J. Yang, S. Haskey, T. Cote, and T. Carter, “Density wavenumber spectrum measurements, synthetic diagnostic development, and tests of quasilinear turbulence modeling in the core of electron-heated DIII-D H-mode plasmas,” *Nucl. Fusion* **64**, 016001 (2024).
- ⁴¹¹V. H. Hall-Chen, F. I. Parra, and J. C. Hillesheim, “Beam model of Doppler backscattering,” *Plasma Phys. Controlled Fusion* **64**, 095002 (2022).
- ⁴¹²C. Zhou, A. Liu, J. Hu, M. Wang, X. Zhang, H. Li, C. Yu, W. Liu, T. Lan, and J. Xie, “Ray tracing for Doppler backscattering system in the experimental advanced superconducting tokamak,” *Plasma Sci. Technol.* **17**, 728–732 (2015).
- ⁴¹³A. Yashin, N. Teplova, G. Zadviyskiy, and A. Ponomarenko, “Modelling of backscattering off filaments using the code IPF-FD3D for the interpretation of Doppler backscattering data,” *Sensors* **22**, 9441 (2022).
- ⁴¹⁴V. H. Hall-Chen, J. Damba, F. I. Parra, Q. T. Pratt, C. A. Michael, S. Peng, T. L. Rhodes, N. A. Crocker, J. C. Hillesheim, R. Hong, S. Ni, W. A. Peebles, C. E. Png, and J. Ruiz Ruiz, “Validating and optimizing mismatch tolerance of Doppler backscattering measurements with the beam model (invited),” *Rev. Sci. Instrum.* **93**, 103536 (2022).

- ⁴¹⁵J. Damba, Q. Pratt, V. H. Hall-Chen, R. Hong, R. Lantsov, R. Ellis, and T. L. Rhodes, "Evaluation of a new DIII-D Doppler backscattering system for higher wavenumber measurement and signal enhancement," *Rev. Sci. Instrum.* **93**, 103549 (2022).
- ⁴¹⁶J. Damba, R. Hong, R. Lantsov, W. A. Peebles, and T. L. Rhodes, "A Q-band frequency tunable Doppler backscattering (DBS) system for pedestal and scrape-off layer density fluctuation and flow measurements in the DIII-D tokamak," *Rev. Sci. Instrum.* **95**, 083512 (2024).
- ⁴¹⁷X. H. Zhang, A. D. Liu, C. Zhou, J. Q. Hu, M. Y. Wang, X. Feng, C. H. Li, X. M. Yang, L. Sang, and J. Q. Ai, "Observation of geodesic acoustic mode in EAST using Doppler backscattering system," *Phys. Plasmas* **25**, 092503 (2018).
- ⁴¹⁸X. L. Zou, L. Colas, M. Paume, J. M. Chareau, L. Laurent, P. Devynck, and D. Gresillon, "Internal magnetic turbulence measurement in plasma by cross polarization scattering," *Phys. Rev. Lett.* **75**, 1090–1093 (1995).
- ⁴¹⁹N. Ohyaibu, T. Morisaki, S. Masuzaki, R. Sakamoto, M. Kobayashi, J. Miyazawa, M. Shoji, A. Komori, and O. Motojima, "Observation of stable superdense core plasmas in the large helical device," *Phys. Rev. Lett.* **97**, 055002 (2006).
- ⁴²⁰G. Motojima, H. Okada, H. Okazaki, S. Kobayashi, K. Nagasaki, R. Sakamoto, H. Yamada, S. Kado, S. Ohshima, T. Minami, N. Kenmochi, Y. Ohtani, Y. Nozaki, Y. Yonemura, Y. Nakamura, S. Konoshima, S. Yamamoto, T. Mizuchi, and K. Y. Watanabe, "High-density experiments with hydrogen ice pellet injection and analysis of pellet penetration depth in Heliotron J," *Plasma Phys. Controlled Fusion* **61**, 075014 (2019).
- ⁴²¹J. Baldzuhn, H. Damm, C. D. Beidler, K. McCarthy, N. Panadero, C. Biedermann, S. A. Bozhnikov, A. Dinklage, K. J. Brunner, G. Fuchert, Y. Kazakov, M. Beurskens, M. Dibon, J. Geiger, O. Grulke, U. Höfel, T. Klinger, F. Köchl, J. Knauer, G. Kocsis, P. Kornejew, P. T. Lang, A. Langenberg, H. Laqua, N. A. Pablant, E. Pasch, T. S. Pedersen, B. Ploekel, K. Rahbarnia, G. Schlisio, E. R. Scott, T. Stange, A. Von Stechow, T. Szepesi, Y. Turkin, F. Wagner, V. Winters, G. Wurden, and D. Zhang, "Enhanced energy confinement after series of pellets in Wendelstein 7-X," *Plasma Phys. Controlled Fusion* **62**, 055012 (2020).
- ⁴²²I. García-Cortés, K. J. McCarthy, T. Estrada, V. Tribaldos, D. Medina-Roque, B. Van Milligen, E. Ascasiar, R. Carrasco, A. A. Chmyga, R. García, J. Hernández-Sánchez, C. Hidalgo, A. S. Kozachek, F. Medina, M. A. Ochando, J. L. De Pablos, N. Panadero, and I. Pastor, "Enhanced confinement induced by pellet injection in the stellarator TJ-II," *Phys. Plasmas* **30**, 072506 (2023).
- ⁴²³G. Vayakis, C. Walker, F. Clairet, R. Sabot, V. Tribaldos, T. Estrada, E. Blanco, J. Sánchez, G. Denisov, V. Belousov, F. D. Silva, P. Varela, M. Manso, L. Cupido, J. Dias, N. Valverde, V. Vershkov, D. Shelukhin, S. Soldatov, A. Urazbaev, E. Y. Frolov, and S. Heurax, "Status and prospects for mm-wave reflectometry in ITER," *Nucl. Fusion* **46**, S836–S845 (2006).
- ⁴²⁴C. Muscatello, C. Anderson, J. Anderson, A. Basile, R. Boivin, M. Duco, D. Finkenthal, A. Gattuso, J. Klabacha, G. Kramer, M. LeSher, L. Meneses, G. Neilson, R. O'Neill, W. Peebles, R. Seraydarian, M. Sibilia, P. Slichta, D. Sieving, A. Sirinelli, G. Wang, W. Wang, and A. Zolfaghari, "Preliminary design overview and performance assessment of the ITER low-field side reflectometer," *Nucl. Fusion* **60**, 066005 (2020).
- ⁴²⁵D. Carralero, T. Happel, T. Estrada, T. Tokuzawa, J. Martínez, E. De La Luna, A. Cappa, and J. García, "A feasibility study for a Doppler reflectometer system in the JT-60SA tokamak," *Fusion Eng. Des.* **173**, 112803 (2021).
- ⁴²⁶S. Zhongbing, J. Min, C. Yonglong, W. Bin, Y. Yong, M. Lin, Z. Wulu, C. Wei, S. Peiwan, L. Zhetian, F. Binzhong, D. Xuantong, L. Yi, Y. Qingwei, and D. Xuru, "Development of microwave imaging reflectometry on the HL-2A tokamak," *Rev. Sci. Instrum.* **85**, 11D816 (2014).
- ⁴²⁷E. Mazzucato, "Microwave imaging reflectometry for the visualization of turbulence in tokamaks," *Nucl. Fusion* **41**, 203–213 (2001).
- ⁴²⁸T. Munsat, E. Mazzucato, H. Park, B. H. Deng, C. W. Domier, N. C. Luhmann, J. Wang, Z. G. Xia, A. J. H. Donné, and M. Van De Pol, "Microwave imaging reflectometer for TEXTOR (invited)," *Rev. Sci. Instrum.* **74**, 1426–1432 (2003).
- ⁴²⁹T. Munsat, E. Mazzucato, H. Park, C. W. Domier, N. C. Luhmann, A. J. H. Donné, and M. V. D. Pol, "Laboratory characterization of an imaging reflectometer system," *Plasma Phys. Controlled Fusion* **45**, 469–487 (2003).
- ⁴³⁰H. Park, E. Mazzucato, T. Munsat, C. W. Domier, M. Johnson, N. C. Luhmann, J. Wang, Z. Xia, I. G. J. Classen, A. J. H. Donné, and M. J. Van De Pol, "Simultaneous microwave imaging system for density and temperature fluctuation measurements on TEXTOR (invited)," *Rev. Sci. Instrum.* **75**, 3787–3792 (2004).
- ⁴³¹R. Sabot, J. C. Giacalone, Y. Nam, A. Berne, C. Brun, D. Elbèze, F. Faisse, L. Gargiulo, M. Kim, W. Lee, P. Lotte, H. K. Park, B. Santraine, G. Yun, and WEST Team, "Development of microwave imaging diagnostics for WEST tokamak," *J. Fusion Energy* **38**, 394–405 (2019).
- ⁴³²C. M. Muscatello, C. W. Domier, X. Hu, G. J. Kramer, N. C. Luhmann, X. Ren, P. Riemenschneider, A. Spear, B. J. Tobias, E. Valeo, and L. Yu, "Technical overview of the millimeter-wave imaging reflectometer on the DIII-D tokamak (invited)," *Rev. Sci. Instrum.* **85**, 11D702 (2014).
- ⁴³³Y. L. Zhu, J. L. Xie, C. X. Yu, Z. L. Zhao, B. X. Gao, D. X. Chen, W. D. Liu, W. Liao, C. M. Qu, C. Luo, X. Hu, A. G. Spear, N. C. Luhmann, C. W. Domier, M. Chen, X. Ren, and B. J. Tobias, "Millimeter-wave imaging diagnostics systems on the EAST tokamak (invited)," *Rev. Sci. Instrum.* **87**, 11D901 (2016).
- ⁴³⁴C. Qu, J. Xie, Y. Zhu, X. Xu, L. Zhang, Z. Li, G. Zhuang, and W. Liu, "The co-located arrangement of ECEI and MIR microwave imaging diagnostics on EAST tokamak," *J. Instrum.* **18**, C10018 (2023).
- ⁴³⁵W. Lee, J. Leem, D. J. Lee, M. J. Choi, H. K. Park, J. A. Lee, G. S. Yun, T. G. Kim, H. Park, K. W. Kim, and the KSTAR Team, "Quasi-coherent fluctuation measurement with the upgraded microwave imaging reflectometer in KSTAR," *Plasma Phys. Controlled Fusion* **60**, 115009 (2018).
- ⁴³⁶Y. Nagayama, A. Ejiri, Y. Takase, N. Tsujii, H. Nakanishi, M. Ohsuna, H. Tsuchiya, and S. Yamaguchi, "Measurement of electron density fluctuations using O-mode microwave imaging reflectometry in a TST-2 spherical tokamak," *Plasma Fusion Res.* **15**, 2402060 (2020).
- ⁴³⁷Y. Nagayama, D. Kuwahara, T. Yoshinaga, Y. Hamada, Y. Kogi, A. Mase, H. Tsuchiya, S. Tsuji-Iio, and S. Yamaguchi, "Development of 3D microwave imaging reflectometry in LHD (invited)," *Rev. Sci. Instrum.* **83**, 10E305 (2012).
- ⁴³⁸Y. Nagayama, S. Yamaguchi, Z. Shi, H. Tsuchiya, S. Hashimoto, N. Ito, M. Jiang, D. Kuwahara, and S. Sugito, "Observation of electron density fluctuations by using the O-mode microwave imaging reflectometry (O-MIR) in LHD," *Plasma Fusion Res.* **11**, 2402111 (2016).
- ⁴³⁹H. K. Park, N. C. Luhmann, A. J. H. Donné, B. Tobias, G. S. Yun, I. Classen, J. E. Boom, M. J. Choi, C. W. Domier, J. C. Kim, X. Kong, W. Lee, T. Liang, and T. Munsat, "2-D microwave imaging on TEXTOR, AUG, DIII-D, and KSTAR," in *Proceedings of the 37th EPS Conference on Plasma Physics (ECA, Dublin, Ireland, 2010)*, Vol. 34A, p. O5.129.
- ⁴⁴⁰X. Ren, M. Chen, X. Chen, C. Domier, N. Ferraro, G. Kramer, N. L. Jr., C. Muscatello, R. Nazikian, L. Shi, B. Tobias, and E. Valeo, "Microwave imaging reflectometry for the study of edge harmonic oscillations on DIII-D," *J. Instrum.* **10**, P10036 (2015).
- ⁴⁴¹X. Chen, K. Burrell, T. Osborne, W. Solomon, K. Barada, A. Garofalo, R. Groebner, N. Luhmann, G. McKee, C. Muscatello, M. Ono, C. Petty, M. Porkolab, T. Rhodes, J. Rost, P. Snyder, G. Staebler, B. Tobias, and Z. Yan, "Stationary QH-mode plasmas with high and wide pedestal at low rotation on DIII-D," *Nucl. Fusion* **57**, 022007 (2017).
- ⁴⁴²X. Chen, K. Burrell, N. Ferraro, T. Osborne, M. Austin, A. Garofalo, R. Groebner, G. Kramer, N. Luhmann, G. McKee, C. Muscatello, R. Nazikian, X. Ren, P. Snyder, W. Solomon, B. Tobias, and Z. Yan, "Rotational shear effects on edge harmonic oscillations in DIII-D quiescent H-mode discharges," *Nucl. Fusion* **56**, 076011 (2016).
- ⁴⁴³W. Lee, J. Lee, D.-J. Lee, and H. K. Park, "Study of the origin of quasi-coherent modes in low-density KSTAR ECH plasmas," *Nucl. Fusion* **61**, 016008 (2021).
- ⁴⁴⁴L. Zhang, J. Yu, J. Yang, G. Zhuang, and J. Xie, "The commissioning progress of microwave imaging reflectometer on EAST tokamak," *J. Instrum.* **20**, T03008 (2025).
- ⁴⁴⁵X. Liu, Y. Wang, T. Zhang, L. Gan, J. Nan, and X. Gao, "A compact multiband quasi-optical system for plasma detection," *IEEE Trans. Antennas Propag.* **68**, 4916–4924 (2020).
- ⁴⁴⁶R. Anwar, L. Mao, and H. Ning, "Frequency selective surfaces: A review," *Appl. Sci.* **8**, 1689 (2018).
- ⁴⁴⁷W. Liao, F. Gao, C. Qu, X. Xu, L. Zhang, Z. Li, S. Yang, C. Domier, Y. Zhu, G. Zhuang, W. Liu, N. L. Jr., and J. Xie, "Bench test of microwave imaging reflectometry system for EAST tokamak," *J. Instrum.* **15**, C03036 (2020).

- ⁴⁴⁸L. Zhang, Y. Han, J. Yu, C. Qu, and J. Xie, "A wavefront measurement platform for W band microwave," in *2022 47th International Conference on Infrared, Millimeter and Terahertz Waves (IRMMW-THz)* (IEEE, Delft, Netherlands, 2022), pp. 1–2.
- ⁴⁴⁹Z. Li, J. Xie, S. Yang, and G. Zhuang, "Development of synthetic diagnostics platform for microwave imaging diagnostics on EAST," in *2022 47th International Conference on Infrared, Millimeter and Terahertz Waves (IRMMW-THz)* (IEEE, Delft, Netherlands, 2022), pp. 1–2.
- ⁴⁵⁰D. Kuwahara, N. Ito, Y. Nagayama, T. Yoshinaga, S. Yamaguchi, M. Yoshikawa, J. Kohagura, S. Sugito, Y. Kogi, and A. Mase, "Development of horn antenna mixer array with internal local oscillator module for microwave imaging diagnostics," *Rev. Sci. Instrum.* **85**, 11D805 (2014).
- ⁴⁵¹Y. Nagayama, N. Ito, D. Kuwahara, H. Tsuchiya, and S. Yamaguchi, "Development of 2-D horn-antenna millimeter-wave imaging device (HMID) for the plasma diagnostics," *Rev. Sci. Instrum.* **88**, 044703 (2017).
- ⁴⁵²A. J. Fenn, D. H. Temme, W. P. Delaney, and W. E. Courtney, "The development of phased-array radar technology," *Lincoln Lab. J.* **12**, 321–340 (2000).
- ⁴⁵³P. Rohmann, S. Wolf, W. Kasperek, B. Plaum, and J. Hesselbarth, "A 32-element frequency-steered array antenna for reflectometry in W-band," in *2013 IEEE International Symposium on Phased Array Systems and Technology* (IEEE, Waltham, MA, 2013), pp. 559–563.
- ⁴⁵⁴T. Windisch, S. Wolf, G. M. Weir, S. A. Bozhrenkov, H. Damm, G. Fuchert, O. Grulke, M. Hirsch, W. Kasperek, T. Klinger, C. Lechte, E. Pasch, B. Plaum, E. A. Scott, and W7-X Team, "Phased array Doppler reflectometry at Wendelstein 7-X," *Rev. Sci. Instrum.* **89**, 10H115 (2018).
- ⁴⁵⁵C. Koenen, "Steerable Millimeter-wave Gaussian beam shaping phased array antenna for Doppler reflectometry of nuclear fusion plasma turbulence in ASDEX upgrade tokamak," Ph.D. thesis (Technische Universität München, 2020).
- ⁴⁵⁶S.-H. Seo, B. Kim, and K.-D. Lee, "Design of a Doppler reflectometer based on frequency steering phased array antenna," in *16th International Reflectometry Workshop, Greifswald, Germany* (IRW, 2024), available at <https://event.ipg-hgw.mpg.de/event/954/>.
- ⁴⁵⁷K. D. Lee, Y. U. Nam, S.-H. Seo, and Y. S. Kim, "Design of a Doppler reflectometer for KSTAR," *Rev. Sci. Instrum.* **85**, 11D858 (2014).
- ⁴⁵⁸T. Tokuzawa, T. Nasu, S. Inagaki, C. Moon, T. Ido, H. Idei, A. Ejiri, R. Imazawa, M. Yoshida, N. Oyama, K. Tanaka, and K. Ida, "3D metal powder additive manufacturing phased array antenna for multichannel Doppler reflectometer," *Rev. Sci. Instrum.* **93**, 113535 (2022).
- ⁴⁵⁹R. G. L. Vann, K. J. Brunner, R. Ellis, G. Taylor, and D. A. Thomas, "Preliminary measurements of the edge magnetic field pitch from 2-D Doppler backscattering in MAST and NSTX-U (invited)," *Rev. Sci. Instrum.* **87**, 11D902 (2016).
- ⁴⁶⁰J. Allen, "Design of the synthetic aperture microwave imager-2 for measurement of the edge current density on MAST-U," Ph.D. thesis (University of York, 2021).
- ⁴⁶¹R. Manabe, H. Tsuchiya, and M. Koga, "Trial of deep learning for image reconstruction of lens-less microwave holography," *Plasma Fusion Res.* **17**, 2401072 (2022).
- ⁴⁶²F. Da Silva, S. Heuraux, T. Ribeiro, E. Ricardo, J. Santos, A. Silva, J. Ferreira, J. Vicente, G. De Masi, O. Tudisco, R. Cavazzana, G. Marchiori, R. Luis, and Y. Nietiadi, "An overview of the evolution of the modeling of reflectometry diagnostics in fusion plasmas using finite-difference time-domain codes," *Fusion Eng. Des.* **202**, 114354 (2024).
- ⁴⁶³Y. Zhu, Y. Chen, J.-H. Yu, C. Domier, G. Yu, X. Liu, G. Kramer, Y. Ren, A. Diallo, N. C. Luhmann, and X. Li, "System-on-chip approach microwave imaging reflectometer on DIII-D tokamak," *Rev. Sci. Instrum.* **93**, 113509 (2022).
- ⁴⁶⁴T. Verdier, R. Vann, A. Jacobsen, T. Jensen, J. Rasmussen, R. Ragona, and S. Nielsen, "An ultrafast digitizer for continuous measurements from microwave fusion diagnostics," *Fusion Eng. Des.* **206**, 114597 (2024).
- ⁴⁶⁵G. H. Neilson, A. Basile, A. Cohen, F. Cometa, M.-A. De Looz, R. Fair, A. Gattuso, A. Jariwala, C. Muscatello, N. Pablant, G. Paraiso, S. Shirey, M. Smith, and A. Zolfaghari, "Diagnostics for burning plasmas," *IEEE Trans. Plasma Sci.* **50**, 4144–4149 (2022).
- ⁴⁶⁶H. Jalili and O. Momeni, "23.2 A 436-to-467 GHz lens-integrated reconfigurable radiating source with continuous 2D steering and multi-beam operations in 65 nm CMOS," in *2021 IEEE International Solid-State Circuits Conference (ISSCC)* (IEEE, San Francisco, CA, 2021), pp. 326–328.
- ⁴⁶⁷W. Biel, M. Ariola, I. Bolshakova, K. Brunner, M. Cecconello, I. Duran, T. Franke, L. Giacomelli, L. Giannone, F. Janky, A. Krimmer, R. Luis, A. Malaquias, G. Marchiori, O. Marchuk, D. Mazon, A. Pironi, A. Quercia, N. Rispoli, S. E. Shawish, M. Siccino, A. Silva, C. Sozzi, G. Tartaglione, T. Todd, W. Treutterer, and H. Zohm, "Development of a concept and basis for the DEMO diagnostic and control system," *Fusion Eng. Des.* **179**, 113122 (2022).
- ⁴⁶⁸C. Torregrosa-Martin, A. Ibarra, J. Aguilar, F. Ambi, F. Arranz, F. Arbeiter, A. Bagnasco, S. Becerril, D. Bernardi, B. Bolzon, E. Botta, B. Brenneis, M. Cappelli, P. Cara, J. Castellanos, D. Cosic, C. De La Morena, A. Diez, G. Ericsson, A. García, M. García, B. Garcinuño, J. Gutiérrez, V. Gutiérrez, D. Jimenez-Rey, T. Deysi, M. J. Ferreira, S. Fiore, W. Krolas, R. Lorenzo, M. Luque, L. Maciá, J. Marroncle, F. Martin-Fuertes, J. Marugán, J. Maestre, C. Meléndez, G. Micciché, J. Mollá, A. Moreno, F. Nitti, C. Núñez, F. Ogando, T. Pinna, C. Oliver, I. Podadera, C. Prieto, R. Prokopowicz, Y. Qiu, D. Rapisarda, D. Regidor, E. Rodríguez, A. Sabogal, D. Sánchez-Herranz, M. Sanmarti, L. Seguí, A. Serikov, T. Tadić, A. Talarowska, U. Wiacek, M. Weber, J. Valenzuela, and A. Zsakai, "Overview of IFMIF-DONES diagnostics: Requirements and techniques," *Fusion Eng. Des.* **191**, 113556 (2023).
- ⁴⁶⁹A. Ibarra, W. Królas, and D. Bernardi, "Preface to the Special Issue on the IFMIF-DONES fusion neutron source," *Nucl. Fusion* (in press) (2025).
- ⁴⁷⁰C. Sozzi, K. Kajiwara, T. Kobayashi, L. Figini, L. Garzotti, A. Moro, S. Nowak, and D. Taylor, "ECRF stray radiation studies in preparation of the operations of JT-60SA," *EPJ Web Conf.* **277**, 01008 (2023).
- ⁴⁷¹A. Moro, J. Ayllon, L. Figini, S. Garavaglia, K. Kajiwara, T. Kobayashi, C. Piccinni, A. Simonetto, C. Sozzi, H. Urano, and M. Yoshida, "Electron Cyclotron stray radiation detector studies for JT-60SA," *Fusion Eng. Des.* **191**, 113535 (2023).
- ⁴⁷²J. W. Oosterbeek, V. S. Udintsev, F. Gandini, M. Hirsch, H. P. Laqua, N. Maassen, Y. Ma, A. Polevoi, A. Sirinelli, G. Vayakis, and M. J. Walsh, "Loads due to stray microwave radiation in ITER," *Fusion Eng. Des.* **96–97**, 553–556 (2015).
- ⁴⁷³L. Krier, K. A. Avramidis, H. Braune, G. Gantenbein, S. Illy, Z. Ioannidis, J. Jellonek, H. P. Laqua, S. Marsen, D. Moseev, F. Noke, I. Gr. Pagonakis, T. Ruess, T. Rzesnicki, T. Stange, M. Thumm, and R. C. Wolf, "Frequency stabilization of megawatt-class 140 GHz gyrotrons at W7-X using an off-the-shelf PLL system," in *2021 46th International Conference on Infrared, Millimeter and Terahertz Waves (IRMMW-THz)* (IEEE, Chengdu, China, 2021), pp. 1–2.
- ⁴⁷⁴G. Dammertz, S. Alberti, A. Arnold, E. Borie, V. Erckmann, G. Gantenbein, E. Giguet, R. Heidinger, J. Hogge, S. Illy, W. Kasperek, K. Koppenburg, M. Kuntze, H. Laqua, G. LeCloarec, Y. LeGoff, W. Leonhardt, C. Lievin, R. Magne, G. Michel, G. Muller, G. Neffe, B. Piosczyk, M. Schmid, K. Schworer, M. Thumm, and M. Tran, "Development of a 140-GHz 1-MW continuous wave gyrotron for the W7-X stellarator," *IEEE Trans. Plasma Sci.* **30**, 808–818 (2002).
- ⁴⁷⁵S.-T. Han, R. G. Griffin, K.-N. Hu, C.-G. Joo, C. D. Joye, J. R. Sirigiri, R. J. Temkin, A. C. Torrezan, and P. P. Woskov, "Spectral characteristics of a 140-GHz long-pulsed gyrotron," *IEEE Trans. Plasma Sci.* **35**, 559–564 (2007).
- ⁴⁷⁶G. Wang, T. L. Rhodes, N. T. Howard, and W. A. Peebles, "A new synthetic correlation electron cyclotron emission diagnostic for validating nonlinear gyrokinetic simulations of electron temperature turbulence," *Rev. Sci. Instrum.* **95**, 083520 (2024).
- ⁴⁷⁷J. R. Pinzón, T. Happel, E. Blanco, G. D. Conway, T. Estrada, and U. Stroth, "Enhanced Doppler reflectometry power response: Physical optics and 2D full wave modelling," *Plasma Phys. Controlled Fusion* **59**, 035005 (2017).
- ⁴⁷⁸T. Happel, T. Görler, P. Hennequin, C. Lechte, M. Bernert, G. D. Conway, S. J. Freethy, C. Honoré, J. R. Pinzón, U. Stroth, and The ASDEX Upgrade Team, "Comparison of detailed experimental wavenumber spectra with gyrokinetic simulation aided by two-dimensional full-wave simulations," *Plasma Phys. Controlled Fusion* **59**, 054009 (2017).
- ⁴⁷⁹X. Feng, A. Liu, C. Zhou, X. Zou, G. Zhuang, S. Wang, M. Wang, H. Liu, W. Ding, S. Zhang, M. Wu, X. Zhu, B. Hao, J. Zhang, Z. Liu, J. Ji, X. Zhong, S. Liu, J. Xie, X. Lin, J. Huang, X. Gao, and Y. Wan, "Investigation of phase modulation and propagation-route effect from unmatched large-scale structures for Doppler reflectometry measurement through 2D full-wave modeling," *Plasma Sci. Technol.* **25**, 115101 (2023).

- ⁴⁸⁰F. Imbeaux, S. Pinches, J. Lister, Y. Buravand, T. Casper, B. Duval, B. Guillerminet, M. Hosokawa, W. Houlberg, P. Huynh, S. Kim, G. Manduchi, M. Owsiak, B. Palak, M. Plociennik, G. Rouault, O. Sauter, and P. Strand, "Design and first applications of the ITER integrated modelling & analysis suite," *Nucl. Fusion* **55**, 123006 (2015).
- ⁴⁸¹M. Romanelli, R. Coelho, D. Coster, J. Ferreira, L. Fleury, S. Henderson, J. Hollocombe, F. Imbeaux, T. Jonsson, L. Kogan, O. Meneghini, A. Merle, S. D. Pinches, O. Sauter, G. Tardini, D. Yadykin, S. Smith, P. Strand, and WPCD Team, "Code integration, data verification, and models validation using the ITER integrated modeling and analysis system (IMAS) in EUROfusion," *Fusion Sci. Technol.* **76**, 894–900 (2020).
- ⁴⁸²X. Ren, C. W. Domier, G. Kramer, N. C. Luhmann, C. M. Muscatello, L. Shi, B. J. Tobias, and E. Valeo, "Process to generate a synthetic diagnostic for microwave imaging reflectometry with the full-wave code FWR2D," *Rev. Sci. Instrum.* **85**, 11D863 (2014).
- ⁴⁸³F. Da Silva, E. Ricardo, J. Ferreira, J. Santos, S. Heuraux, A. Silva, T. Ribeiro, G. De Masi, O. Tudisco, R. Cavazzana, and O. D'Arcangelo, "Benchmarking 2D against 3D FDTD codes for the assessment of the measurement performance of a low field side plasma position reflectometer applicable to IDTT," *J. Instrum.* **17**, C01017 (2022).
- ⁴⁸⁴N. Q. X. Teo, V. H. Hall-Chen, K. Barada, R. J. H. Ng, L. Gu, A. K. Yeoh, Q. T. Pratt, X. Garbet, and T. L. Rhodes, "Using convolutional neural networks to detect edge localized modes in DIII-D from Doppler backscattering measurements," *Rev. Sci. Instrum.* **95**, 073528 (2024).
- ⁴⁸⁵B. Kim, S.-H. Seo, D. K. Oh, and Y.-S. Na, "Classification of the L-, H-mode, and plasma-free state: Convolutional neural networks and variational autoencoders on the edge reflectometer for KSTAR," *Rev. Sci. Instrum.* **95**, 104701 (2024).
- ⁴⁸⁶R. M. Churchill, C. S. Chang, J. Choi, R. Wang, S. Klasky, R. Kube, H. Park, M. J. Choi, J. S. Park, M. Wolf, R. Hager, S. Ku, S. Kampel, T. Carroll, K. Silber, E. Dart, and B. S. Cho, "A framework for international collaboration on ITER using large-scale data transfer to enable near-real-time analysis," *Fusion Sci. Technol.* **77**, 98–108 (2021).
- ⁴⁸⁷J. Farthing, T. Ozeki, S. Clement Lorenzo, N. Nakajima, F. Sartori, G. De Tommasi, G. Manduchi, P. Barbato, A. Rigoni, V. Vitale, G. Giruzzi, M. Mattei, A. Mele, F. Imbeaux, J.-F. Artaud, F. Robin, J. Noe, E. Joffrin, A. Hynes, O. Hemming, M. Wheatley, S. O'hira, S. Ide, Y. Ishii, M. Matsukawa, H. Kubo, T. Totsuka, H. Urano, O. Naito, N. Hayashi, Y. Miyata, M. Namekawa, A. Wakasa, T. Oshima, H. Nakanishi, and K. Yamanaka, "Status of the ITER remote experimentation centre," *Fusion Eng. Des.* **128**, 158–162 (2018).
- ⁴⁸⁸C. Allen and D. M. A. Mehler, "Open science challenges, benefits and tips in early career and beyond," *PLoS Biol.* **17**, e3000246 (2019).
- ⁴⁸⁹E. G. Carayannis, M. Vincenzi, and J. Draper, "The economic logic of open science in fusion energy research: A policy perspective," *Energy Policy* **186**, 113983 (2024).
- ⁴⁹⁰H. Van Den Brand, "Modelling and measurements for control of magnetic instabilities in tokamak plasmas," Ph.D. thesis (Technische Universiteit Eindhoven, 2016).